2020-09-30

Neuroendocrine Modulation of Complex Behavior and Physiology in C. elegans

Jeremy T. Florman
University of Massachusetts Medical School

NEUROENDOCRINE MODULATION OF COMPLEX BEHAVIOR AND PHYSIOLOGY IN *C. ELEGANS*

A Dissertation Presented

By

Jeremy Tyler Florman

Submitted to the Faculty of the
University of Massachusetts Graduate School of Biomedical Sciences, Worcester
In partial fulfillment of the requirements for the degree of

DOCTOR OF PHILOSOPHY

SEPTEMBER 30th, 2020

BIOMEDICAL SCIENCE
PROGRAM IN NEUROSCIENCE

NEUROENDOCRINE MODULATION OF COMPLEX BEHAVIOR AND

PHYSIOLOGY IN *C. ELEGANS*

A Dissertation Presented
By

Jeremy Tyler Florman

The signatures of the Dissertation Defense Committee signify completion and approval as to style and content of the Dissertation

_____
Mark Alkema, Ph.D., Thesis Advisor

_____
Claire Bénard Ph.D., Member of Committee

_____
Alexandra Byrne, Ph.D., Member of Committee

_____
Patrick Emery, Ph.D., Member of Committee

_____
Jagan Srinivasan, Ph.D., External Examiner

The signature of the Chair of the Committee signifies that the written dissertation meets the requirements of the Dissertation Committee

_____
Michael Francis, Ph.D., Chair of Committee

The signature of the Dean of the Graduate School of Biomedical Sciences signifies that the student has met all graduation requirements of the school

_____
Mary Ellen Lane, Ph.D., Dean of the Graduate School of Biomedical sciences

Program in Neuroscience
September 30th, 2020

Dedication

To my parents Joyce and Harvey

for raising me well,

and to my loving wife Laura

for putting up with the results of that upbringing.

Acknowledgements

Looking back on my years at UMass medical school I am stunned and gladdened by both the changes that I have witnessed and the constants that remain. Unlike many of my peers who crossed vast oceans and continents to move to the Worcester area to attend graduate school, I merely crossed the town of Shrewsbury. Having grown up in Northborough, I often joke that you can see my childhood home from the top floor of the LRB. You can't, but that is only because there is a hill in the way. While I may have missed out on traveling to an exotic new locale for school, this meant that my family and friends were always close at hand during the ups and downs of my career as a graduate student.

I would not be where I am today without the support and inspiration of my family. My parents, Joyce and Harvey, have been a source of encouragement throughout my life, and instilled in me a sense of wonder and scientific curiosity from a young age. My mother would sometimes bring me into work as a child, and to keep me out of her hair she would let me look at histology slides through a microscope. I remember being fascinated by the intricate color and detail of the microscopic realm, but I was equally fascinated by the mechanical cell counter, which was probably much more distracting. My father also led me down the path towards science from an early age, allegedly reciting the laws of thermodynamics to get me to sleep as a baby, and when I was older letting me hold starfish and sea-urchins in the lab at the Worcester Foundation. Their continued support has made me who I am today. My brother Murphy has always been a someone I can

turn to for a laugh and he is equally likely to be on the receiving end of a “nerd-rant” as to be delivering one to me, which I always appreciate.

I met my wife Laura the year before starting graduate school and wooed her with my talk of volumetric reconstruction of butterfly brains. For some reason that did not send her running and in the years since then we have built a beautiful life together. She has been with me through all the discoveries and all the dark times that are an inevitable part of science and I am truly grateful to her for that. Without her as a pillar of support I do not know where I would be.

My time in Mark Alkema’s lab has allowed me to grow as a scientist and as a person and I am extremely thankful to him for that. I first became interested in Mark’s lab when I learned about his research into how worms escape predatory fungus. At the core of this work was understanding the sensory motor coding of complex behavior but layered on top of that was an evolutionary arms race between worms and fungi. I found this incredibly interesting and wanted to join the lab to be a part of research like this.

I relate this because it highlights an important lesson that I have learned from Mark: A large part of science is story telling. You can have the most solid results in the world, but they won’t make an impact if you can’t convey them in a compelling way. Of course, it is hard to tell a good story without good science, and as a mentor Mark has given me the assistance, and the independence, to grow as a researcher, to lean experimental design and how to approach questions in a scientific way.

The other reason I wanted to join Mark's lab, aside from thinking predatory fungus was awesome, was the people and atmosphere he cultivated. Chris Clark, Jenn Ingemi and Yung-Chi Huang were my original mentors, my "Worm-Sensei", and are true friends. I remember lots of laughter and shenanigans, but I learned so much from them. Over the years the faces have changed but I feel a bond with everyone who has passed through the lab. Amit Sinha, Jeff Grant, Diego Rayes and all his students that have come up from Argentina. I also am deeply thankful to my current lab mates. Andrea Thackery, who brought order to our chaos and who is basically the heart of the lab. Her patience and care working with undergrad volunteers and rotation students allowed me to be the distant and reclusive senior grad student I needed to be to finish my degree. Wookyu Kang, who is a tireless and dedicated scientist and an incredibly kind human being. And Antonia Budnik, who's scientific and botanical prowess is on track to surpass mine before she reaches her second decade of life.

I am also deeply grateful to the past and current members of our fellow worm labs, the Francis lab, the Byrne lab and Bénard lab who have made working in the department feel like being part of a community. Particularly Navonil Banerjee, Raja Bhattacharya, Devyn Oliver, Victoria Julian.

Thanks also to Ross Lagoy, Kyra Burnett and Agustin Almoril-Porras, who's comradery helped me survive my first year teaching the Neural Systems and Behavior course at the MBL in Woods Hole and will always be friends of mine.

I owe a large portion of whatever remaining sanity I still possess to my network of friends outside the scientific community so thanks to Charlie and Liz Thebado, Steve Schwartz, Hrothgar And Alex Lane, Kyle Rivers, Alex Hanelt, Charlie Lynch, Pete Kellogg and Sean Coulson and everyone else who I am forgetting.

And finally, I would like to thank my committee members for their mentorship over the years and all the advice and support they have provided me during my scientific development. My committee chair Michael Francis, Clair Bénard, Patrick Emery, Alexandra Byrne former committee member José Lemos and to my external examiner Jagan Srinivasan.

Thesis Abstract

To survive, animals must adapt to a complex and challenging world in a way that is flexible and responsive, while maintaining internal homeostasis. Neuromodulators provide a means to systemically alter behavioral or physiological state based on intrinsic or extrinsic cues, however dysregulated neuroendocrine signaling has negative consequences for fitness and survival. Here I examine neuroendocrine function and dysfunction using the escape response in *Caenorhabditis elegans*. The RFamide neuropeptide FLP-18 is a co-transmitter with the monoamine tyramine and functions both synergistically and antagonistically to tyramine in coordinating escape behavior. Using behavioral analysis and calcium imaging, I show that FLP-18 functions primarily through the G-protein coupled receptor (GPCR) NPR-5 to increase calcium levels in muscle, enhancing locomotion rate, bending and reversal behavior during the escape response.

Furthermore, I examine the relationship between persistent acute stress and resilience using repeated activation of the escape response as a model of neuroendocrine dysregulation. Repeated activation of the escape response shortens lifespan and renders animals more susceptible to thermal, oxidative, and nutritional stress. Tyramine release is necessary and sufficient for this effect and activity of the tyraminergic RIM neurons is differentially regulated by acute versus long-term stressors. Impaired stress resistance requires both the GPCR TYRA-3 in the intestine and intestinal neuropeptide release. Activation of the

insulin receptor DAF-2 is downstream of TYRA-3 and inhibits the transcription factors DAF-16/FOXO, SKN-1/Nrf2 and HSF-1, linking monoamine signaling in acute stress to the insulin signaling pathway and impaired resilience to long-term stressors.

Table of Contents

List of Figures

List of Movies

Chapter II

List of Abbreviations

Acronyms and nomenclature:

AMP	adenosine monophosphate
ANOVA	analysis of variance
ARS	area restricted search
ATP	adenosine triphosphate
ATR	*all-trans* retinal
CCD	charge coupled device
ChR2	channelrhodopsin-2
cAMP	cyclic adenosine monophosphate
CMOS	complementary metal-oxide-semiconductor
DAG	diacylglycerol
DIC	differential interference contrast
DNA	deoxyribonucleic acid
FLP	FMRF-like peptide
FMRF	Phe-Met-Arg-Phe-amide peptide
FOXO	forkhead box O transcription factor
GABA	gamma aminobutyric acid
GFP	greed fluorescent protein
GPCR	G-protein coupled receptor
GTP	guanosine-5'-triphosphate
HA	histamine

HisCL	histamine gated chloride channel
HPA	hypothalamic-pituitary-adrenal
IGF	insulin-like growth factor
IGFR	insulin-like growth factor receptor
IIS	insulin/insulin-like growth factor signaling
ILP	insulin-like peptide
IP_3	inositol triphosphate
ITR	inositol triphosphate receptor
Kb	kilobase
LDCV	large dense core vesicle
L1-L4	larval stage 1-4
LED	light emitting diode
LGC	ligand gated channel
N2	*C. elegans* wild-type Bristol strain
NA	noradrenaline
NGM	nematode growth media
NLP	neuropeptide-like peptide
NLS	nuclear localization signal
NMJ	neuromuscular junction
NPR	neuropeptide receptor
NPY	neuropeptide Y
NPYR	neuropeptide Y receptor

P	promoter
PIP2	phosphatidylinositol 4,5-bisphosphate
PKA	protein kinase A
PKC	protein kinase C
PLC	phospholipase C
PTSD	post-traumatic stress disorder
RFP	red fluorescent protein
RNA	ribonucleic acid
ROI	region of interest
ROS	reactive oxygen species
SEM	standard error of the mean
SNS	sympathetic nervous system
STNS	stomatogastric nervous system
TA	tyramine
TRN	touch receptor neuron
VNC	ventral nerve cord
YFP	yellow fluorescent protein
(+)	transgenic expression, rescue
(+++)	transgenic overexpression

Symbols and units

α	alpha
A	anterior
C	Celsius
°	degree
Δ	delta
D	dorsal
R	fluorescence ratio (GFP/RFP)
F	fluorescence
fps	frames per second
g	gram
l	liter
m	meter
µl	microliter
µm	micrometer
µM	micromolar
ml	milliliter
mm	millimeter
mM	millimolar
ms	millisecond
min	minute

M	molar
ng	nanogram
nm	nanometer
nmol	nanomole
ns	not significant
Ω	omega
P	posterior
s, sec	seconds
t	time
V	ventral

Copyrighted Materials

The following figures or chapters were reproduced or adapted from copyrighted materials.

List of third party Copyrighted materials:

Figure I-1:

Cannon, W. B. (1915) Bodily Changes in Pain, Hunger, Fear and Rage; An Account of Recent Researches into the Function of Emotional Excitement. NEW YORK AND LONDON D. APPLETON AND COMPANY.

No permission required.

Figure I-2:

Burnstock, G. and Verkhratsky, A. (2010) 'Vas deferens - A model used to establish sympathetic cotransmission', *Trends in Pharmacological Sciences.* Elsevier Ltd, 31(3), pp. 131–139. http://doi.org/10.1016/j.tips.2009.12.002

Publisher: Elsevier License #: 4892631097301

Figure I-4:

Selye, H. (1946) 'The General Adaptation Syndrome and the Diseases of Adaptation', *The Journal of Clinical Endocrinology*, 6(2), pp. 117–230. http://doi.org/10.1210/jcem-6-2-117

Publisher: Oxford University Press License #: 4892640270485

Figure I-5:

Jasper, H. (2008) 'SKNy Worms and Long Life', *Cell*, pp. 915–916. http://doi.org/10.1016/j.cell.2008.03.002

Publisher: Elsevier License #: 4892640044618

List of Copyrighted materials produced by the Author:

Chapter III is adapted from a published manuscript and was modified to include supplemental figures. No permission is required from Nature Publishing Group for the author to reproduce their contribution in full or in part.

De Rosa, M.J., Veuthey, T., **Florman, J.** et al. (2019) The flight response impairs cytoprotective mechanisms by activating the insulin pathway. *Nature* 573, 135–138. https://doi.org/10.1038/s41586-019-1524-5

Portions of *Appendix I*, including Figure AI-1, are adapted from an unpublished manuscript that the Author contributed to in the lab of Mark Alkema. Portions of that manuscript were used in the doctoral dissertation of Christopher M Clark.

Clark, C. M. (2014) Neural Orchestration of the C. elegans Escape Response: A Dissertation. University of Massachusetts Medical School. doi: https://doi.org/10.13028/M24S4T.

CHAPTER I: INTRODUCTION

For an animal to survive it must be able to sense and adapt to an ever-changing environment. Behavior is an overt form of response, but cellular and physiological adaptations are just as vital to an animal's ability to survive. Apart from Poriferans and Placozoans, all other animal phyla rely on a nervous system to coordinate both behavior and physiological reactions to their environment. From the simple nerve nets of Cnidarians and Ctenophores to the complex, centralized brains of vertebrates, containing millions or billions of neurons, all nervous systems share the same basic function: to detect information about the external or internal environment, integrate and process that information, and produce an appropriate response. Behavioral responses can take the form of courting a mate, foraging for food or fleeing from a predator, while physiological responses can be shifting metabolic pathways based on nutrient availability, altering circadian rhythms in response to changes in photoperiod or elevating heart rate in response to danger. Often behavioral and physiological responses must act in concert across multiple levels to achieve an adaptive outcome. A central question in biology remains understanding how the nervous system can switch between behavioral and physiological states and how this is coordinated on a systemic level in the organism?

Shifting state through modulation of neural circuits

In species across the animal kingdom, modulatory substances such as hormones, monoamines and neuropeptides can have a dramatic and long-lasting impact on the functional properties of neurons, muscle and other tissues. Release of these modulators provides a mechanism by which the nervous system can translate sensory input into a persistent shift in the behavioral state of an animal. Early insights into the modulation of behavioral states came from the work of Walter B. Cannon (1915) on catecholamine signaling from the sympathetic nervous system during states of intense physical or psychological distress. Cannon found that diverse stressors such as cold, hemorrhage, pain or fear induced the release of adrenaline and noradrenaline into circulation which impact the physiology of nearly every tissue in the body (Figure I-1). These effects, the “fight-or-flight” response, resulted in vasoconstriction to draw blood away from digestive and reproductive organs in favor of muscle, heart and lungs, increased the contractile force of heart and skeletal muscle, increased blood glucose levels and in general prepared the body for decisive physical action. By acting simultaneously on multiple target sites, modulatory transmitters can effectively bias behavior from one state to another.

In the century since Cannon, a plethora of modulatory peptides have been discovered in numerous species, many of which have a surprising degree of conservation in the physiological and behavioral functions they regulate. Take, for example, the oxytocin signaling system. In mammals oxytocin is associated

with the regulation of maternal behavior, pair bonding and reproduction (Insel, 1992; Lim and Young, 2006). Oxytocin-like peptides and cognate receptors are evolutionarily ancient and are found in the genomes of many bilaterian species (Moore, 1992; Jékely, 2013; Mirabeau and Joly, 2013; Lockard, Ebert and Bargmann, 2017). Interestingly, oxytocin-like peptides are involved in the regulation of similar behaviors in mammals and in distantly related invertebrates, for example oxytocin-like signaling promotes copulatory behavior in the nematode *Caenorhabditis elegans* (Garrison *et al.*, 2012), the medicinal leech *Hirudo verbena* (Wagenaar *et al.*, 2010) and the snail *Lymnaea stagnalis* (Van Kesteren *et al.*, 1995; De Boer *et al.*, 1997). This deep conservation of not just sequence but of function indicates the importance of peptide signaling in the modulation of behavior.

Neuropeptide signaling

Neuropeptides have such wide-ranging effects on the output of neural circuits, and thus on behavior, in part because of the difference in their mechanism of action when compared to that of classical neurotransmitters. The basis of information in the nervous system is the flow of current into and out of cells in the form of charge carrying ions. When membrane potential of a neuron passes a certain threshold, voltage gated ion channels open and further depolarize the cell. This wave of depolarization propagates down the axon until it reaches the presynaptic terminal where the opening of voltage gated calcium channels

causes an influx of calcium ions and the fusion of transmitter filled synaptic vesicles. Exocytosis of vesicles releases neurotransmitter molecules into the synaptic cleft where they bind to ligand gated ion channels on the postsynaptic membrane. Channel activation causes an influx of ions into the postsynaptic neuron and converts the chemical message back to an electrical one. Signaling by classical neurotransmitters is 1) fast, with ion channel conductance operating on the scale of milliseconds, 2) mediated by ionic currents, either cationic or anionic, which depolarize or hyperpolarize the membrane, respectively, and 3) direct, with transmitter being released across a synaptic cleft spanning tens of nanometers.

Neuropeptide signaling operates in a parallel or orthologous fashion to that of classical neurotransmitters and as a result enhances the complexity and flexibility of neural computation. Unlike classical neurotransmitters, neuropeptides signal through metabotropic G-protein coupled receptors (GPCRs) which, when activated, result in a G-protein mediated second messenger cascade. These second messenger cascades rely on diffusion of proteins in the membrane and can involve the phosphorylation of multiple proteins, and as a result are slow compared to ionotropic receptors. However once initiated, the effects of second messenger signaling can persist from fractions of a second to minutes. Another key difference between classical transmitter and neuropeptides is that the consequences of GPCR activation rarely lead to direct depolarization of a neuron, rather, they modulate neuronal properties, for example through

phosphorylation of ion channels, changes in the quantal content of vesicles or activation of transcription factors to effect long lasting changes in neuronal function. Finally, neuropeptides differ from classical neurotransmitters in their packaging and release. Neurotransmitters are released from small synaptic vesicles at synaptic active zones and are rapidly reabsorbed or degraded preventing diffusion of transmitter. Neuropeptides, on the other hand, are packaged into large dense core vesicles (LDCVs) and are usually released outside of the active zone, referred to as extra-synaptic transmission. As a result neuropeptides can diffuse up to a distance of several millimeters (Jan and Jan, 1982) and thereby modulate the activity of large numbers of neurons within a circuit. These features of neuropeptides, to act on long timescales and over large distances to alter neuronal properties, make peptidergic signaling an effective means to alter behavior and physiology in response to stimuli.

Co-transmission of peptides and classical transmitters.

Initially it was thought that neuronal communication was mediated by the release of a single transmitter, however in the 1970s evidence began to emerge that neurons synthesize and release multiple signaling molecules, a phenomenon known as co-transmission (Burnstock, 1976). It has now been demonstrated that this is a common feature of the nervous system with neurons often releasing peptides and other substances in addition to classical transmitters. Co-transmission increases the flexibility and dynamic range of signaling in the

nervous system as different transmitters can be released in response to different inputs, such as low versus high frequency stimulation. Co-transmitters can act on the same postsynaptic targets or on distinct targets, referred to as convergent and divergent transmission, respectively. The action of co-transmitted substances on their targets can be synergistic, both having a complementary effect, or there can be negative crosstalk where one substance antagonizes the effect of the other.

Adrenergic neurons of the sympathetic nervous system innervate smooth muscle and have been shown to use multiple signaling molecules to regulate muscle contraction (Figure I-2). In addition to noradrenaline (NA), these neurons also release neuropeptide Y (NPY) and adenosine triphosphate (ATP) (Kasakov *et al.*, 1988; Ellis and Burnstock, 1990; Westfall, Yang and Curfman-Falvey, 1995). Release of NA and ATP onto smooth muscle induces contraction with ATP mediating a fast, initial response while NA driving a slower persistent contraction, and NPY potentiates the actions of ATP and NA, enhancing contraction (Ellis and Burnstock, 1990; Boland *et al.*, 1992; Honner and Docherty, 1999; Smith and Burnstock, 2004). All three transmitters also activate receptors on preganglionic terminals which mediate negative feedback and inhibit their own release (Lundberg and Stjarne, 1984; Queiroz, Talaia and Gonçalves, 2003). Co-transmission of classical neurotransmitters and modulatory neuropeptides can have complex outcomes for the activity of neural circuits but understanding the functional impact of co-transmission on behavior

remains challenging. Work in invertebrates has demonstrated the impact of co-transmission in the modulation of rhythmic motor behavior (Weiss *et al.*, 1992; Katz, 1998; Blitz *et al.*, 1999; Eve Marder and Dirk Bucher, 2001), however these studies have been conducted in dissected preparations or used neuronal activity as a read-out of behavior rather than in intact behaving animals.

C. elegans and its nervous system

The nematode *Caenorhabditis elegans* is a soil dwelling round worm that has become an important model system to understand aspects of biology from programed cell death, nervous system development and maintenance to longevity and aging. *C. elegans* presents a number of advantages to studying the impact of peptidergic co-transmission on behavior. *C. elegans* has a completely sequenced genome and a relatively simple nervous system containing only 302 neurons. Importantly, *C. elegans* is the only animal to have its nervous system entirely reconstructed (White *et al.*, 1986), allowing us to know the topography of neural circuits that mediate behavior. Because the cuticle of *C. elegans* is optically transparent, neuronal activity can be monitored and manipulated at single cell resolution in freely behaving animals through expression of genetically encoded calcium indicators or light gated ion channels driven by cell specific promoters (Shipley *et al.*, 2014; Venkatachalam *et al.*, 2015). Finally, the genome of *C. elegans* contains over 100 neuropeptide precursor genes, many of which encode multiple peptide sequences to bring the total number of potential mature

peptides to over 250 (Li and Kim, 2008). In *C. elegans,* neuropeptides are grouped into three families based on sequence similarity, these are the insulin like peptides (ILPs), the FMRF-like peptides (FLPs) and a group of peptides that lack obvious orthologs which are referred to as neuropeptide-like proteins (NLPs) (Li *et al.*, 1999; Li, Kim and Nelson, 1999). *C. elegans* also has a large number of neuropeptide GPCRs, many of which remain to be de-orphanized (Frooninckx *et al.*, 2012). Many *C. elegans* neurons co-express one or more neuropeptides along with their classical transmitter and over 80% of all neurons are part of a peptidergic signaling network (Bentley *et al.*, 2016). Given the relative simplicity of the nervous system, it is likely that peptidergic co-transmission provides additional flexibility to the hard-wired connectome, allowing circuits to respond differently under specific conditions. Together, these reasons make *C. elegans* an ideal system in which to study the impact of neuromodulatory peptides on behavior.

The C. elegans escape response.

In the wild, *C. elegans* lives in decaying vegetable matter and feeds upon bacteria. *C. elegans* itself is preyed upon by numerous species of nematophagous fungi that have evolved specific adaptations to trap nematodes for consumption, including toxins, adhesive nets or knobs and noose-like constricting rings (Drechsler, 1937; Thorn and Barron, 1984). Constricting rings are composed of mechanosensitive cells which are activated by contact and

cause the ring to inflate after a brief delay. If a worm is within the ring when it inflates, the animal will be trapped for eventual digestion by hyphae which invade the immobilized body. Similar to the fight-or-flight response triggered by detection of a predator in other animals, *C. elegans* too has evolved a flight response, also referred to as the escape response, which is an adaptation that increases their chances of survival in an encounter with a predator (Maguire *et al.*, 2011).

The escape response is a highly stereotyped compound motor sequence which is elicited by anterior touch, be it from a hyphal ring or from other gentle mechanical stimuli. During normal foraging activity, *C. elegans* moves forward by propagating sinusoidal waves from head to tail while scanning the olfactory environment with exploratory head oscillations. When the escape response is triggered by anterior touch, the animal relaxes its neck muscles, suppressing head oscillations, and initiates a rapid reversal. Animals that fail to suppress head oscillations cannot back out of hyphal rings effectively and are trapped more frequently as a result (Maguire *et al.*, 2011). Following several seconds of backward motion, animals will frequently execute a sharp ventral turn during which they slide their head along the side of the body, referred to as an omega turn as the shape of the animal looks like the Greek letter Ω (Figure I-3, a; Croll, 1975). The omega turn is synchronized to occur with the resumption of forward locomotion and functions to reorient the worm in the opposite direction. Following the omega turn the worm will accelerate forward, away from the stimulus, and maintain elevated velocity for several minutes.

The *C. elegans* escape response is an ideal model to study peptidergic modulation of behavior for several reasons. First, the escape response is a highly stereotyped behavior that is easy to quantify and can be elicited in the lab either by hand or in an automated fashion by delivering a mechanical tap to the side of a plate. Using automated tap delivery in conjunction with computer assisted worm tracking software enables reproducible, high throughput analysis of changes in escape behavior after experimental manipulation (Swierczek *et al.*, 2011). Second, the escape response has the hallmarks of being a modulated state in that a specific stimulus can induce an alteration in behavior that persists for up to several minutes. Also, most of the neurons in the escape circuit express neuropeptides or neuropeptide receptors(Li and Kim, 2008; Frooninckx *et al.*, 2012), indicating that it is a system that is subject to neuromodulation. Finally, and perhaps most importantly, like other systems used to study peptide function, such as the crustacean stomatogastric nervous system (STNS), the neural circuit that mediates the escape response is extremely well understood, (Chalfie *et al.*, 1985; White *et al.*, 1986; Wicks and Rankin, 1995), but unlike the STNS, we can observe the behavioral output of the escape circuit as well as its neuronal activity in freely behaving animals (Wang *et al.*, 2020; Appendix I). No other system is better suited to study the impact of neuropeptide signaling on the activity of a completely defined circuit and what affect that has on behavior.

Neuronal basis of the escape response

The *C. elegans* wiring diagram describes the synaptic connections between all 302 neurons in the nematode (White *et al.*, 1986). This provided the framework for Chalfie and coworkers (Chalfie *et al.*, 1985; Wicks and Rankin, 1995) to dissect the neural circuit that mediates the escape response to gentle touch in *C. elegans* (Figure I-3, b). The mechanosensory AVM and ALM neurons detect anterior touch and make synapses onto groups of interneurons that control both backward and forward locomotion. The PVC and AVB interneurons synapse onto the B type motor neurons which drive forward locomotion whereas the AVD, AVE and AVA interneurons synapse onto the A type motor neurons which drive backward locomotion. Output from the anterior mechanosensory AVM and ALM likely inhibit the forward motion interneurons and activate the backward locomotion interneurons (Wicks and Rankin, 1995). The AVA and AVE are electrically coupled to the RIM inter/motor-neurons which are in turn coupled to the AIB by both chemical and electrical synapses. The RIM and AIB both synapse onto the SMD and RMD motor neurons which innervate neck muscle to control head movements (Gray, Hill and Bargmann, 2005). The AIB is also electrically coupled to the RIV inter/motor-neurons which asymmetrically innervate ventral neck muscle and establish the ventral bias to the omega turn (White *et al.*, 1986; Gray, Hill and Bargmann, 2005).

The RIM inter/motor-neurons synthesize and release the monoamine tyramine (Alkema *et al.*, 2005), the invertebrate analog of adrenaline. Tyramine

functions both as a classical transmitter and as a neuromodulator to coordinate behavior during several phases of the escape response (Pirri *et al.*, 2009; Donnelly *et al.*, 2013; Figure II-7, c). The RIM is presynaptic to the AVB, which drive forward locomotion, and to the SMD, RMD and neck muscle, which control head movements. Acting as a classical transmitter, tyramine inhibits these neurons and muscles through activation of the tyramine gated chloride channel LGC-55 (Pirri *et al.*, 2009). Inhibition of the AVB suppresses forward locomotion and thus results in a longer reversal, and inhibition of the SMD, RMD and neck muscle prevents head movements resulting in the suppression of head oscillations during the reversal (Pirri *et al.*, 2009). Tyramine is also released extra-synaptically and acts as a neuromodulator to promote deep bending during the omega turn. The VD motor neurons are GABAergic neurons that innervate ventral body-wall muscle to mediate relaxation. Tyramine activates the $G\alpha_o$ coupled GPCR SER-2 in the VD motor neurons, which suppresses their activity, resulting in reduced inhibitory input into ventral body wall muscles, allowing enhanced contraction during the deep ventral bend of the omega turn (Donnelly *et al.*, 2013).

While the connectivity and, to some degree, the functionality of individual neurons in the escape circuit are clearly defined, there is still much we do not understand about how this circuit operates to orchestrate the escape response. What is the role of peptide neuromodulators in shaping circuit activity and behavior? In addition to tyramine, the RIM neurons also express the RFamide

neuropeptide FLP-18 (Rogers *et al.*, 2003), and the FLP-18 receptors NPR-1, NPR-4 and NPR-5 are expressed in neurons in the escape circuit including the backwards locomotion interneurons, AVA, the ventral turn motor neurons, RIV, as well as in motor neurons in the ventral nerve cord and in muscle (Coates and Bono, 2002; Kubiak *et al.*, 2003, 2008; Cohen *et al.*, 2009). Is FLP-18 a co-transmitter with tyramine in the RIM and if so, what are the functional consequences of co-transmission on behavior? It is also unclear how activity in the circuit differs during normal locomotion and foraging compared to when engaging in the escape response. Many of these neurons function in coordinating basal locomotion. Does peptidergic modulation shift their activity during the escape response to get more behavioral flexibility out of a simple, hard-wired circuit?

Homeostasis and endocrine regulation.

The state induced by adrenal secretion, the fight-or-flight response, is adaptive to an organism in certain circumstances, such as when faced with a predatory threat, because it promotes a behavioral response that helps the animal survive. But adrenal secretion affects not just behavior, but physiology and metabolism as well, for example it prevents the secretion of digestive enzymes and the contractions of the stomach (Cannon, 1915). Similarly, modulatory peptidergic signaling from the autonomic nervous system and the hypothalamic-pituitary-adrenal (HPA) axis can promote fight-or-flight, driving energy utilization and

physical exertion or it can promote “feed-and-breed”, driving energy storage, growth and reproduction, but it can’t simultaneously drive both processes. As a result, it is vital that the nervous system be able to downregulate modulatory signaling when it is no longer adaptive so as to maintain physiological balance.

Dysregulation of the neuroendocrine systems that modulate physiology and behavior is linked to pathological conditions, therefore it is important to understand how these systems are coordinated by the nervous system. Pioneering research into what we now think of as chronic stress came from the work of Hans Selye in the 1930s and 1940s. Similar to the work done by Walter Cannon, Selye found that animals exposed to prolonged trauma or “diverse noxious agents” exhibited a characteristic response that he referred to as the “General Adaptation Syndrome”, which followed a similar progression regardless of the specific treatment (Selye, 1936, 1946). When first exposed to a stressor, animals would enter a state of shock, however, in time they would develop resistance to that stressor and to other stressors as well (“crossed-resistance”) until eventually they would succumb to death if the stressor did not cease (Selye, 1946; Figure I-4). What was remarkable about this work was the finding that the cause of death is not the stressor *per se* but the body’s response to it, in the form of chronic adrenal and corticoid secretion (Selye, 1946). This response is adaptive in the short term, enhancing resistance, but is ultimately maladaptive if not properly regulated.

Systemic responses like adrenal secretion act on an organismal level to increase stress resistance, by allowing an animal to run longer or fight harder. In contrast to these behavioral responses, there are stress response pathways that operate on a cellular level to increase resistance to threats such as oxidation, hypoxia and heat stress. Cells are protected from damage through the activation of evolutionarily conserved transcriptional response pathways mediated by proteins like the heat shock factor HSF-1, the fork-head box O transcription factor DAF-16/FOXO and SKN-1/Nrf (Hsu, Murphy and Kenyon, 2003; An *et al.*, 2005; Prahlad and Morimoto, 2009; Landis and Murphy, 2010; Chiang *et al.*, 2012; Tullet *et al.*, 2017). Activation of these transcriptional cascades increases resistance to reactive oxygen species, misfolded proteins and functions to protect cells and extend lifespan (Kenyon *et al.*, 1993; Dorman *et al.*, 1995; Kimura *et al.*, 1997; Lithgow and Walker, 2002; Arantes-Oliveira, Berman and Kenyon, 2003; Fontana, Partridge and Longo, 2010).

However, as with the antagonism between fight-or-flight and feed-and-breed, activation of cellular stress response pathways comes at a cost to cell growth, protein synthesis and reproduction (Feder *et al.*, 1992; Krebs and Feder, 1997; Kenyon, 2010). To manage proper development and reproduction, multicellular animals must coordinate stress responses throughout the body. In favorable conditions such as in the presence of abundant food, animals shift to a state of growth energy utilization and reproductive development and down regulate stress response pathways through the conserved insulin/insulin like

growth factor (IGF-I) signaling (IIS) pathway(Kimura *et al.*, 1997; Honda and Honda, 1999; Barbieri *et al.*, 2003; Fontana, Partridge and Longo, 2010). Activation of the IIS pathway results in the phosphorylation of stress response transcription factors and precludes their translocation to the nucleus and thereby inhibits their activity(Lin *et al.*, 2001; Matsuzaki *et al.*, 2003; Figure I-5).

In *C. elegans* there is a single gene encoding the insulin receptor/IGFR homolog *daf-2* (Kimura *et al.*, 1997), but there are 40 putative insulin like peptide (ILP) genes. As DAF-2/IIS activation mediates the switch from stress resistance to growth and reproduction, endocrine signaling by ILPs are key modulators of an animal's physiological and metabolic state. While the function of some ILPs have been investigated in relation to sensory processing and DAF-2/IIS activity (Pierce, 2001; Murphy, Lee and Kenyon, 2007), it remains unclear how an animal integrates internal and external sensory cues to control cellular homeostasis and stress resistance.

Finally, is there interaction between behavioral response to stress like the fight-or-flight response and cellular responses to stress? In vertebrates, activation of the HPA stress response downregulates reproductive and anabolic cellular functions to mobilize energy for immediate use, does a similar interaction occur between the escape response and *C. elegans* and the pathways mediating cytoprotection versus growth? Given the high degree conservation of insulin signaling pathways across species, understanding how peptidergic modulatory

programs interact in *C. elegans* could have major impact on our understanding of nervous system control of physiology and behavior.

Thesis Outline

The work presented in this thesis uses the escape response in *Caenorhabditis elegans* as a model to understand the molecular and genetic mechanisms underlying neuromodulatory signaling in the coordination of behavioral states and explores the consequences of neuroendocrine dysregulation. I will show how neuropeptide and monoamine signaling molecules act as physiological switches which have adaptive outcomes in the appropriate circumstances yet if not properly regulated can have a negative impact on stress resistance and survival. The genetic tractability and known wiring diagram of the nematode *C. elegans* allows study of these responses at the level of individual neurons, from sensory transduction to motor output.

I will show how co-transmission of the monoamine tyramine and the RFamide neuropeptide FLP-18 act synergistically and antagonistically to coordinate distinct behavioral phases of the compound motor sequence that makes up the *C. elegans* escape response. Tyramine is released during the escape response and coordinates reversal behavior, head bending and omega turning during the escape response (Alkema *et al.*, 2005; Pirri *et al.*, 2009; Donnelly *et al.*, 2013). In appendix I, I will demonstrate that tyramine also plays a

role in coordinating the transition from reversal to omega turn. Using laser ablation of individual neurons and genetic mutants I will show that disruption of tyramine signaling affects the duration of reversals. Using pharmacological assays and optogenetics I will show that tyramine also affects the timing of the ventral head bend that initiates the omega turn thus linking the two motor programs, reversal and turn. Additionally, I will reveal how tyramine shapes the dynamics of neuronal activity by simultaneous calcium imaging of the neurons of the escape circuit in freely behaving animals executing the escape response in wild type or tyramine deficient mutants.

In Chapter II, I will show that FLP-18 is co-expressed with tyramine in the RIM and is released upon activation of the escape response indicating a role as a co-transmitter. Using behavioral analysis of FLP-18 signaling mutants and transgenic overexpression I will demonstrate that FLP-18 acts through the G-protein coupled receptor (GPCR) NPR-5 primarily in the muscle to enhance reversals, body bending and locomotion rate during the escape response. Using calcium imaging I will show that FLP-18 acts to enhance calcium levels in body wall muscle in an NPR-5 dependent manner to facilitate escape behavior. FLP-18 acts as a divergent, synergistic co-transmitter to tyramine in omega turning, but as a convergent, antagonistic co-transmitter in the modulation of head movements. These results highlight the importance of studying co-transmission in intact behaving animals and reveal new mechanisms of peptidergic motor control.

The escape response is a form of “fight-or-flight” response and is mediated in part by the invertebrate analog of adrenaline, tyramine. In Chapter III, I use repeated activation of the *C. elegans* flight response as a model for chronic acute stress and discover novel mechanisms for monoamine modulation of cellular stress resistance. Repeated activation of the flight response shortens an animal’s lifespan, and transient activation of the flight response reduces resistance to environmental oxidative or heat stress. Through analysis of tyramine defective tdc-1 mutants, application of exogenous tyramine, and direct optogenetic activation of the tyramine releasing RIM neurons, I will show that tyramine is both necessary and sufficient to reduce resistance to environmental stressors. Through calcium imaging I discover that the activity of the RIM, as well as tyramine release, is differentially regulated by acute versus environmental stressors, becoming active during the flight response but suppressed when exposed to oxidation, fasting, or heat. Through analysis of tyramine receptor mutants and rescue experiments I reveal that the GPCR TYRA-3 is required in the intestine to mediate the effect of tyramine on stress resistance.

Lastly, I examine the downstream mechanisms mediating the negative effect of tyramine on resistance. When exposed to environmental stressors the transcription factor FOXO/ DAF-16 translocates to the nucleus and activates a transcriptional cascade to regulate cellular protective pathways. Activation of the insulin receptor DAF-2 leads to DAF-16 phosphorylation and precludes nuclear translocation. I will show that activation of the escape response or exposure to

exogenous tyramine leads to the activation of DAF-2 and prevents DAF-16 from entering the nucleus. The nuclear exclusion of DAF-16 requires peptide release from the intestine as this effect is blocked in hid-1 mutants. Together this suggests that tyramine is released from the RIM during the flight response and activates TYRA-3 in the intestine. TYRA-3 activation leads to activation of DAF-2, likely through the release of insulin like peptides, which results in the phosphorylation of DAF-16 preventing nuclear translocation and reducing resistance to chronic stressors.

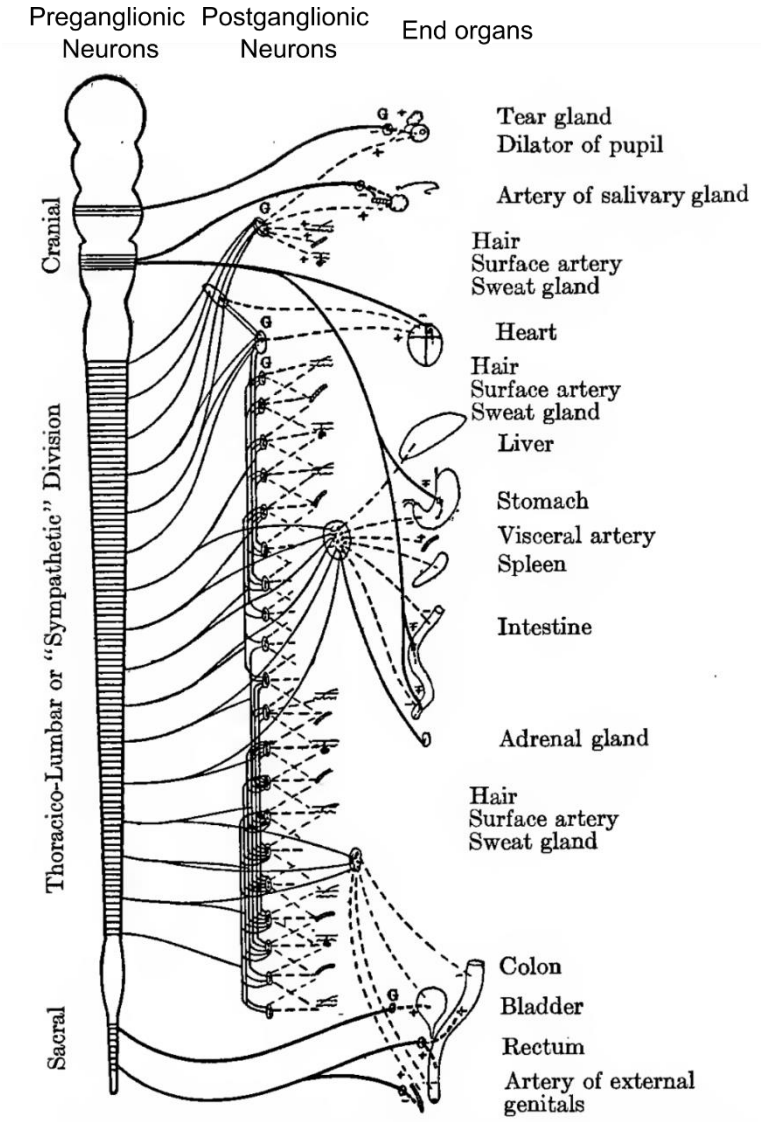

Figure I-1. Organization of the autonomic nervous system in humans.

Activation of the sympathetic nervous system affects nearly every tissue in the body. Cholinergic preganglionic neurons from the thoracic and lumbar divisions (solid lines) project to postganglionic neurons in the sympathetic chain denoted with “G”. Sympathetic postganglionic neurons project to end organs where they release noradrenaline and co-transmitters such as neuropeptide Y and ATP.

Preganglionic projections to the adrenal gland also release adrenaline and noradrenaline hormonally. Parasympathetic neurons from the cranial and sacral divisions oppose the action of sympathetic neurons on end organs. (Adapted from Cannon, 1915)

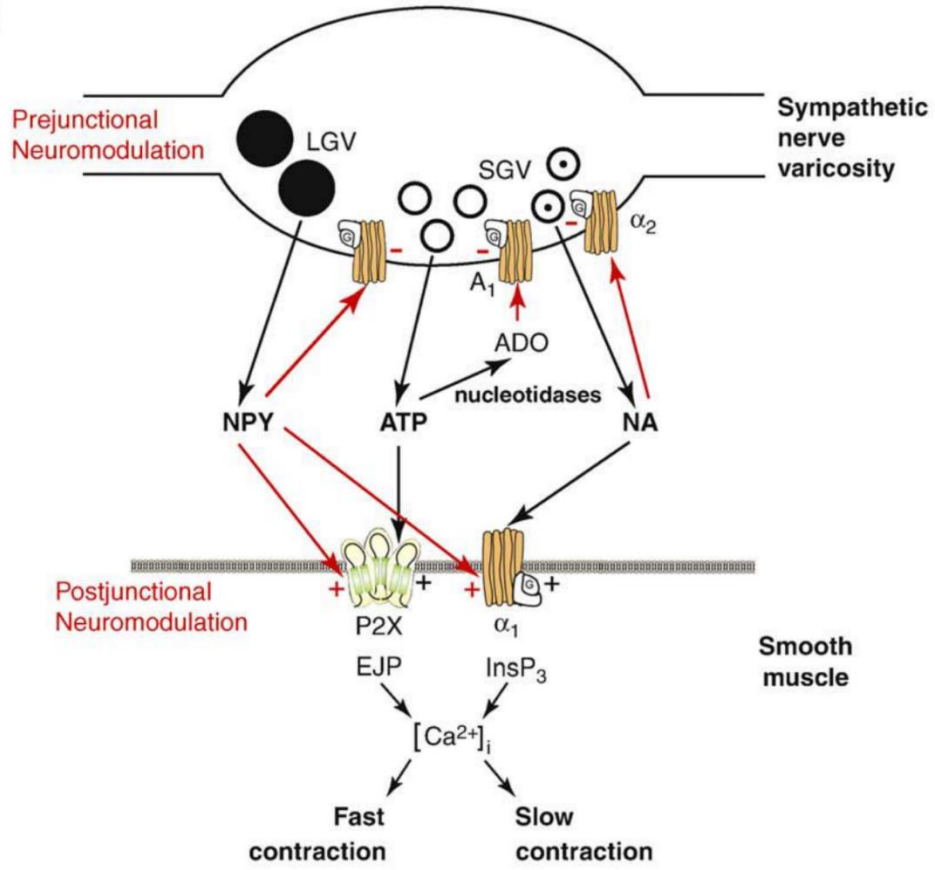

Figure I-2. Sympathetic co-transmission at vascular smooth muscle.

Sympathetic neurons signal using multiple transmitters to modulate the contractility of vascular smooth muscle. Noradrenaline (NA), adenosine triphosphate (ATP) and neuropeptide Y (NPY) are stored in distinct pools of vesicles in sympathetic neurons. ATP mediates fast contraction by activation of purinergic P2X cation channels. NA mediates slow contraction through $G\alpha_q$ coupled α_1 adrenergic receptors which cause release of calcium from intracellular stores. NPY potentiates the effects of NA and ATP enhancing muscle contraction through Y_1 receptors. ATP, NA and NPY all suppress their own release through

presynaptic inhibition by activating A_1, α_2 and Y_2 receptors, respectively. LGV, large granular vesicle; SGV, small granular vesicle; EJP, excitatory junctional potential; $InsP_3$, inositol triphosphate; ADO, adenosine (reproduced with permission from Burnstock and Verkhratsky, 2010).

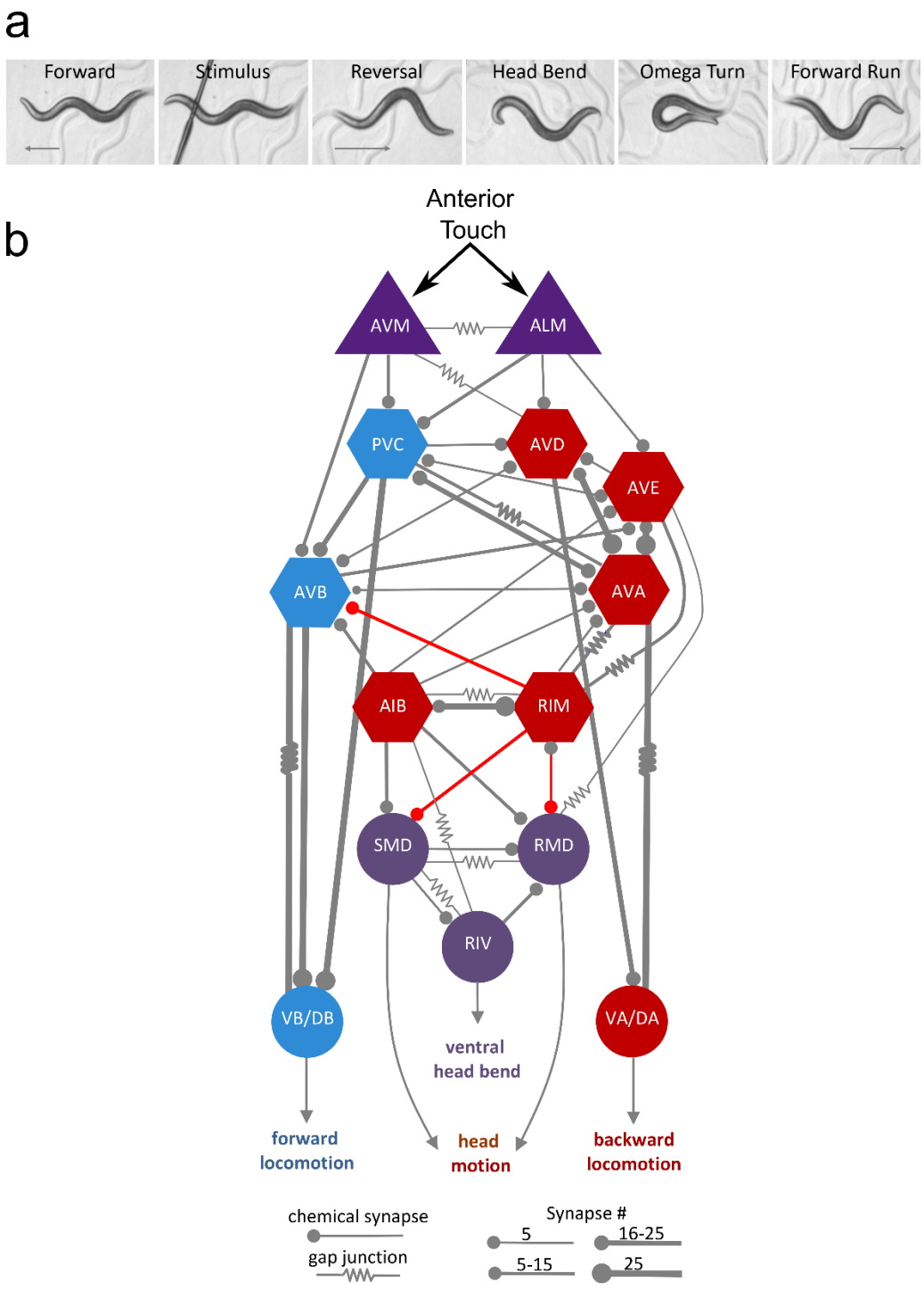

Figure I-3. The *C. elegans* escape response and neural circuit. a) Sequence of the motor programs in the escape response to gentle touch. Stimulus is

anterior touch with an eyelash. arrows indicate direction of travel. b) Schematic of the neural circuit mediating the escape response. Sensory neurons are depicted as triangles, interneurons as hexagons and motor neurons as circles. Chemical synapses are denoted as lines ending in circles, electrical synapses as lines with resistor symbol. Thickness of lines indicates the number of synaptic connections between neurons. Neurons colored in blue are part of the forward locomotion motor circuit, those in red are part of the backward locomotion motor circuit and neurons in purple are involved in controlling head movements. Inhibitory tyraminergic synapses are colored in red. See text for details on function of specific neurons.

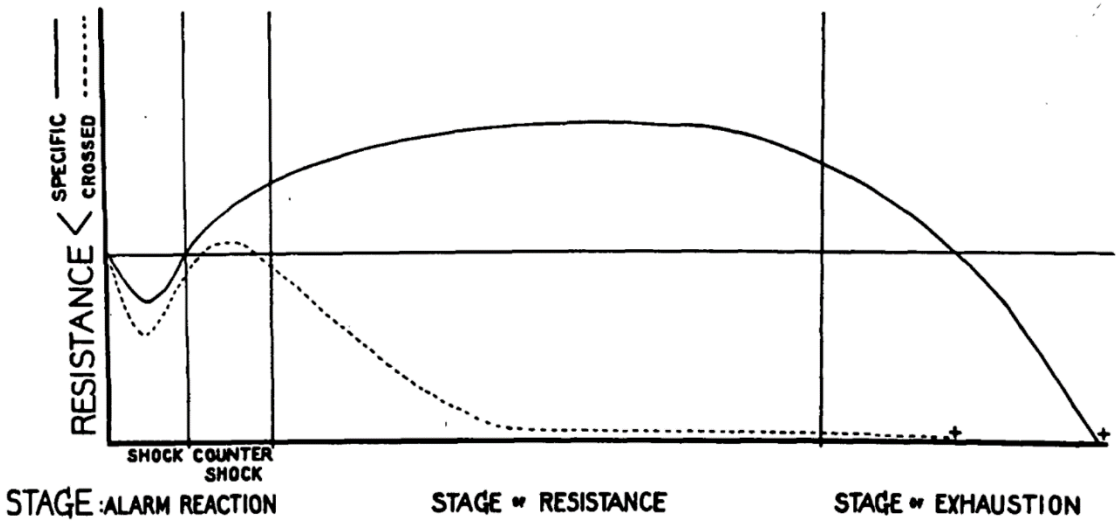

Figure I-4. Schematic representing stress resistance during the general adaptation syndrome. During initial exposure to trauma or a noxious agent, resistance to that specific stressor (sold line) or different stressor ("crossed resistance" dotted line) is reduced in what was known as the state of shock. Following shock, a state of "counter shock" is entered where the body's response to the stressor (activation of the sympathetic nervous system (SNS) and hypothalamic-pituitary-adrenal (HPA) axis) results in an increase in both specific and crossed resistance to subsequent stress. This bi-phasic shock-countershock response is referred to as the Alarm Reaction. Following the Alarm Reaction is the Stage of Resistance, where the output of SNS and HPA activity maintains high resistance to further exposure to stressors. If SNS and HPA activity are not downregulated a final Stage of Exhaustion where resistance is depleted and death will occur. The + symbol indicates death. (Reproduced with permission from Selye, 1946).

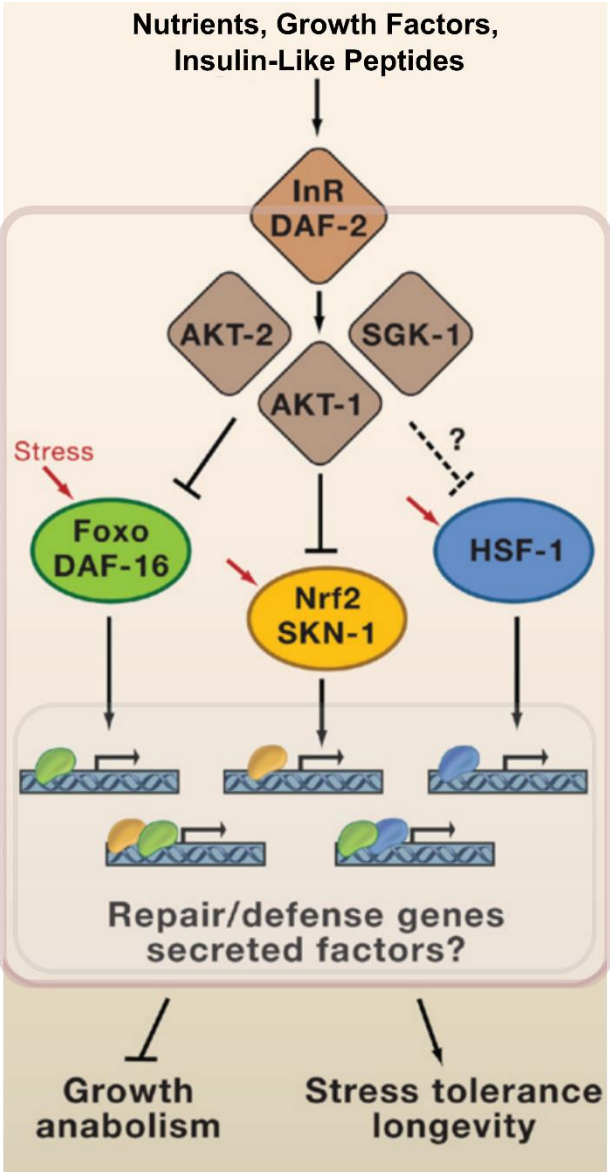

Figure I-5. Repression of stress response pathways by insulin receptor homolog DAF-2. The insulin receptor (InR) DAF-2 responds to various nutritional and endocrine cues through the activation of kinases including AKT-1/2 and SGK-1. Phosphorylation of transcription factors DAF-16/FOXO, SKN-1/Nrf2 and HSF-1 precludes their nuclear translocation and prevents the

activation of cytoprotective stress resistance transcriptional activity while allowing transcription of anabolism and growth-related transcriptional activity. In the absence of DAF-2/InR activity, stress induces nuclear translocation of DAF-16/FOXO, SKN-1/Nrf2 and HSF-1 where transcription of antioxidant, heat shock factors and protein chaperone genes protects cells from damage (Adapted with permission from Jasper, 2008).

PREFACE TO CHAPTER II

The work presented in chapter II examines the role of monoamine-neuropeptide co-transmission in the coordination of complex behavior. In response to touch *C. elegans* exhibits a characteristic escape response consisting of several linked motor programs. The monoamine neurotransmitter tyramine is released from the RIM interneurons and functions to coordinate distinct aspects of escape behavior. In this study we show that the RFamide neuropeptide FLP-18 is also released from the RIM during the escape response and functions both synergistically and antagonistically to tyramine in the coordination of different aspects of escape behavior. We find that FLP-18 exerts its effects through activation of the G-protein coupled receptor NPR-5 in neck and body wall muscle. NPR-5 activation leads to increased muscle calcium levels which facilitates forward acceleration as well as bending and turning behavior during the escape response. Jeremy Florman generated strains, performed the experiments, developed Matlab scripts and analyzed the data. Mark Alkema and Jeremy Florman designed the experiments and co-wrote the manuscript. This work was prepared for publication at the time of this writing.

CHAPTER II: CO-TRANSMISSION OF NEUROPEPTIDES AND MONOAMINES CHOREOGRAPH THE *C. ELEGANS* ESCAPE RESPONSE.

Jeremy Florman[1] and Mark J. Alkema[1*]

1. Department of Neurobiology, University of Massachusetts Medical School, Worcester, MA, 01605

*Correspondence to: mark.alkema@umassmed.edu

Abstract

Co-expression and co-transmission of neurotransmitters and neuropeptides is a core property of neural signaling across species. While co-transmission can increase the flexibility of cellular communication, understanding the functional impact on neural dynamics and behavior remains a major challenge. Here we examine the role of neuropeptide/monoamine co-transmission in the orchestration of the *C. elegans* escape response. The tyraminergic RIM neurons, which coordinate distinct motor programs of the escape response, co-expresses the neuropeptide encoding gene *flp-18*. We find that in response to a mechanical stimulus, *flp-18* mutants have defects in locomotory arousal and head bending that facilitates the omega turn. We show that the induction of the escape response leads to the release of FLP-18. FLP-18 modulates distinct motor programs of the escape response through the activation the G-protein coupled receptor NPR-5. FLP-18 increases intracellular calcium levels in neck and body wall muscles to promote body bending and locomotion rate. Our result show that FLP-18 and tyramine act in different tissues in both a complementary and antagonistic manner to control distinct motor programs during different phases of the *C. elegans* flight response. Our study reveals basic principles by which co-transmission of monoamines and neuropeptides orchestrate in arousal and behavior in response to stress.

Introduction

Animals encounter a variety of challenges in their environment that require specific behavioral responses to survive. An attack, or even the perception of a predator elicits a rapid “fight-or-flight” response to enhance the animal’s chance of survival. In vertebrates, the acute fight-or-flight response leads to the activation of the sympathetic nervous system (SNS) and the release of “stress hormones”, such as adrenaline and noradrenaline (Cannon, 1915). Adrenergic and noradrenergic neurons in the SNS trigger an increase in heart rate, blood flow, respiration and release of glucose from energy stores, which prepare the animal for vigorous muscle activity and physical exertion (Li and Sawchenko, 1998; Horn and Swanson, 2013). Neuropeptide Y (NPY), one of the most abundant neuropeptides in the mammalian nervous system, is a co-transmitter with noradrenaline (NA) in many neurons of the SNS (Lundberg *et al.*, 1983, 1989; Everitt *et al.*, 1984). Co-transmitted signaling molecules can activate receptors on a common target (convergence) or different targets (divergence) and induce complementary or antagonistic effects, making the functional outcome of co-transmission challenging to anticipate. The sympathetic co-transmission of NA and NPY suggest that they may coordinate aspects of the flight response, however, the physiological and behavioral impact of co-transmission can be difficult to dissect in mammalian systems. For instance, studies in mammals have shown that the stress related modulatory functions of NPY and NA co-transmission are complex, with complementary actions in some

tissues and antagonistic actions in others. For example, both NA and NPY increase blood pressure through peripheral vasoconstriction, however NPY inhibits presynaptic NA release from sympathetic neurons and opposes the action of NA on cardiac contraction (Lundberg *et al.*, 1982; Wahlestedt *et al.*, 1985, 1990; Zukowska-Grojec, Marks and Haass, 1987; Balasubramaniam *et al.*, 1988; Zukowska-Grojec and Vaz, 1988; Westfall *et al.*, 1988; Toth *et al.*, 1993; McDermott *et al.*, 1997; Allen *et al.*, 2006; Oki, Teraoka and Kitazawa, 2017). Co-transmission of NPY and catecholamines may induce a longer lasting state of arousal that enhances alertness and the ability to deal with environmental threats. Unraveling the precise effects of co-transmission of neural stress hormones is challenging in vertebrates given the complexity of the nervous system, the multiple central and peripheral release sites and the diversity of tissues expressing NA and NPY receptor (NPYR) subtypes.

The nematode *Caenorhabditis elegans* provides an excellent system to study the co-transmission of aminergic and peptidergic neuromodulators due to its compact and completely defined nervous system and wealth of genetic tools (Brenner, 1974; White *et al.*, 1986). The *C. elegans* genome encodes a large family of NPY related peptides and G-protein coupled receptors (GPCRs) (Li *et al.*, 1999; Li and Kim, 2014). Like other invertebrates, *C. elegans* lacks NA, however the structurally related tyramine fulfills a similar role to NA in coordinating stress responses and flight behavior (Alkema *et al.*, 2005; Bauknecht and Jékely, 2017; De Rosa *et al.*, 2019).

In response to a mechanical stimulus *C. elegans* can engage in a flight- or an escape-response, where the worm quickly reverses and turns in the opposite direction to move away from the noxious stimulus. Tyramine plays a crucial role in the coordination of independent motor programs, which increases the animal's chances to escape predation (Alkema *et al.*, 2005; Pirri *et al.*, 2009; Maguire *et al.*, 2011; Donnelly *et al.*, 2013; De Rosa *et al.*, 2019). The escape response triggers the release of tyramine from a single pair of neurons called the RIM. The RIM neurons co-express a NPY like peptide, FLP-18 (Rogers *et al.*, 2003; Kim and Li, 2004). The RFamide FLP-18 and its associated receptors are related to the NPY/NPYR signaling system (Elphick and Mirabeau, 2014). I*n vitro* experiments have shown that FLP-18 can activate a human NPYR and weak activation of NPR-5 is produced by human NPY (Gershkovich *et al.*, 2019). In *C. elegans* FLP-18 has been shown to play a role in foraging and metabolism (Cohen *et al.*, 2009), arousal and homeostasis (Stawicki *et al.*, 2013; Sanders *et al.*, 2014; Choi *et al.*, 2015), chemosensation (Luo *et al.*, 2014), reversal behavior (Bhardwaj *et al.*, 2018; Bhardwaj, Pandey and Babu, 2020), and swimming rates in *C. elegans* (Kim and Li, 2004; Chang *et al.*, 2015). FLP-18 acts through several neuropeptide receptors including NPR-1, NPR-4, and NPR-5 (Rogers *et al.*, 2003; Kubiak *et al.*, 2008; Cohen *et al.*, 2009).

Here we investigate the role of tyramine and FLP-18 co-transmission in the coordination of the *C. elegans* escape response. We find that FLP-18 plays a central role in coordinating distinct phases of the escape response in *C. elegans.*

FLP-18 is released from the tyraminergic RIM and the AVA interneurons in response to mechanical stimuli. FLP-18 activates the GPCR NPR-5 in body wall muscle to enhance reversals, turning behavior and locomotion speed during the escape response by increasing muscle excitability. Our result show that FLP-18 and tyramine act in different tissues in both a complementary and antagonistic manner to orchestrate distinct motor programs during different phases of the *C. elegans* flight response.

Results

Mechanical stimulation transiently increases forward velocity

Handling of *C. elegans*, such as the transfer with a platinum wire, bumping the plate on microscope stage or removing the lid of a plate can induce a temporary increase in locomotion rate (Swierczek *et al.*, 2011; Chew *et al.*, 2018). This indicates that mechanical stimulation can lead to longer lasting changes to the internal state of the animal. To quantify locomotion patterns upon mechanical stimulation we compared the locomotion rate of animals subjected to a tap to the side of the plate. Mechanical tap can trigger an escape response, in which *C. elegans* reverses, turns and resumes forward locomotion in the opposite direction (Chalfie and Sulston, 1981; Wicks and Rankin, 1995). We compared locomotion rates of animals before, during and after spontaneous reversals and tap induced reversals. In animals that initiated a spontaneous

reversal, forward locomotion rate remained the same before and after the reversal (Figure II-1, a). Furthermore, the absolute velocity during spontaneous reversals was similar to the velocity of forward movement.

When an escape response was triggered with a tap stimulus, reversal velocity was distinctly higher than during spontaneous reversals. Forward locomotion rate following the reversal was slightly increased after a weak tap (Figure II-1, b). In response to a strong tap, animals initiated a rapid reversal; double the speed of spontaneous reversals. Furthermore, following a strong tap induced reversal, animals exhibited a markedly elevated forward locomotion rate for approximately 3 minutes (Figure II-2) - a behavior we termed the 'forward run' (Figure II-1, c). The sustained increase in forward velocity in response to a strong tap indicated longer lasting changes in the internal state of the animal.

flp-18 affects locomotion

Neuropeptides are potent neuromodulators, whose action can lead to longer lasting changes in behavior. We focused our attention on FLP-18 neuropeptide since it is the only RFamide known to be expressed in the tyraminergic RIM and in the AVA (Rogers *et al.*, 2003; Kim and Li, 2004), pre-motor interneurons that play a central role in the escape response to mechanical touch (Alkema *et al.*, 2005; Pirri *et al.*, 2009; De Rosa *et al.*, 2019). *flp-18* null mutants are healthy (Figure II-3 a.) and had no obvious defects in locomotion velocity, body curvature, speed of foraging head movements, or spontaneous

reversal frequency (Figures II-1, a, II-3, c-f). *flp-18* mutants propagated regular body bends as they moved across the agar surface (Figure II-3, g).

flp-18 mutants initiated reversals in response to weak and strong tap stimuli similar to wild-type (Figure II-1, f), indicating that *flp-18* is not required for mechanosensation or initiation of the escape response. In response to a weak or strong tap, *flp-18* mutants reversal velocity was slightly reduced compared to wild-type animals (Figure II-1, b-d). In response to a strong tap, *flp-18* mutants had significantly slower forward run velocity than the wild-type (Figure II-1, c & e). This indicates that FLP-18 signaling is required for the shift to sustained rapid movement during the forward run of the escape response.

flp-18 mutants have defects in head and body bending during the escape response.

We further analyzed *flp-18* mutants for defects in other aspects of the escape response. During the initial phase of the escape response elicited by gentle anterior touch animals reverse while suppressing head movements (Figure II-4, b, II-6, a, Video II-3). The reversal is often followed by an omega turn which consists of two linked motor programs: an initial ventral head swing followed by a deep body bend where the animal slides its head along the ventral side of the body to resume locomotion in the opposite direction (Figure II-4, a). In response to gentle anterior touch *flp-18* mutants reversed and suppressed head

movements like the wild type (Figure II-4, b). Following a reversal, *flp-18* mutants, often initiate an omega turn similar to the wild type. However, *flp-18* mutants made a shallower ventral head bends compared to wild-type animals (Figure II-4, c). *flp-18* mutants executed omega turns (> 90 degree turn) less frequently than wild-type animals (37% vs 57% respectively) (Figure II-4, d). Furthermore, when *flp-18* mutants did make high-angled omega turns, the head often fails to contact the ventral side of the body during the turn (open omega turn (Donnelly *et al.*, 2013; Figure II-4, a)) resulting in a much higher proportion of open omega turns compared to wild-type animals (62% vs 22% respectively) (Figure II-4, e). Expression of a low-copy transgenic *flp-18* genomic construct, which includes a 3 kb endogenous promoter [P*flp-18*::FLP-18::SL2::mCherry] (referred to as FLP-18+), rescued the omega turning defects seen in *flp-18* mutants (Figure II-4, d & e).

Flp-18 overexpression enhances bending and omega turning

To further assess the effect of FLP-18 signaling on behavior we overexpressed *flp-18* using a high-copy transgene [P*flp-18*::FLP-18::SL2::mCherry] (referred to as FLP-18+++). *flp-18 o*verexpression caused uncoordinated locomotion (Rogers *et al.*, 2003) with strikingly deep body bends (Figure II-3, a & g). Animals overexpressing *flp-18* also displayed hyperactive foraging head movements, increased body curvature and elevated spontaneous reversal frequency (Figure

II-3, c-f). Overexpression of FLP-18 in a subset of neurons of the escape circuit using the *Pcex-1* promoter [*Pcex-1::*FLP-18::SL2::mCherry] in a *flp-18* mutant background was sufficient to cause exaggerated body bends and reversals, similar to FLP-18 expression under its native promoter (Videos II-1, II-2). The *cex-1* promoter drives expression in the RIM, AVA and the AVD (Starich *et al.*, 2009), but not in the AIY, RIG or motor neurons that also express endogenous FLP-18 (Rogers *et al.*, 2003; Figure II-5, a & b). This suggests that FLP-18 release from the escape circuit neurons AVA and RIM is sufficient to enhance body bending and reversals.

FLP-18 overexpression had an opposite effect on the escape response compared to *flp-18* deficiency. In contrast to *flp-18* mutants, which have reduced ventral head bend angle, FLP-18 overexpressing animals made high angled head bends (Figure II-4, c). Furthermore, overexpression of FLP-18 resulted in increased omega turn frequency and a reduced proportion of open omega turns compared to wild-type or *flp-18* mutant animals (Figure II-4, d-e). Moreover, in response to a mechanical stimulus FLP-18 overexpressing animals failed to suppress head movements during reversals (Figures II-4, b, II-6, b, Video II-4). This phenotype is similar to tyramine deficient *tdc-1* mutants and *lgc-55* mutants that lack the tyramine-gated chloride channel LGC-55 (Alkema *et al.*, 2005; Pirri *et al.*, 2009). In wild-type animals suppression of head oscillations during touch induced reversals is mediated by tyraminergic activation of LGC-55 in neck muscles and SMD and RMD head motor-neurons. The suppression of head

oscillations during reversals increases *C. elegans* chances to escape from predatory fungi that use hyphal nooses to entrap nematodes (Maguire *et al.*, 2011). The fact that FLP-18 overexpression causes a failure to suppress head movements suggests that FLP-18 may oppose the tyraminergic inhibition of neck muscles.

The escape response induces FLP-18 release from the AVA and RIM

flp-18 is expressed in the AVA and RIM neurons (Rogers *et al.*, 2003; Kim and Li, 2004), which are activated during the escape response (Kawano *et al.*, 2011; Shipley *et al.*, 2014; De Rosa *et al.*, 2019). To analyze FLP-18 release we generated transgenic animals with a fluorescently tagged the FLP-18 pro-peptide with the YFP variant Venus (P*flp-18::*FLP-18::Venus). Venus is resistant to quenching in low pH environments and has been used to monitor neuropeptide secretion from dense core vesicles in *C. elegans* (Nagai *et al.*, 2002; Sieburth, Madison and Kaplan, 2007; Hoover *et al.*, 2014). To determine whether FLP-18 is released from the AVA and RIM neurons we measured changes in fluorescent intensity in these neurons after repeated activation of the escape response (Figure II-7, a,c). FLP-18::Venus fluorescence was observed in the RIM and AVA escape circuit neurons, as well as the AIY and RIG (Figure II-7, b). In contrast to a *Pflp-18*::GFP transcriptional reporter, fluorescence in P*flp-18::*FLP-18::Venus transgenic animals was also detected in coelomocytes, which are endocytic

scavenger cells which internalize material from the pseudocoelomic fluid (Fares and Greenwald, 2001). The observed fluorescence in coelomocytes indicates that the FLP-18::Venus protein was secreted and cleared by these scavenger cells. Confocal imaging revealed that repeated mechanical tap to the plate caused a progressive reduction in fluorescent intensity in the AVA and RIM compared to animals that did not receive the tap stimuli (Figure II-7, d-e). This suggests that activation of the escape response results in the release of FLP-18 from the AVA and RIM. The fluorescent intensity in coelomocytes did not change as a result of tap treatment (Figure II-7, f). This could be due to protein break down in the coelomocytes and/or the high basal levels of coelomocyte fluorescence due to FLP-18 release from other neurons (e.g. the AIY and RIG) and regulation of foraging and metabolism (Cohen *et al.*, 2009).

FLP-18's modulation of the escape response depends on npr-5.

How does FLP-18 affect locomotion and the escape response? FLP-18 peptides have been shown to activate the G-protein coupled receptors (GPCRs) NPR-1, NPR-4 and NPR-5 *in vitro* (Rogers *et al.*, 2003; Kubiak *et al.*, 2008; Cohen *et al.*, 2009). We analyzed *npr-1, npr-4* and *npr-5* loss-of-function mutants for defects in the escape response. *npr-1, npr-4* and *npr-5* mutants displayed largely normal locomotion and initiated an escape response upon anterior touch. While loss of *npr-1* had no impact on the frequency of omega turns and loss of *npr-4* slightly decreased omega turns, however, *npr-5* mutants executed significantly fewer

omega turns compared to the wild-type (Figure II-4, f). The decrease in omega turning of *npr-5* mutants was comparable to those in *flp-18* mutants. Furthermore, like *flp-18* mutants, *npr-5* mutants also display a higher proportion of open omega turns (Figure II-4, g). This suggests that FLP-18 released during the escape response enhances head and body bending to promote turning through activation of the GPCR NPR-5.

Next, we examined whether neuropeptide receptor mutants could suppress the hyper bending phenotype of the FLP-18 overexpression strain. Loss of *npr-5*, but not *npr-1* or *npr-4* suppressed the increased body curvature (Figure II-8, a-b) and hyper bending during the omega turn (Figure II-8, d) caused by FLP-18 overexpression. While the fraction of *npr-5*; FLP-18(+++) animals that make an omega turns in response to touch is similar to wild type, the proportion of open omega turns made by *npr-5*; FLP-18(+++) animals is significantly increased and similar to *npr-5* single mutants (Figures II-8, e, II-4, g).

npr-1; FLP-18(+++) and *npr-4;* FLP-18(+++) were indistinguishable from FLP-18(+++) in their failure to suppress head oscillations in response to touch. In contrast, *npr-5;* FLP-18(+++) animals suppressed head movements in response to anterior touch like wild-type animals (Figure II-8, c). Loss of both *npr-1* and *npr-5* reduced the high spontaneous reversal frequency caused by FLP-18 overexpression (Figure II-8, f). *npr-1* single mutants displayed significantly fewer spontaneous reversals compared to wild-type animals (Figure II-9, a), likely due to the fact that *npr-1* mutants avoid high ambient oxygen concentrations (Busch

et al., 2012). Under low oxygen conditions loss of *npr-1* failed to suppress the increased reversal frequency caused by FLP-18 overexpression while *npr-5*; FLP-18(+++) animals were indistinguishable from wild-type (Figure II-9, b). This suggests that the effect of *npr-1* on reversal frequency reflects its role in oxygen sensation and may act in parallel with *npr-5*. Taken together these data indicate that FLP-18 modulates locomotion behavior and the escape response primarily through the activation of the NPR-5 receptor.

NPR-5 acts in body wall muscle to drive body bending

To determine NPR-5 expression and subcellular localization we generated transgenic animals that express a GFP tagged NPR-5 translational fusion [P*npr-5::*NPR-5::GFP]. NPR-5::GFP is expressed in body wall muscle and several neurons (Figure II-10, a), consistent with previously described transcriptional reporters for *npr-5* (Cohen *et al.*, 2009). NPR-5::GFP expression was particularly strong in head and neck muscles. NPR-5::GFP localizes to dense bodies within muscle cells, and is highly enriched in muscle arms and the muscle plate around the nerve ring (Figure II-10, a). Animals overexpressing NPR-5 driven by the endogenous promoter (*Pnpr-5::*NPR-5) promoter did not cause elevated curvature during basal locomotion (Figure II-10, b). However, in response to a mechanical stimulus, *Pnpr-5::*NPR-5 animals displayed increased body curvature comparable to FLP-18(+++) animals (Figure II-10, c). This suggests that the effect of NPR-5 overexpression under control of the endogenous promoter is

uncovered when FLP-18 is released during the escape response. Cell specific overexpression of NPR-5 in body wall muscles (*Pmyo-3::*NPR-5), on the other hand, did increase body curvature during both basal and tap induced locomotion, similar to FLP-18 overexpressors (Figure II-10, b-c). The discrepancy in basal curvature between the *Pnpr-5::*NPR-5 and *Pmyo-3::*NPR-5 transgenic animals may be due to differences in expression level and/or pattern of NPR-5. *Pmyo-3* is expressed strongly in all body wall muscle, while high expression of the endogenous *Pnpr-5* promoter is largely restricted to head and neck muscles. Overexpression of NPR-5 under control of its endogenous promotor increased spontaneous reversal frequency to a level similar FLP-18 overexpression, whereas muscle specific expression did not increase reversals (Figure II-10, d). These results suggest that FLP-18 acts through NPR-5 in muscle to enhance body bending and through NPR-5 in neurons to increase reversal frequency.

FLP-18 increases calcium levels in body wall muscle.

How does FLP-18 stimulate body bending? Muscle contractions are triggered by the rapid entry of calcium into the muscle cytosol (Maryon, Saari and Anderson, 1998; Jospin *et al.*, 2002). To determine if FLP-18 signaling affects calcium levels in body wall muscle we generated a strain expressing the fluorescent calcium indicator GCaMP6s in body wall muscles [P*myo-3::*GCaMP6] (Figure II-11, a). *C. elegans* locomotion is driven by alternating waves of contraction and relaxation in dorsal and ventral musculature. As animals moved,

the highest GCaMP fluorescence was observed when muscles were contracted and faded upon relaxation, consistent with calcium influx driving muscle contraction. *flp-18* mutants showed a reduction in GCaMP fluorescence in the muscle compared to a wild-type background (Figure II-11, a,b). In sharp contrast, overexpression of FLP-18 resulted in a striking increase of GCaMP fluorescence in body-wall muscles (Figure II-11, a,b). This indicates that FLP-18 increases calcium transients in muscles that facilitate body bending.

Loss of *npr-5* resulted in a similar decrease in GCaMP fluorescence in body wall muscles similar to *flp-18* mutants. Furthermore, *npr-5* mutations completely suppressed the increase in GCaMP fluorescence of FLP-18 overexpression (Figure II-11, a,b). *In vitro* experiments indicate that the GPCR NPR-5 signals primarily through the $G_{\alpha}q$ pathway (Kubiak *et al.*, 2008). Activation of $G_{\alpha}q$ coupled receptors can cause the release of calcium from intracellular stores (Streb *et al.*, 1983; Garcia, Mehta and Sternberg, 2001). EGL-30 encodes the *C. elegans* $G_{\alpha}q$ ortholog (Brundage *et al.*, 1996). To determine whether NPR-5 signaling is $G_{\alpha}q$ dependent *in vivo* we examined the effect of mutations in *egl-30* on muscle calcium levels. Loss of *egl-30* substantially decreased GCaMP fluorescence in muscle. In *egl-30;* FLP-18(+++) double mutants muscle GCaMP fluorescence was strongly reduced and indistinguishable from *egl-30* single mutants (Figure II-11, a,b). These results are consistent with the idea that FLP-18 activates NPR-5 and EGL-30/$G_{\alpha}q$ signaling cascades, resulting in increased calcium levels in the muscle (Figure II-11, c).

Discussion

In this study we identify FMRFamide-like peptides encoded by the *flp-18* gene as key modulators of the distinct phases in the *C. elegans* escape response. We showed that FLP-18 neuropeptides are released from the RIM and AVA neurons during an escape response elicited by a mechanical stimulus. FLP-18 promotes head and body bending during the omega turn and increases forward run velocity following the turn. We find that the effects of FLP-18 on locomotion are largely mediated through activation of the $G_{\alpha}q$ coupled NPR-5 receptor in head and body wall muscles. Studies in both vertebrates and *C. elegans* have shown that EGL-30/$G_{\alpha}q$ activates phospholipase Cβ (PLCβ) (Miller, Emerson and Rand, 1999; Bastiani *et al.*, 2003) . EGL-8/PLCβ increases IP_3 levels which can lead to the release of Ca^{2+} from internal stores (Gollasch *et al.*, 1991; Xu and Chisholm, 2011). We find that FLP-18 activation of NPR-5 increases calcium levels in muscles *in vivo* in an EGL-30/$G_{\alpha}q$ dependent manner. Our findings are consistent with *in vitro* studies that show that NPR-5 activation by FLP-18 peptides resulted in rises in intracellular Ca^{2+} levels (Kubiak *et al.*, 2008). Our data support a model in which FLP-18 release during the flight response stimulates Ca^{2+} release in head and body wall muscle through the NPR-5 - EGL-30/$G_{\alpha}q$ signaling pathway (Figure II-11, c). Increases in calcium levels would stimulate muscle tension, required for head and body bending the during the omega turn and may increase forward velocity following the turn. Previous

studies have indicated that FLP-18 acts in part through NPR-5 in body wall muscles to decrease the convulsion phenotype of nicotinic acetylcholine receptor *acr-2(gf)* mutants. Our data raise the possibility that FLP-18 dependent increase in intracellular Ca^{2+} concentrations may reduce the Ca^{2+} gradient across the muscle membrane and thus provides a homeostatic response in muscles to the elevated neuronal activity of cholinergic motor-neurons in *acr-2(gf)* mutants. Recent reports have shown FLP-18 acts through the NPR-4 and NPR-5 in the AVA and sensory neurons to control of reversal lengths (Bhardwaj *et al.*, 2018; Bhardwaj, Pandey and Babu, 2020). Our observation that NPR-5 overexpression under control of the endogenous promoter (neurons and muscle) increases, while overexpression just in muscle did not affect reversal frequency, supports this hypothesis.

Together, our results show that FLP-18 signaling functions to enhance motor output during the escape response and locomotory arousal through activation of NPR-5 in muscle. FLP-18 thus may contribute a locomotory arousal state that enhances vigilance and the ability to escape from predation. Other studies have shown that FLP-18 activation of NPR-1, dampens the activity of sensory neurons to promote the sleep like quiescent period associated with larval molts (Choi *et al.*, 2013, 2015; Sanders *et al.*, 2014; Chen *et al.*, 2016). Interestingly, release of the peptide FLP-20 from mechanosensory neurons functions to enhance arousal and motor output across multiple sensory modalities through activation of NPYR like receptor FRPR-3 in the

neurosecretory RID neurons (Chew *et al.*, 2018). Together these findings highlight the multilevel nature of RFamide neuropeptides in the modulation of arousal in *C. elegans.*

We have previously shown that tyramine release from the RIM neurons during the escape response coordinates independent motor programs of the escape response (Alkema *et al.*, 2005; Pirri *et al.*, 2009; Donnelly *et al.*, 2013; De Rosa *et al.*, 2019). Our findings indicate that activation of the flight response results in the co-transmission of tyramine and FLP-18 from the RIM. The RIM neurons contain dense core vesicles (Witvliet *et al.*, 2020) which can store both neuropeptides and monoamines (Hokfelt, Elfvin and Elde, 1977; Liu *et al.*, 1994). However, it is currently unclear whether tyramine and FLP-18 are co-released from the same vesicle. Nonetheless, both tyramine and FLP-18 together choreograph the execution of the escape response. There are intriguing similarities in mammals where neuropeptide Y (NPY) is co-released with noradrenaline (NA) in response to stress (Lundberg *et al.*, 1982, 1983, 1985; Everitt *et al.*, 1984; Zukowska-Grojec, Konarska and McCarty, 1988; Zukowska-Grojec and Vaz, 1988). In mammals, co-transmission of NA and NPY has both complementary and antagonistic actions. For example, both NA and NPY produce a pressor response through contraction in vascular smooth muscle (Wahlestedt *et al.*, 1985, 1990; Zukowska-Grojec and Vaz, 1988), while NPY and NA have opposing inotropic and chronotropic effects on cardiac muscle

(Zukowska-Grojec, Marks and Haass, 1987; Michael Piper, Cherie Millar and McDermott, 1989; Allen *et al.*, 2006; Oki, Teraoka and Kitazawa, 2017). Similarly to the co-transmission of NPY and NA in the mammalian sympathetic nervous system, the co-transmission of FLP-18 and tyramine from the RIM are convergent in some aspects of the escape response but divergent in others. For example, FLP-18 and tyramine both act to facilitate deep bending during the omega turn but do so through distinct mechanisms in different tissues. Tyramine inhibits the GABAergic VD motor-neurons through activation of the $G_{\alpha}o$ coupled receptor SER-2 (Donnelly *et al.*, 2013). The inhibition of GABA release onto ventral body wall muscle facilitates the deep ventral contraction during the omega turn. FLP-18 on the other hand activates NPR-5 in the neck and body wall muscles resulting in increased calcium levels and enhanced head and body bending. Thus, co-transmission of FLP-18 and tyramine exert excitatory and inhibitory effects in different tissues resulting in functional synergism that enhances omega bending (Figure II-11. c).

In contrast to the complementary function of tyramine and FLP-18 on body bending, we observe convergent but antagonistic effects of these neuromodulators on exploratory head oscillations. During the reversal phase of the escape response, wild-type *C. elegans* suppress head oscillations to increase its chances to escape encounters with hyphal nooses of predatory fungi (Maguire *et al.*, 2011). The RIM synapses directly onto neck muscle and tyramine release mediates the suppression of head oscillations through the activation of a

tyramine-gated chloride channel, LGC-55, in neck muscle and in cholinergic motor-neurons that synapse onto neck muscles (Pirri *et al.*, 2009). Animals that overexpress FLP-18 fail to suppress head oscillations during reversals (Figure II-4, b II-6, b; Video II-2), but this defect is rescued by loss of *npr-5* (Figure II-8, c). The simplest explanation is that in FLP-18 overexpressing animals, the tyramine induced hyperpolarization of neck muscles is no longer sufficient to overcome the excess of FLP-18 induced depolarization. In the behavioral sequence of the escape response, head oscillations are reinitiated during the forward run that follows the omega turn. The tyraminergic activation of a fast-acting ionotropic LGC-55 receptor and FLP-18 activation of the slow-acting metabotropic NPR-5 receptor may contribute to temporal dynamics in the suppression and re-initiation of head oscillations.

The similarities between NA/NPY signaling pathways in vertebrates and nematodes indicate that co-transmission monoamines and neuropeptides is a central feature of the signaling pathways that underlie arousal in response to stress. In the presence of danger, heightened arousal can prepare an animal to respond more effectively to a threat and increase the chance of survival. The stereotyped *C. elegans* escape response provides opportunities to unravel the basic mechanisms of neuropeptide/and monoamine co-transmission. Future work could exploit this system to further understand the principles that regulate

network signaling principles by which monoamines and neuropeptides orchestrate in arousal and physiology in response to stress.

Acknowledgments Some strains were provided by the CGC, which is funded by NIH Office of Research Infrastructure Programs (P40 OD010440). We thank Mario de Bono and Rex Kerr.

Author contributions JF performed the experiments and analyzed the data. JF and MJA conceived the study and wrote the paper.

Materials and Methods

Strains used in this study: N2: Wild Type, CX4148: *npr-1*(ky13), QW940: *npr-4*(tm1782), QW953: *npr-5*(ok1583), QW1379 *flp-18*(gk3063), QW1223: *flp-18(tm2179)*; zfex528[Pcex-1::FLP-18::SL2::mCherry], QW1526: *lin-15(n765ts)*, zfex713[Pnpr-5::NPR-5 unc-122::RFP +PL15EK], QW1646: *lin-15(n765ts)*; zfex813[Pmyo-3::NLSwCherry::SL2::GCaMP6 +PL15EK], QW1655: zfis149[Pflp-18(3kb)::mCherry::SL2::FLP-18 +PL15EK], QW1675: *npr-4(tm1782)*; zfis149[Pflp-18(3kb)::mCherry::SL2::FLP-18 +PL15EK], QW1677: zfex813[Pmyo-3::NLSwCherry::SL2::GCaMP6]; zfis149[Pflp-18(3kb)::mCherry::SL2::FLP-18 +PL15EK], QW1680: *flp-18(gk3063)*; zfex821[pflp-18::FLP-18, unc-122::gfp], QW1714: *lin-15(n765ts)*, zfex837[pflp-18::FLP-18::Venus +PL15EK], QW1754:

lin-15(n765ts); zfex845[Pmyo-3::NPR-5::SL2::mCherry +PL15EK], QW1770: *lin-15(n765ts)*; zfex852[Pnpr-5::NPR-5::GFP +PL15EK], QW1784: *npr-5(ok1583)*; zfex813[Pmyo-3::NLSwCherry::SL2::GCaMP6]; zfis149[Pflp-18(3kb)::mCherry::SL2::FLP-18 +PL15EK], QW1802: *flp-18(gk3063)*; zfex813[Pmyo-3::NLSwCherry::SL2::GCaMP6], QW1818: *npr-5(ok1583)*; zfis149[Pflp-18(3kb)::mCherry::SL2::FLP-18 +PL15EK], QW1819: *npr-5(ok1583)*; zfex813[pmyo-3::NLSwcherry::SL2::GCamp6], QW1827: *egl-30(ad805)*; zfex813[Pmyo-3::NLSwCherry::SL2::GCaMP6]; zfis149[Pflp-18(3kb)::mCherry::SL2::FLP-18 +PL15EK], QW1855: *egl-30(ad805)*; zfex813[Pmyo-3::NLSwCherry::SL2::GCaMP6], QW2169: *npr-1(ky13)*; zfis149[Pflp-18(3kb)::mCherry::SL2::FLP-18 +PL15EK].

Molecular Biology and Transgenics

Standard molecular biology methods were used. Transgenic strains were made through microinjection of plasmid DNA into lin-15(n765ts). A lin-15 rescuing plasmid (PL15EK) was used as a co-injection marker and transgenics were identified based on rescue of the lin-15 multivulva phenotype. FLP-18 transgenic strains were created by amplifying a 5.8kb sequence of genomic DNA beginning 3.3kb upstream of the open reading frame and containing the flp-18 coding region as well as the 3’ UTR. The extrachromosomal array was stably integrated into the genome using X-ray irradiation and were backcrossed to wild type N2

animals 4 times. NPR-5 transgenics were created by amplifying a 7.7kb sequence of genomic DNA beginning 3kb upstream of the npr-5 open reading frame and including the npr-5 coding sequence and 3' UTR.

Behavioral experiments

All behavioral experiments were carried out using young adult animals which had been staged as L4s the previous day. Behavioral experiments were performed on medium (60mm) thin-lawn NGM plates where a single drop of OP50 (~30µl) was spread across the plate and allowed to grow at room temperature overnight. Thin lawn plates older than 24hrs were discarded. Prior to behavioral experiments, animals were transferred from standard plates to thin lawn plates and allowed to acclimate for at least 5 minutes. All experiments were conducted with 20 worms to a plate unless otherwise stated and were run in parallel with wild type controls across at least 3 days.

Worm Tracking

Quantification of locomotion was performed using one of two different worm tracking systems. For quantification of foraging speed (figure 2, c), the Worm Tracker 2.0 system was used (Eviatar Yemini and Tadas Jucikas, https://www.mrc-lmb.cam.ac.uk/wormtracker) and "absolute foraging speed" was reported. A single animal on a thin lawn plate was tracked for 5 minutes at 30fps

using a USB digital microscope (DinoLite Pro AM413T, Dino-Lite US) on a motorized stage (Zaber TNA08A50 linear actuator and Zaber TSB60-M motorized stage, Zaber Technologies Inc.).

Quantification of velocity, body curvature and reversal frequency was done using the Multi-Worm Tracker (Rex Kerr, https://sourceforge.net/projects/mwt/). When tracking experiments included a tap stimulus, the stimulus was delivered by a tubular push solenoid (Saia-Burgess/Ledex #195205-127) controlled by the Multi-Worm Tracker software. The tap stimulus consisted of a train of taps (3 taps for the “weak tap” stimulus and 20 taps for all other stimuli) with an inter tap interval of 10 milliseconds. Tap stimuli were always delivered after 5 minutes of tracking had elapsed.

Experiments were analyzed using custom Matlab (The MathWorks, Inc.) scripts to interface with the Multi-Worm Tracker feature extraction software Choreography. Analysis was limited to objects that had been tracked for a minimum of 20 seconds and had moved a minimum of 5 body lengths. All experiments were conducted on thin lawn plates with 20 animals on each plate.

Body curvature

For comparisons of basal versus tap stimulated curvature animals were tracked using the Multi-Worm Tracker. The body curvature of the population was averaged over 3 seconds either just prior to the tap stimulus for basal curvature or just after the tap stimulus for stimulated curvature.

Reversal frequency

20 animals were tracked while freely moving on a thin lawn plate with the Multi-Worm Tracker. The total number of reversals made by the population in a 3 minute window was extracted using the Multisensed plugin for Choreography (Rex Kerr) and divided by the average number of worms tracked during that time to get the number of reversals per worm in 3 minutes. For simplicity this value was divided by 3 and plotted as number of reversals per worm per minute.

Touch assays

Experiments quantifying omega turning, suppression of head oscillations and ventral turn head angle were conducted by gently touching an animal just posterior to the pharynx with a fine paint brush bristle taped to a glass pipette as previously described(Chalfie and Sulston, 1981). Animals were transferred to a thin lawn plate and allowed to acclimate for at least 5 minutes. 20 animals were assayed in each experiment and the population average was reported for each behavior. Animals were touched a single time and animals that failed to reverse were ignored.

Suppression of head oscillations

Animals that moved their head from side to side during a reversal were considered to be defective in the suppression of head oscillations.

Omega turns

Omega turns were defined as any turn which results in a reorientation greater than 90° from their initial forward bearing before the reversal. Turns that were greater than 90° where the animal failed to touch its body with its head were considered open omega turns. Percent omega turns for a given experiment was calculated as the number of open plus the number of closed turns divided by the total number of animals that reversed. The percentage of open omegas was calculated as the number of open omega turns divided by the total number of omega turns (open + closed) in that experiment.

Ventral turn angle

To calculate the angle of the head during the initiation of a ventral turn animals were touched with an eyelash while video was being recorded through a dissecting microscope (SZ6TR1 Olympus) with a digital camera (AVT Pike F421-b, Allied Vision Technologies) using Fire-I image acquisition software (Unibrain inc.). Videos of animals that made omega turns were loaded into ImageJ / Fiji (Schindelin *et al.*, 2012) and the first frame of forward movement following the

touch initiated reversal was identified. To calculate the head deflection angle two lines were drawn, one running from the tip of the nose to the beginning of the intestine and the second running from the beginning of the intestine to a point on the midline 1 pharynx length further posterior. The angle between these two lines was measured using the angle tool in Fiji.

Confocal imaging

Animals were immobilized with 60mM sodium azide and placed on a 2% agarose pad under a coverslip. Images were acquired using a Zeiss LSM700 confocal microscope (Carl Zeiss AG)

Venus quantification

A population of animals expressing the *Pflp-18*::FLP-18::Venus transgene were subjected to a plate tap every 2 minutes for up to 2 hours. Individuals were removed at 0, 1 and 2 hours and immediately mounted and anesthetized as described above. Z-stacks were acquired with a confocal microscope (LSM 700, Carl Zeiss Microscopy GmbH) using a 40x objective (C-Apochromat 40x/1.20 W Korr, Carl Zeiss Microscopy GmbH). Images were loaded into ImageJ and the soma of the RIM and AVA were identified from their anatomical location. A

circular region of interest (ROI) with a diameter of 13.5µm was placed around the soma or coelomocyte to measure the mean grey value of each neuron. An additional measurement was taken adjacent to the soma to quantify background fluorescence; this value was subtracted from the gray values of the RIM, AVA and coelomocyte in that animal. The values obtained for each condition were normalized to the average intensity of the relevant neuron or coelomocyte in the control condition.

Calcium Imaging

Young adult animals expressing a *Pmyo-3::*GCaMP6::SL2::mCherry transgene were placed into a drop of M9 buffer on a 2% agarose pad atop a microscope slide and a coverslip was gently placed onto the pad. Animals were able to move freely under the coverslip and were imaged on an inverted fluorescent microscope (Axio Observer A.1, Carl Zeiss Microscopy GmbH) using a Hammamatsu ORCA-Flash4.0 camera within 10 minutes of mounting. Images were analyzed using ImageJ software by drawing a 1075µm x 630µm rectangular ROI which could be rotated or translated to fit the position of an animal and the mean gray value was measured. The same ROI was placed in a position containing no animals to measure the mean grey value of the background which was then subtracted from the grey value of the ROI containing the animal. Wild type animals expressing the *Pmyo-3::*GCaMP6::SL2::mCherry

transgene were imaged in parallel with mutants and the average background-subtracted grey value of the wild type animals for that day was used to normalize the values obtained from imaging the mutants.

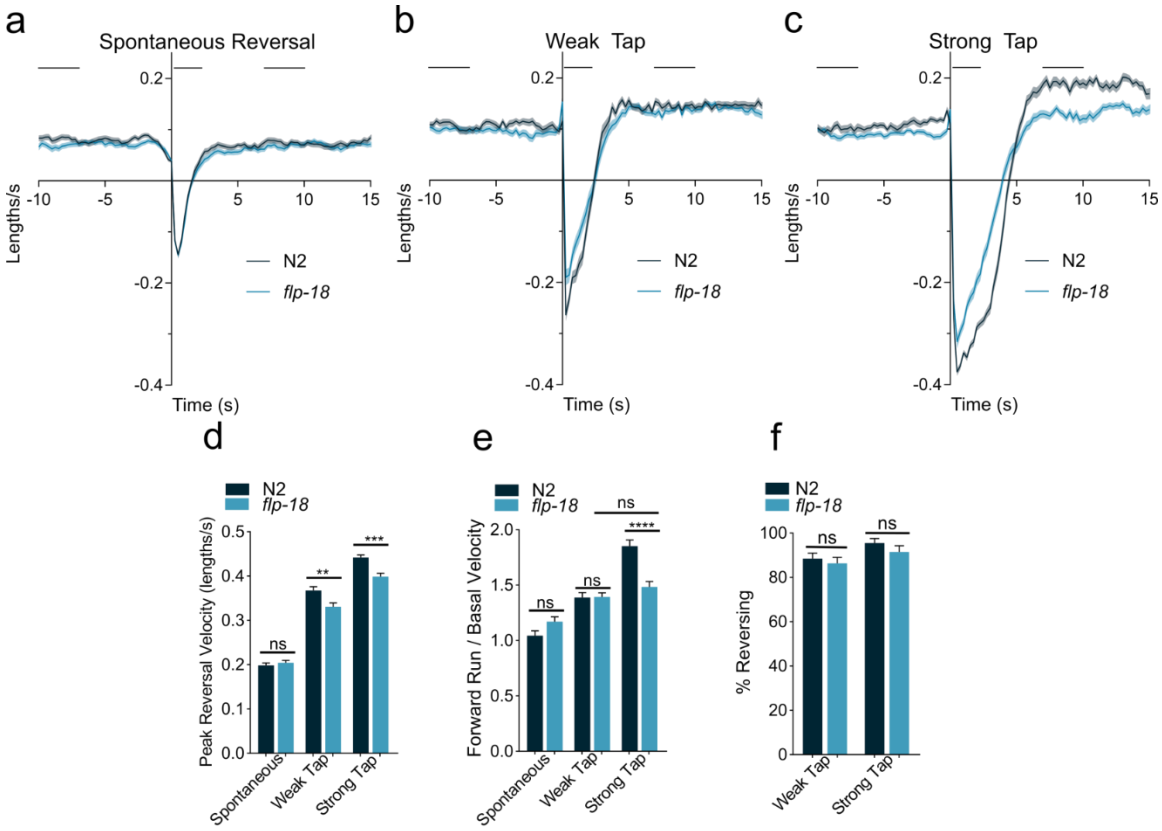

Figure II-1. Increase in locomotion speed following of a mechanical stimulus. Backward- and forward-velocity upon a spontaneous or tap induced reversal. Wild-type animals show a persistent increase in locomotion speed in response to a strong tap stimulus ("forward run"). *flp-18* mutants do not show a robust increase locomotion speed in response to a strong tap stimulus. (a-c) Velocity traces from wild-type and *flp-18* mutants aligned to reversal events, negative velocity indicates backward locomotion. Dark lines represent mean velocity and shaded region represents standard error. Reversals were spontaneous (a), in response to a 3 tap burst (b) or a 20 tap burst (c). (d) Peak backward velocity during the reversal phase (t=0.25-2.25s). (e) Quantification of

the change in velocity during the forward run phase (t=7-10s) relative to the average baseline speed (t=-10- -7s) for each genotype in each condition. Black bars over the traces indicate relevant time windows. (f) Quantification of the percentage of animals initiating a reversal within 1 second after a tap was delivered. Graphs represent mean ± SEM, significance was calculated using ANOVA with Sidak's multiple comparison test (P> 0.05=ns, P<0.005 = **, P<0.0001 = ****). Sample size (a-e): spontaneous reversal N2 and *flp-18* (n=256), weak tap N2 (n=210), *flp-18 (*n=199), strong tap, N2 (n=146) *flp-18* (n=209). Sample size (f) (n=16 experiments per genotype per condition, 20 worms per experiment)

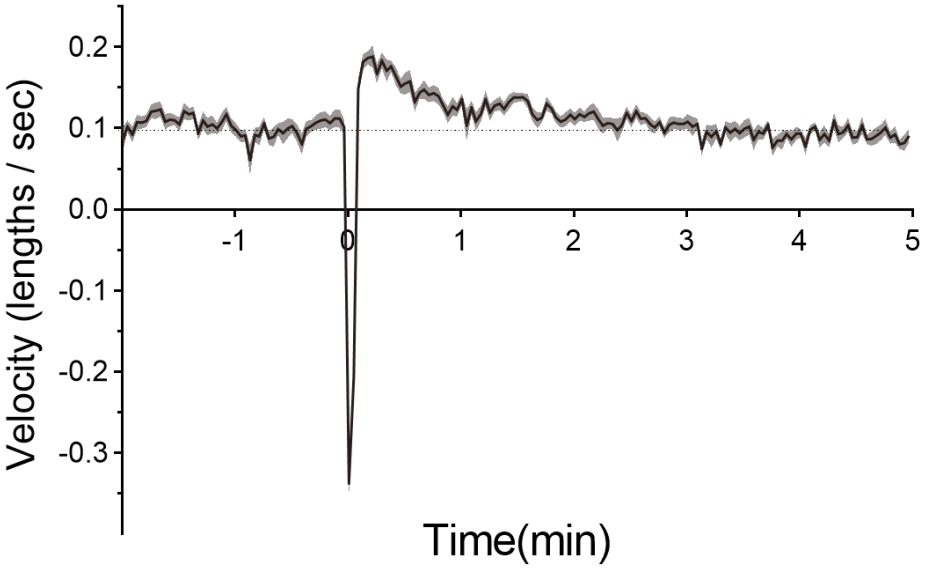

Figure II-2 Elevated forward velocity persists for minutes following tap. Locomotion velocity of wild type animals aligned relative to the time when a mechanical plate tap was delivered to trigger the escape response at t=0 min. negative velocity indicates backward locomotion. Dotted line indicates approximate average speed prior to the plate tap. Solid line in trace represents mean velocity shaded area indicates standard error of the mean. Sample size: n=14 independent trials with 20 worms recorded during each trial and their mean velocity was quantified.

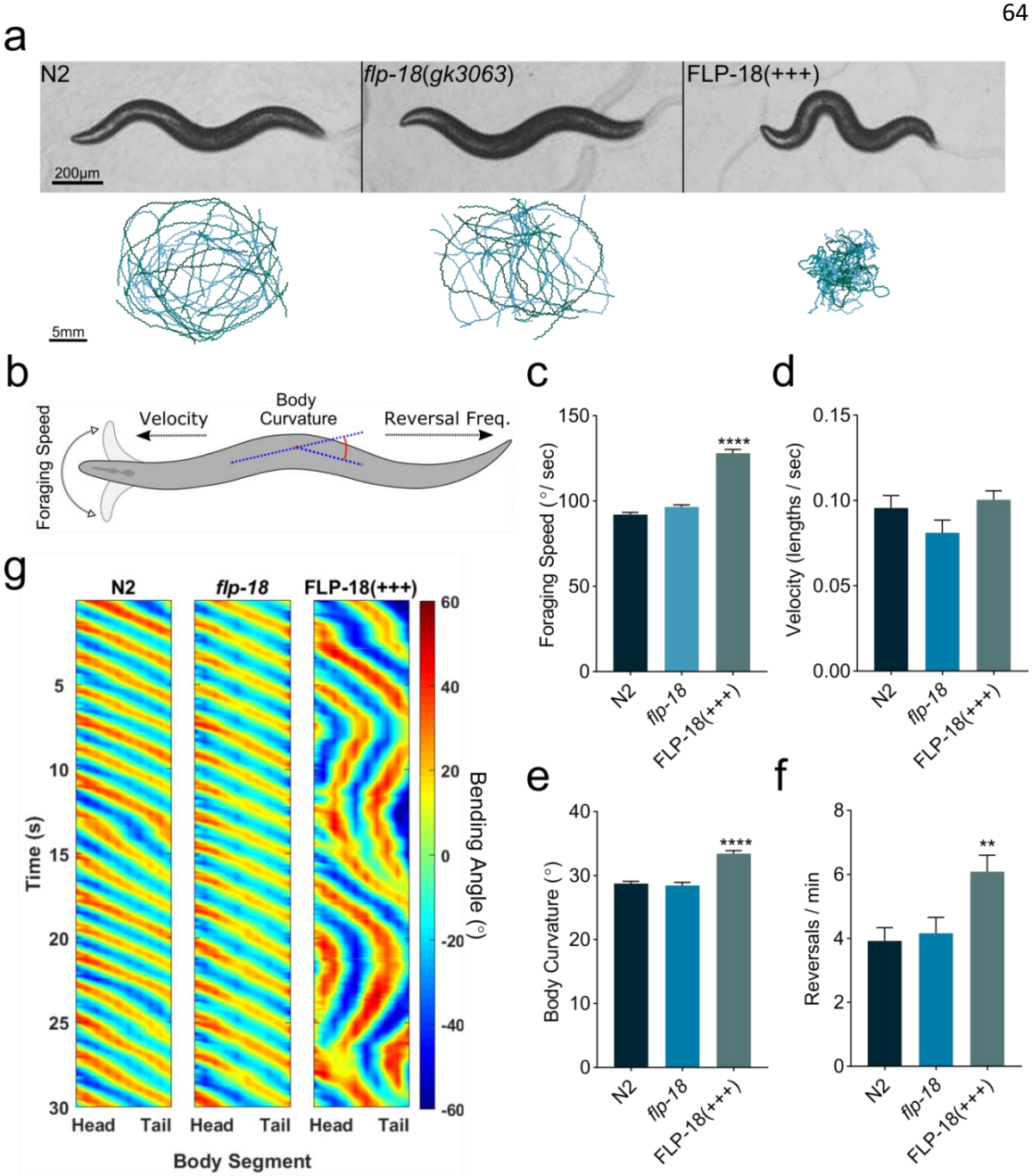

Figure II-3. Overexpression of FLP-18 causes locomotion defects. (A) Behavioral tracking of wild-type, *flp-18(gk3063)* and FLP-18 overexpressors (FLP-18(+++)). Representative images of each genotype (upper panel) and locomotion tracks recorded from multiple animals freely moving on a plate for 5 min (lower

panel). Scale bars represent 200 µm (top) and 5 mm (bottom) respectively. (B) Schematic illustrating quantified behaviors. (C-F) Quantification of basal locomotion behavior by Single-Worm Tracker (c) and Multi-Worm Tracker (d-f). (G) Kymographs showing body bending along the body over 30 s of locomotion. Color map represents degrees of bending, positive values represent dorsal bends and negative values represent ventral bends. Graphs represent mean ± SEM, significance was calculated using ANOVA with Dunnett's multiple comparison test ($P<0.005$ = **, $P<0.0001$ = ****). Sample sizes: Single Worm Tracking (c), N2 (n=38), *flp-18* (n=28), FLP-18(+++) (n=31). Multi-Worm Tracking (d-f) N2, *flp-18* and FLP-18(+++) (n=16 experiments, 20 animals per experiment)

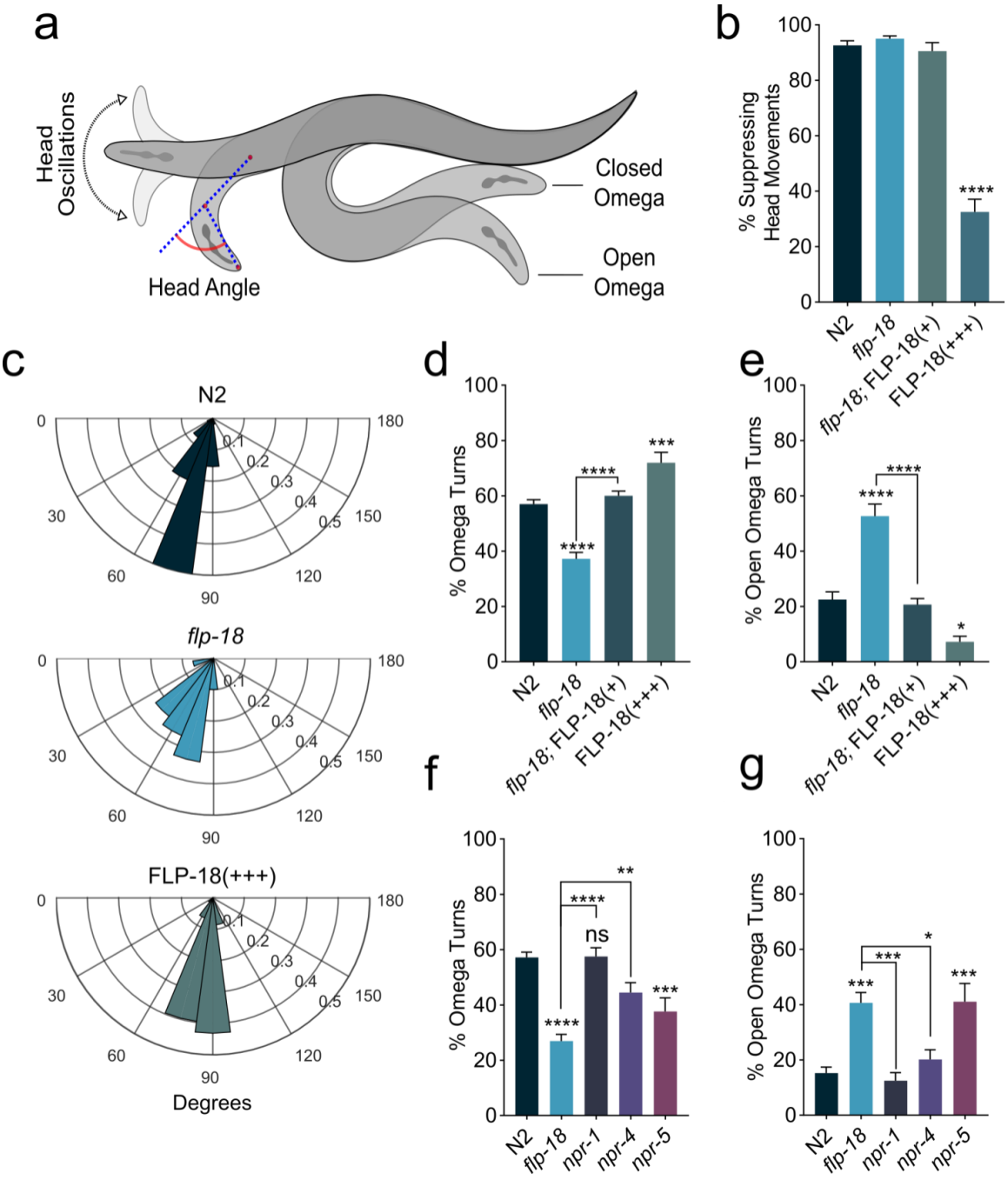

Figure II-4. *flp-18* mutants are defective in head bending and turning during the escape response. (a) Schematic depicting head oscillations, ventral turn head angle and open vs closed omega turns. (b) Quantification of the percentage of

animals suppressing head oscillations upon gentle anterior touch. (c) Angle of ventral head bend following touch induced reversal of animals that make omega turns probability histogram with a bin size of 15°. Each concentric circle represents a probability of 0.1. *flp-18* mutants make a shallower ventral head bend during the initiation of the omega turn (d and f) Percentage of animals that execute omega turns in response to gentle anterior touch. (e and g) Fraction of open omega turns out of total omega turns. When subjected to gentle anterior touch, *flp-18* mutants have defects in omega turning. Mean ± SEM. significance was calculated using ANOVA with Sidak's multiple comparison correction ($P<0.05$ = *, $P<0.005$ = **, $P<0.0001$ = ****). Sample sizes: ventral head bend measurement (c and d), N2 (n=52), *flp-18* (n=30), FLP-18(+++) (n=58). Suppression of head movement and omega quantification (b,d and e) # of experiments, 20 worms per experiment) N2 (n=15), *flp-18* (n=14), *flp-18;* FLP-18(+) (n=7), FLP-18(+++) (n=9). Omega turn quantification (f and g) N2 (n=21), *flp-18* (n=21), *npr-1* (n=12), *npr-4* (n=14), *npr-5* (n=21).

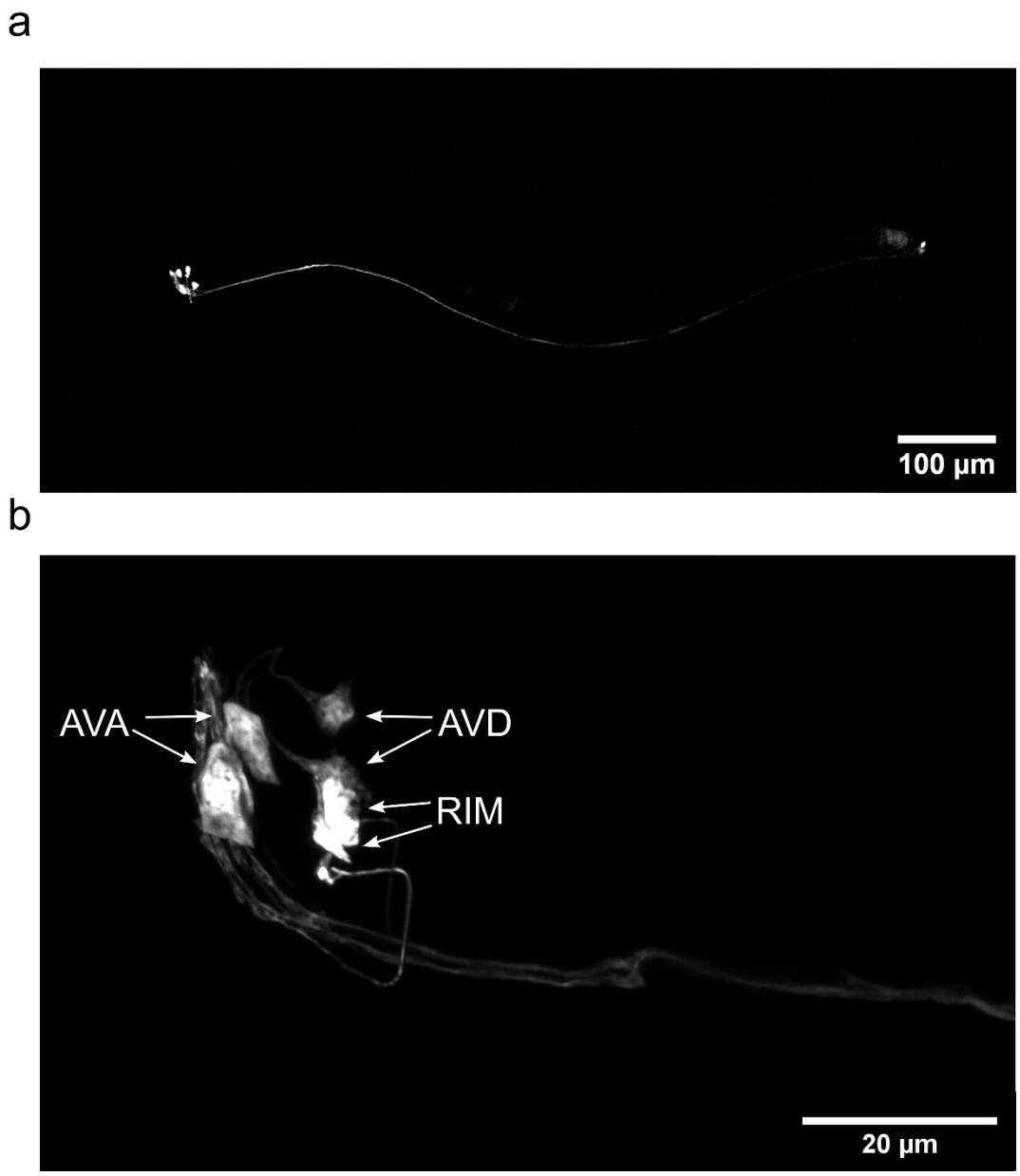

Figure II-5 Expression pattern of *Pcex-1*::FLP-18::SL2::mCherry.

Confocal micrographs of zfex528[*Pcex-1*::FLP-18::SL2::mCherry] (a) 10x objective confocal z-projection showing expression in head neurons, ventral

nerve cord (VNC) and a pair of tail neurons. The ventral cord expression appears to be the process of the AVA rather than motor neurons as no cell bodies were visible in the VNC. (b) 40x objective confocal z-projection showing detail of head neurons. Cell bodies are labeled, neurons were identified based on anatomical position.

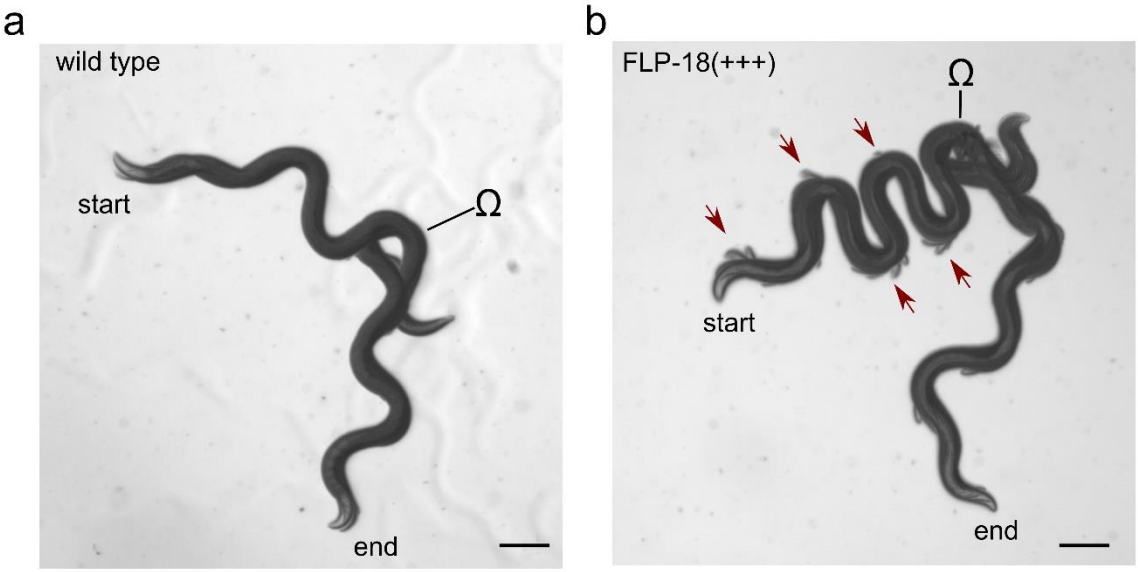

Figure II-6 Animals overexpressing FLP-18 fail to suppress head oscillations in response to touch. Minimum intensity projections from videos recordings of wild type (a) and FLP-18 overexpressing (b) animals after anterior touch. “start” indicates location of head when the animal was touched and initiated a reversal. The omega (Ω) symbol indicates the point where an omega turn was initiated, and the animal switched from reversal to forward motion. “end” indicates the position of the head at the end of the video. The head of the wild type animal remains relaxed and follows the body during the reversal (a). The FLP-18(+++) overexpressing animal continues head oscillations during the reversal which are visible as the tip of the nose projecting out from the sides of the body and are indicated with red arrows (b). Scale bar = 100µm.

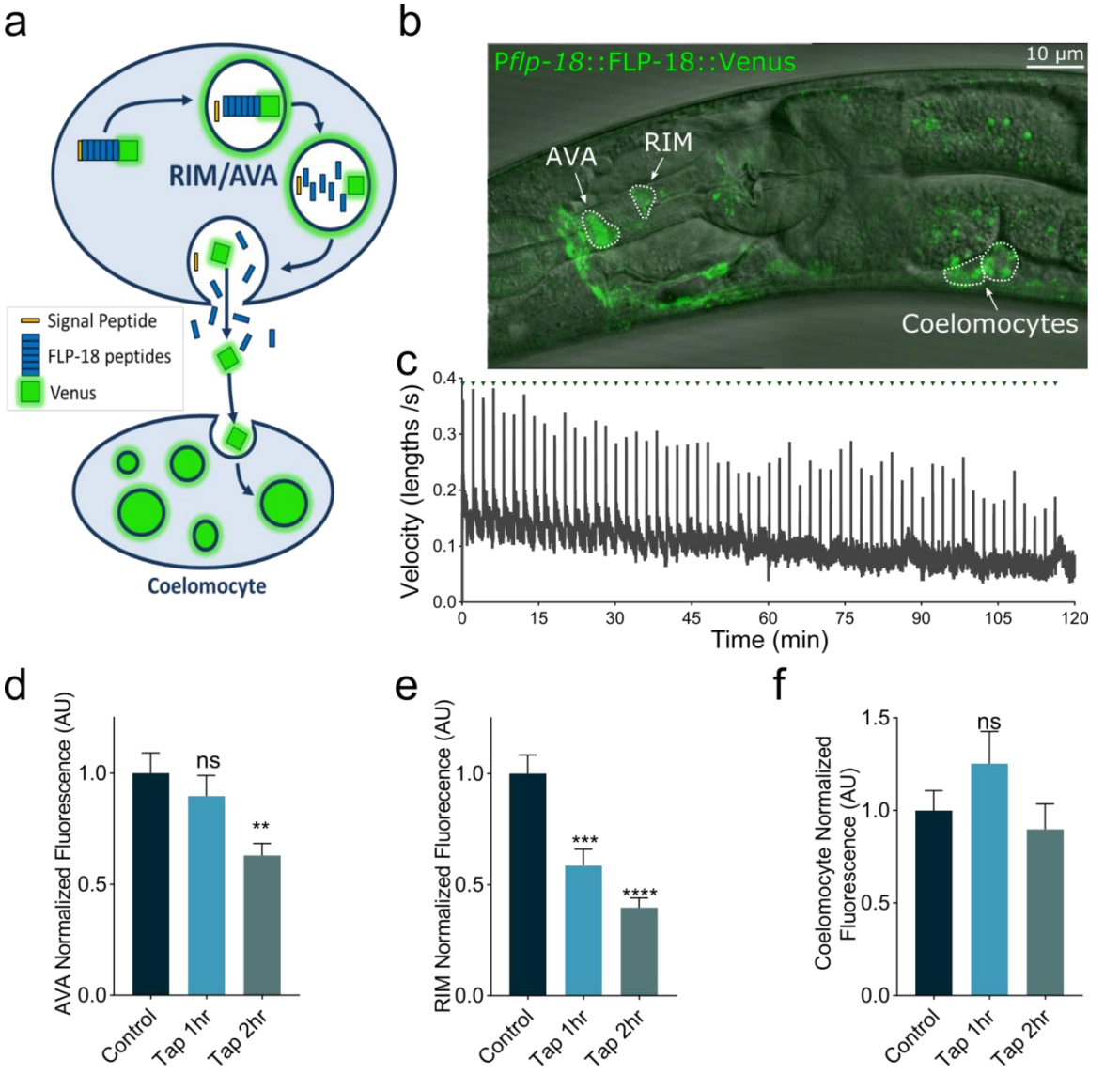

Figure II-7. The escape response triggers FLP-18 release from the AVA and RIM. Animals expressing a FLP-18::Venus fusion protein were subjected to repeated mechanical plate taps. The decrease in fluorescent intensity of the RIM and AVA cell body was quantified as a readout of FLP-18 release. (a) Schematic illustrating the processing and exocytosis of the FLP-18::Venus fusion protein. (b) Representative image showing an animal expressing FLP-18::Venus, DIC and

GFP overlay. Scale bar represents 10 µm. (c) Average velocity of a population of animals as they are subjected to mechanical plate taps. Green arrows indicate the delivery of a tap every 2 min. The spikes in velocity coincide with the initiation of the escape response (d-e) Quantification of fluorescence in the AVA (d) and RIM (e) at 0, 1- and 2-hour time points. RIM fluorescence significantly decreased at 1 hour, and both AVA and RIM florescence was significantly decreased at 2 hours. Graphs represent mean ± SEM, significance was calculated using ANOVA with Dunnett's multiple comparison test ($P>0.05$ = ns, $P<0.005$ = **, $P<0.0005$ = ***, $P<0.0001$ = ****). Sample size: Control (n=32), Tap 1 hr (n=26), Tap 2 hr (n=35).

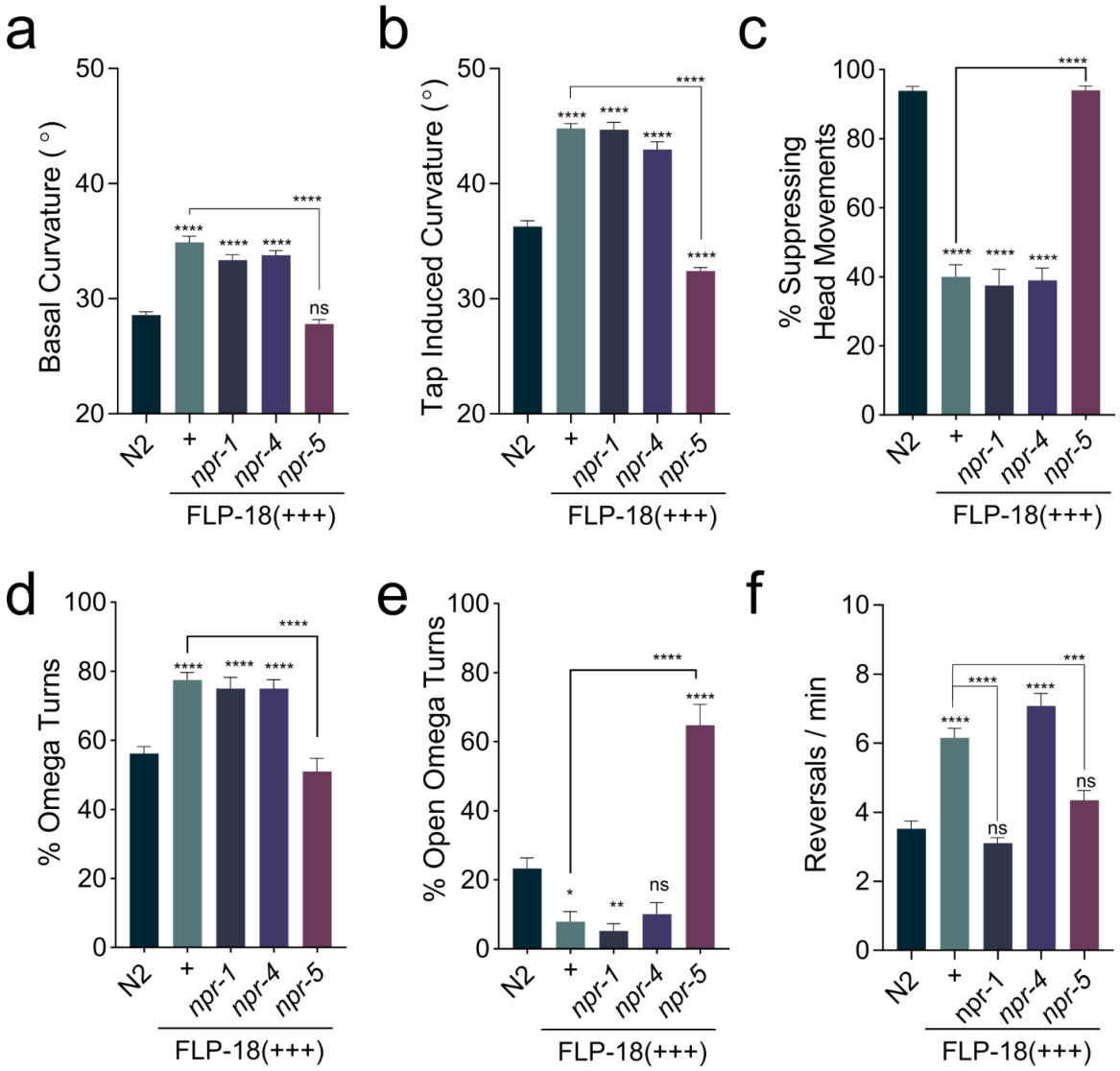

Figure II-8. Loss of *npr-5* suppresses FLP-18 overexpression phenotypes. Overexpression of FLP-18 causes uncoordinated locomotion, frequent reversals and excessive bending, which is suppressed in an *npr-5* mutant background. (a and b) Mean body curvature averaged over 5 seconds prior to a tap stimulus (a) or immediately following a strong tap stimulus (b). (c) Percentage of animals suppressing head movements in response to gentle anterior touch with an eyelash.

(d) Percentage of animals initiating omega turns after gentle anterior touch. (e) Proportion of open omega turns out of total omega turns. (f) Mean number of spontaneous reversals per minute per worm averaged over 3 minutes. Graphs represent mean ± SEM, significance was calculated using ANOVA with Sidak's multiple comparison correction ($P<0.05$ = *, $P<0.005$ = **, $P<0.0005$ = ***, $P<0.0001$ = ****). Sample sizes (# of experiments, 20 animals per experiment): Spontaneous reversals and curvature measurements (a,b and f) N2 (n=46), FLP-18(+++) (n=33), *npr-1;* FLP-18(+++) (n=23), *npr-4;* FLP-18(+++) (n=27), *npr-5;* FLP-18(+++) (n=23). Suppression of head movements and omega turn quantification (c-e) N2 (n=22), FLP-18(+++) (n=10), *npr-1*; FLP-18(+++) (n=12), *npr-4*; FLP-18(+++) (n=10), *npr-5;* FLP-18(+++) (n=10)

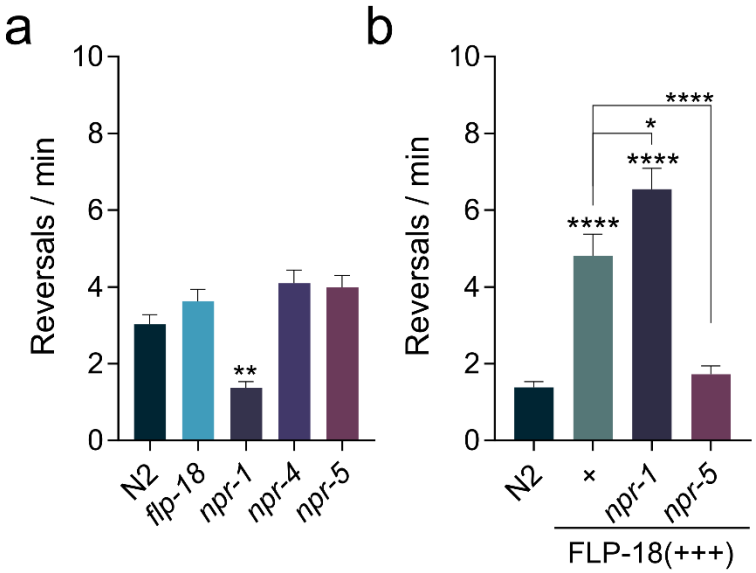

Figure II-9 *npr-5* but not *npr-1* mutation suppresses high spontaneous reversal frequency in low oxygen conditions. Quantification of spontaneous reversal frequency in ambient oxygen (a) or in low oxygen conditions (b). Mean number of spontaneous reversals per minute per worm averaged over 3 minutes. Ambient oxygen experiments (a) were conducted with a standard lid covered plate in room air. Low oxygen experiments (b) were conducted on a plate that had nitrogen gas injected into it with a 5ml syringe prior to placing a lid. Both conditions were allowed to acclimate for 5 minutes prior to recording. Graphs represent mean ± SEM, significance was calculated using ANOVA with Sidak's multiple comparison correction (P<0.05 = *, P<0.005 = **, P<0.0001 = ****). Sample sizes (# of experiments, 20 animals per experiment): (a) N2 (n=26), *flp-18* (n=28), *npr-1* (n=14), *npr-4* (n=23), *npr-5* (n=17). (b) N2 (n=12), FLP-18(+++) (n=12), *npr-1;* FLP-18(+++) (n=15), *npr-5;* FLP-18(+++) (n=13).

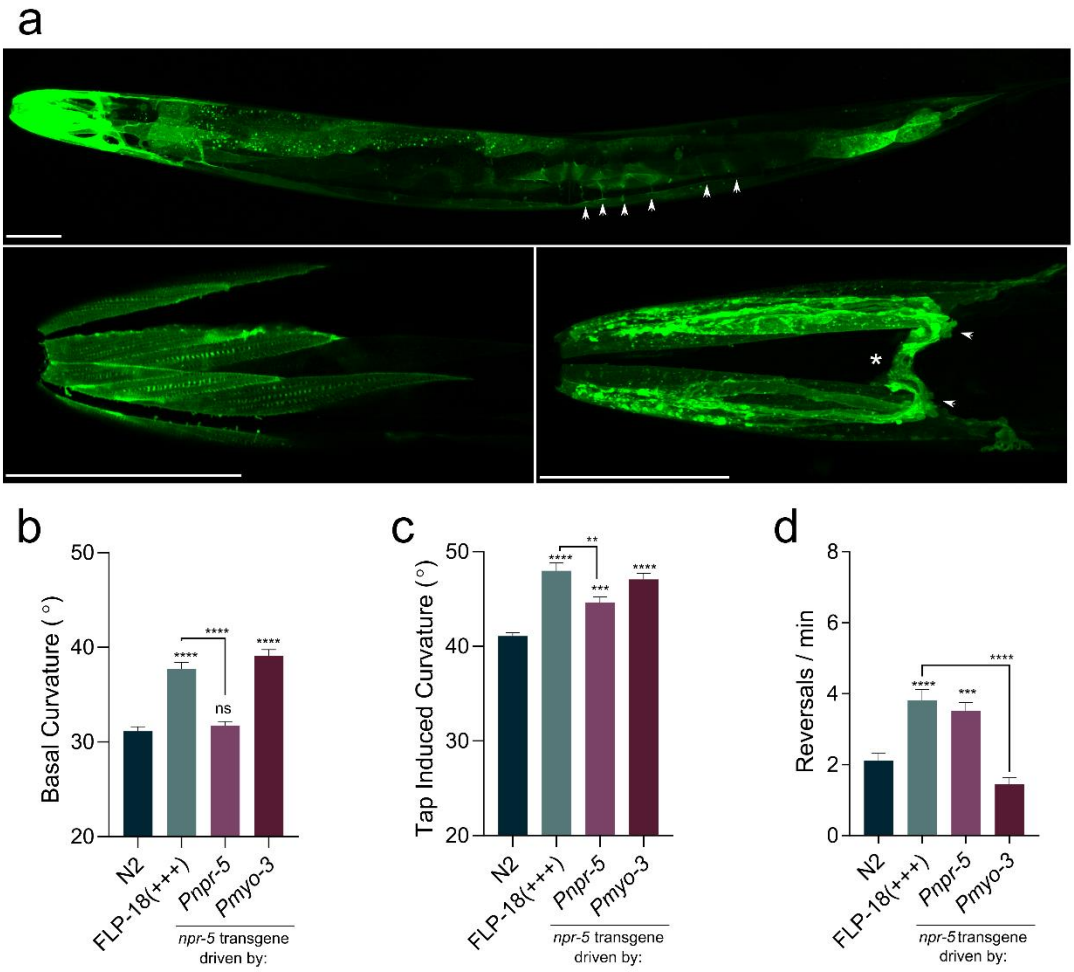

Figure II-10. NPR-5 expression in muscle enhances body bending. (a) Confocal micrographs of animals expressing a translational NPR-5 reporter, *Pnpr-5::*NPR-5::GFP. Upper panel: Z-projection shows strongest expression in head- and neck-muscles and muscle arms. NPR-5::GFP also localized to body-wall and vulval muscle. Body wall muscle arms are visible (arrow heads). Lower left panel: confocal slice showing NPR-5::GFP localization to dense bodies in head muscle. Lower right panel: Confocal projection showing high expression in head- and neck-muscle arms (arrow heads) and in the muscle plate in the nerve ring (asterisk). (b-

d) Quantification of behavior when NPR-5 is overexpressed either from its endogenous promoter or from the muscle specific *Pmyo-3* promotor. Mean body curvature averaged over 5 seconds prior to a tap stimulus (b) or immediately following a strong tap stimulus (c). (d) Quantification of spontaneous reversal frequency. Graphs represent mean ± SEM, significance was calculated using ANOVA with Sidak's multiple comparison correction (P>0.05 = ns, P<0.005 = **, P<0.0005 = ***, P<0.0001 = ****). Sample sizes (# of experiments, 20 animals per experiment): Curvature measurements (b-c) N2 (n=20), FLP-18(+++) (n=13), *Pnpr-5::*NPR-5 (n=12), *Pmyo-3::*NPR-5 (n=14).

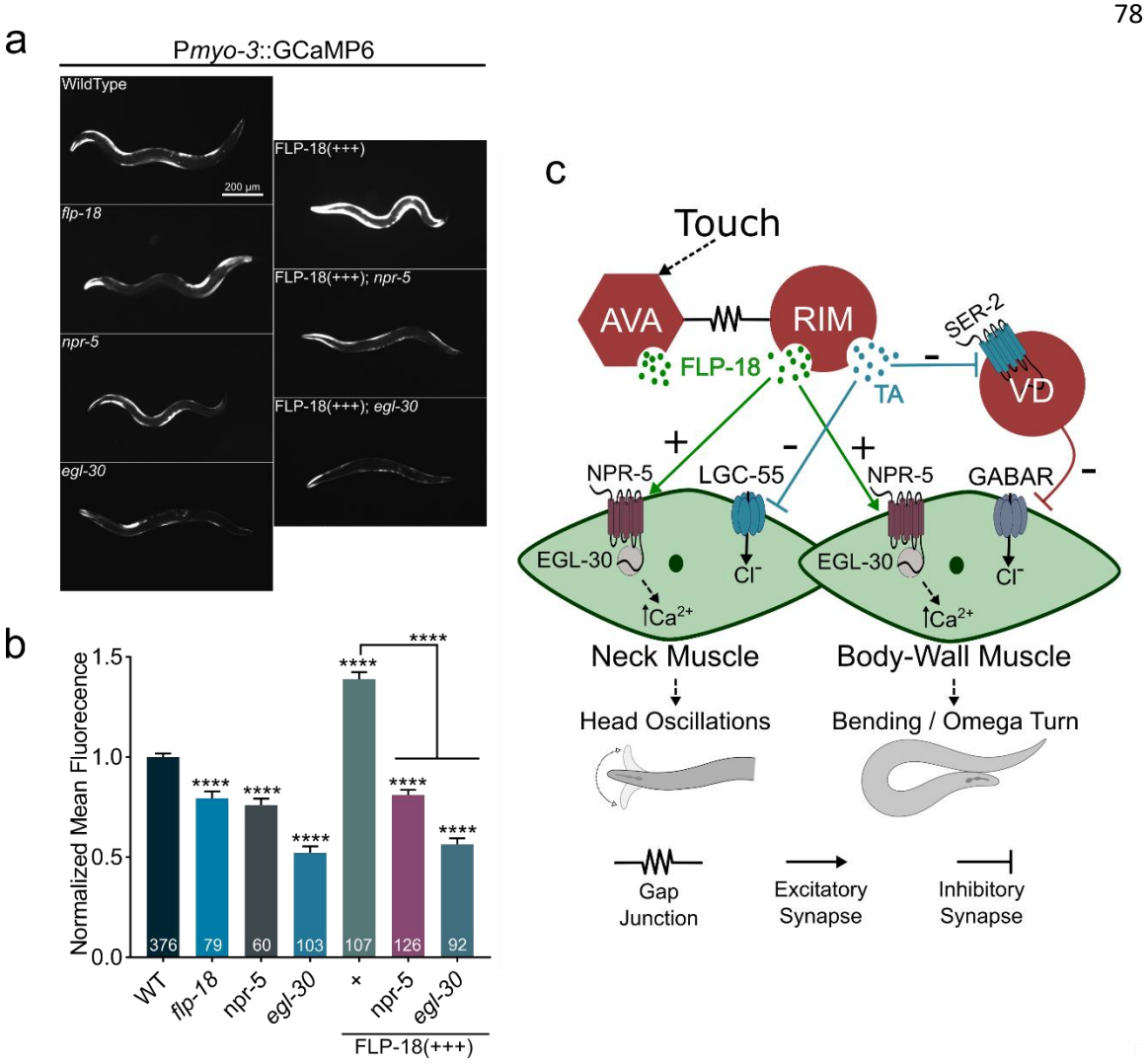

Figure II-11. FLP-18 increases muscle calcium levels and requires NPR-5 and EGL-30/Gαq. (a) Loss of *flp-18* or *npr-5* reduces calcium transients in body wall muscle. FLP-18 overexpression causes a large increase in muscle GCaMP6 fluorescence, which is suppressed by loss of *npr-5* or *egl-30.* Representative images of animals expressing a P*myo-3::*GCaMP6 transgene in different genetic backgrounds. Scale bar represents 200 µm. (b) Quantification of mean GCaMP6 fluorescence in muscle in different genetic backgrounds. Fluorescence is

normalized to same day wild-type controls. Graphs represent mean ± SEM, significance was calculated using ANOVA with Sidak's multiple comparison correction ($P<0.0001$ = ****). Sample size for each genotype is indicated at the base of each bar. (c) Model depicting the role of FLP-18 in modulation of locomotion patterns of the escape response. Touch activates the AVA and RIM neurons resulting in the release of FLP-18 onto body wall muscle where it activates NPR-5. NPR-5 activation causes an increase in muscle calcium levels through activation of EGL-30/Gαq signaling pathways. Increased muscle excitability facilitates head and body bending and omega turning as well as elevated forward run velocity.

PREFACE TO CHAPTER III

The work presented in this chapter addresses the question of how an animal balances physiological responses to different types of stressors and how that balance is regulated by the nervous system. Immediate “acute” stressors like predation require a rapid behavioral fight-or-flight response, however “long-term” environmental stressors such as extreme temperature, oxidation or starvation are best mitigated by conserved cellular protective pathways. The behavioral response to acute stress is regulated by the monoamine tyramine whereas long-term cytoprotective stress responses are regulated by insulin/IGF-1 like signaling (IIS). In this study we find that tyramine is released from the RIM interneurons during the flight response and negatively impacts long-term stress resistance and lifespan in *C. elegans*. This negative interaction is dependent on activation the G-protein coupled receptor TYRA-3 in the intestine which leads to activation of the insulin receptor DAF-2, likely through the release of insulin like peptides from the intestine. DAF-2 activation inhibits stress response transcriptional cascades by preventing nuclear localization of DAF-16/FOXO and other transcription factors. Furthermore, we show that RIM activity and thus tyramine release is differentially regulated by acute versus long term stressors and as a result functions to integrate internal and external information to switch between different stress response pathways.

María José De Rosa, Tania Veuthey, Jeremy Florman, Jeff Grant, María Gabriela Blanco, Natalia Andersen, Diego Rayes and Mark J. Alkema designed

the experiments. Stress resistance and lifespan assays were conducted by María José De Rosa, Tania Veuthey, Jeremy Florman, María Gabriela Blanco, Natalia Andersen, Diego Rayes. Optogenetic experiments were performed by Jeremy Florman. Calcium imaging was done by Jeremy Florman and Jeff Grant. Microscopy and image analysis were conducted by María José De Rosa, Tania Veuthey, María Gabriela Blanco, Natalia Andersen, Diego Rayes. Molecular biology and strain generation were performed by María José De Rosa, Tania Veuthey, Jeremy Florman, Jamie Donnelly. Diego Rayes and Mark J. Alkema conceived the study and wrote the paper. This paper was published in the journal Nature in 2019.

CHAPTER III: THE FLIGHT RESPONSE IMPAIRS CYTOPROTECTIVE MECHANISMS BY ACTIVATING THE INSULIN PATHWAY

María José De Rosa[1#], Tania Veuthey[1#], Jeremy Florman[2#], Jeff Grant[2], María Gabriela Blanco[1], Natalia Andersen[1], Jamie Donnelly[2], Diego Rayes[1,2*] and Mark J. Alkema[2 *]

1. Instituto de Investigaciones Bioquímicas de Bahía Blanca (CONICET), Departamento de Biología, Bioquímica y Farmacia, Universidad Nacional del Sur,- Bahía Blanca, Argentina.

2. Department of Neurobiology, University of Massachusetts Medical School, Worcester, MA, USA

#Equal contribution

*Correspondence to: mark.alkema@umassmed.edu; drayes@criba.edu.ar

An animal's stress response requires different adaptive strategies depending on the nature and duration of the stressor. While acute stressors, like predation, induce a rapid and energy-demanding fight or flight response, long-term environmental stressors induce the gradual and long-lasting activation of highly conserved cytoprotective processes (Cannon, 1915; Essers *et al.*, 2004; Prahlad, Cornelius and Morimoto, 2008). In animals across the evolutionary spectrum the continued activation of the fight-or-flight response weakens the animal's resistance to environmental challenges (Travers *et al.*, 2010; Miller and Sadeh, 2014). However, the molecular and cellular mechanisms that regulate the trade-off between flight response and long-term stressors are poorly understood. Here we show that repeated induction of the C. elegans flight response shortens lifespan and inhibits conserved cytoprotective mechanisms. The flight response activates neurons that release tyramine, the invertebrate analog of adrenaline/noradrenaline. Tyramine stimulates the DAF-2/Insulin/IGF-1 pathway and precludes the induction of stress response genes by activating an adrenergic-like receptor in the intestine. In contrast, long-term environmental stressors, such as heat or oxidative stress, reduce tyramine release allowing the induction of cytoprotective genes. These findings demonstrate that a neural stress-hormone supplies a state-dependent neural switch between acute flight and long-term environmental stress responses and provides mechanistic insights into how the flight response impairs cellular defense systems and accelerates aging.

Like other animals, C. elegans faces challenges that occur either abruptly (e.g. predation) or more progressively (e.g. oxidation, heat, food shortage) (Figure III-1). Prolonged exposure to environmental stressors reduces an animal's lifespan (Rodriguez *et al.*, 2013) (Figures III-2 a, III-3 b). In response to touch, C. elegans engages in an escape- or flight response where it rapidly moves away from the stimulus (Chalfie *et al.*, 1985). We triggered the flight response every 5 min by applying a vibrational stimulus ("tap") to the side of the agar plate containing the animals (Wicks and Rankin, 1995). The repeated induction of the flight response throughout life significantly reduced lifespan (Figure III-2 b). To study the interaction between different stress responses, we analyzed whether a mild stressor can affect C. elegans resistance to subsequent stronger stressors. Low doses of oxidative stress, mild heat or fasting made C. elegans more resistant to a subsequent higher dose of the same and other environmental stressors (Figures III-2 a, III-3 b,c). This adaptive induction of enhanced stress tolerance, called hormesis, has been previously observed in living organisms (Cypser and Johnson, 2002; Rattan and Ali, 2007; Calabrese, 2008; Kumsta *et al.*, 2017). In contrast, the transient induction of the flight response, which does not affect overall lifespan of the animal (Figure III-2 b), markedly reduced resistance to subsequent oxidative or thermal stress (Figures III-2 a, III-3 a-c).

Tyramine, which is structurally and functionally related to adrenaline/noradrenaline, plays a crucial role in the orchestration of the C.

elegans flight response (Alkema *et al.*, 2005; Pirri *et al.*, 2009; Maguire *et al.*, 2011). We found that exogenous tyramine inhibits the hormetic effects of mild oxidative, thermal, or nutritional pre-stressors (Figures III-2 a, III-3 c). Moreover, induction of the flight response in tyramine-deficient tdc-1 animals did not impair their subsequent resistance to either strong oxidative (Figure III-2 c) or thermal stress (Figure III-3 f). This suggests that tyramine release during the flight response impairs the animal's capacity to respond to subsequent environmental stressors. Furthermore, tdc-1 mutants were more resistant to environmental stressors and had an increased lifespan compared to wild-type animals (Figures III-2 c, III-3 f-j, III-4 b-d). In contrast, exogenous tyramine impaired environmental stress resistance and drastically shortened lifespan (Figure III-3 g,j). Tyramine is also a precursor for octopamine biosynthesis (Alkema *et al.*, 2005). However, our results indicate that the lack of tyramine, and not octopamine, underlies the stress resistant phenotype of tdc-1 mutants (Figure III-4).

The flight response and environmental stressors may pose conflicting challenges to the organism. We found that repeated activation of the flight response during exposure to oxidative or heat stress reduced resistance of wild-type animals, but not tdc-1 mutants (Figures III-5 b, III-6 a, c). To exclude the possibility that the mechanical stimulus causes a physical damage that impairs the animal's defense mechanisms, we triggered the flight response by optogenetic activation of mechanosensory neurons (Figure III-6 b). Light induction of the flight response reduced survival to oxidative stress and heat (Figure III-6 b, e). The flight

response can be initiated by stimulation of the touch receptor neurons (TRN), which in turn activate a single pair of tyraminergic RIM neurons (Chalfie *et al.*, 1985; Alkema *et al.*, 2005; Pirri *et al.*, 2009) (Figure III-5 a). Optogenetic activation of RIM was not sufficient to trigger a flight response, but did reduce resistance to environmental stress (Figure III-5 c). In addition, the silencing of tyraminergic RIM neurons increased resistance to oxidative and heat stress (Figure III-6 g, h). Therefore, while tyramine orchestration of the flight response is beneficial to escape from predation (Maguire *et al.*, 2011), it negatively impacts the response to environmental stressors.

We analyzed the activity of RIM neurons during the flight- or environmental stress response. At the onset of the flight response there was an immediate rise in RIM calcium levels (Figure III-5 d), consistent with observations that these neurons are active during reversals (Zheng *et al.*, 2012; Kagawa-Nagamura *et al.*, 2018). In contrast, a gradual but sustained reduction of calcium levels in RIM neurons was detected in animals subjected to heat, oxidative stress or food deprivation (Figures III-5 e, III-6 i, j). This reduction is reversed upon removal of the stressor (Figures III-5 e, III-6 k). Thus, while the activity of the tyraminergic RIM neurons rapidly increased during the flight response, their activity decreased upon exposure to environmental stressors.

C. elegans has four different receptors that are activated by tyramine: three adrenergic-like GPCRs (SER-2, TYRA-2 and TYRA-3) (Tsalik *et al.*, 2003; Komuniecki *et al.*, 2004) and a tyramine-gated chloride channel (LGC-55) (Pirri *et*

al., 2009). Like tyramine-deficient animals, we found that tyra-3 mutants are resistant to oxidative stress, heat and starvation (Figures III-7 a, III-8 a,b). Moreover, exogenous tyramine did not reduce the stress resistance of tyra-3 mutants (Figures III-7 c, III-8 c). This shows that tyraminergic activation of TYRA-3, a predicted Gq-coupled GPCR (Wragg *et al.*, 2007), is required to modulate the stress response. Where does TYRA-3 function? tyra-3 is expressed in a subset of neurons and the intestine (Figure III-7 b). Expression rescue of tyra-3 in the intestine, but not in neurons, was sufficient to restore the stress sensitivity and the negative impact of exogenous tyramine on heat, oxidative stress and starvation survival to wild-type levels (Figures III-7 c, III-9 b, c). Moreover, while repeated induction of the flight response in tyra-3 mutants did not increase sensitivity to subsequent heat or oxidative stress, sensitivity was restored when tyra-3 was expressed in the intestine (Figures III-7 d, III-9 d). Since RIM neurons have no direct synaptic outputs onto the intestine, tyramine acts as a neurohormone to inhibit the environmental stress response through the activation of TYRA-3 in the intestine.

The response to environmental stressors triggers the activation of conserved cytoprotective processes (Henderson and Johnson, 2001). Stress-induced activation of transcription factors, such as the Forkhead box O (FOXO/DAF-16), Heat Shock Factors (HSFs/HSF-1) and NF-E2-related factor 2 (NRF2/SKN-1), increases the expression of antioxidant enzymes and protein chaperones to cope with protein misfolding and aggregation (Essers *et al.*, 2004; Prahlad, Cornelius

and Morimoto, 2008). The insulin/IGF-1 signaling (IIS) pathway regulates growth, reproduction, metabolic homeostasis, lifespan and stress resistance from nematodes to humans (Fontana, Partridge and Longo, 2010). In C. elegans, loss-of-function mutations in the insulin/IGF-1 receptor ortholog, DAF-2, increase stress resistance and longevity (Arantes-Oliveira, Berman and Kenyon, 2003). Stress resistance of tdc-1; daf-2 and tyra-3; daf-2 double mutants was similar to that of daf-2 single mutants (Figure III-10 a) and exogenous tyramine did not impair the stress resistance of daf-2 mutants (Figure III-10 b). This suggests that tyraminergic inhibition of the environmental stress response depends on the DAF-2/IIS pathway.

DAF-16/FOXO mediates a large portion of the physiological processes downstream of DAF-2. Environmental stressors reduce the activity of the DAF-2/IGFR, leading to DAF-16/FOXO translocation to the nucleus where it induces the expression of stress response genes (Henderson and Johnson, 2001). After 10 min of exposure to heat (35˚C), tdc-1 and tyra-3 mutants exhibited significantly higher levels of nuclear DAF-16/FOXO accumulation compared to the wild-type background (Figure III-11 a). Exogenous tyramine inhibited DAF-16/FOXO nuclear localization in wild-type and tdc-1 animals, but not in tyra-3 mutant animals exposed to a prolonged heat stimulus (30 min, Figure III-11 a). Intestinal expression of tyra-3 rescued the DAF-16/FOXO localization phenotype of tyra-3 mutants (Figure III-11 a). As expected, DAF-16/FOXO localized to the nucleus in response to a short exposure to oxidative, heat or nutritional stress

(Figure III-12 a) (Henderson and Johnson, 2001). In contrast, DAF-16/FOXO largely localized to the cytoplasm in response to repeated mechanical stimuli (Figure III-12 a). The induction of the flight response and optogenetic activation of the RIM neurons inhibited DAF-16/FOXO nuclear localization in animals exposed to heat (Figure III-12 b,c). Moreover, the expression of sod-3, a DAF-16/FOXO target gene, is upregulated in tdc-1 and tyra-3 mutants (Figure III-13 a). daf-16; tyra-3 and daf-16; tdc-1 mutants are more resistant to environmental stress than daf-16 single mutants, indicating that TYRA-3 likely interfaces with the DAF-2/IIS pathway upstream of DAF-16/FOXO (Figure III-13 b). Indeed, DAF-2 dependent and DAF-16/FOXO independent stress response genes such as hsp-16.2 (HSF-1) and gst-4 (SKN-1) (Chiang *et al.*, 2012), were also upregulated in tdc-1 and tyra-3 mutant animals (Figure III-13 c,d). In tdc-1 and tyra-3 mutants, cytoprotective mechanisms, such as DAF-16 translocation or hsp-16 and sod-3 induction, were induced not only in the intestine, but also in other tissues (Figures III-11, III-13). To test whether tyramine can activate the DAF-2/IIS pathway in non-intestinal cells through the release of Insulin-Like Peptides (ILPs) from the intestine, we analyzed DAF-16/FOXO localization and stress response in hid-1 mutants. HID-1 is a membrane protein required for neuropeptide sorting and insulin secretion in worms and mice (Mesa *et al.*, 2011; Du *et al.*, 2016). In contrast to the wild type, exogenous tyramine did not impair DAF-16/FOXO translocation and stress resistance in hid-1 mutants (Figure III-11 c). Expression of hid-1 in the intestine restored tyramine's detrimental effect on

the resistance to oxidative and heat stress (Figure III-14). This suggests that TYRA-3 activation stimulates the release of Insulin-Like Peptides (ILPs) from the intestine to further inhibit cytoprotective pathways in non-intestinal cells (Figure III-11 d).

The metabolic rate increases during the animal's flight response (Hawlena and Schmitz, 2010; Rabasa and Dickson, 2016). Since the upregulation of the insulin pathway is linked to increased metabolic rates (Van Voorhies and Ward, 1999; Lee *et al.*, 2012), tyramine-mediated activation of the DAF-2/IIs pathway may induce a metabolic shift to provide the fuel needed for high-energy demands of the C. elegans flight response. While tyramine release facilitates the animal's escape from a threatening stimulus, the down regulation of tyramine signaling is crucial to deal with environmental stressors. Striking parallels exist in vertebrates, where acute stress stimulates the release of adrenaline and noradrenaline: key inducers of the animal's fight-or-flight response. Given the conservation in neural control of stress responses, it will be interesting to determine whether perpetuated activation of the "fight-or-flight" response negatively impacts animal health and aging through the inhibition of insulin-dependent cytoprotective pathways.

Methods

Standard *C. elegans* culture and molecular biology methods were used (Brenner, 1974; Stiernagle, 2006). All strains were cultured at 20°C on NGM agar plates with the *E. coli* OP 50 strain as a food source. The wild-type strain was Bristol N2. Some strains were provided by the CGC, which is funded by NIH Office of Research Infrastructure Programs (P40 OD010440). CX16663 strain was kindly provided by C. Bargmann (Jin, Pokala and Bargmann, 2016). The NM2761, NM3067, NM3139 and NM3154 strains were kindly provided by M. Nonet (Mesa *et al.*, 2011). Worm population density was maintained low throughout their development and during the assays. The strains used were:

N2 (Wild-type)
MT10661 *tdc-1(n3420) II*
MT13113 *tdc-1(n3419) II*
MT9455 *tbh-1(n3247) X*
QW425 *tdc-1(n3420) II; zfIs23[Ptbh-1::TDC-1::GFP]*
CX16663 *kyEx5846[pXJ07(Pgcy-13::HisCl1::SL2::mCherry)]*
QW89 *lgc-55(tm2913) V*
OH313 *ser-2(pk1357) X*
QW42 *tyra-2(tm1815) X*
CX11839 *tyra-3(ok325)X*
QW833 *lgc-55(tm2913)V; tyra-3(ok325)X; tyra-2(tm1846)X; ser-2(pk1357) X*
OAR61 *tyra-3(ok325)X; lin-15(n765ts); nbaEx 1 [pelt-2::TYRA-3 + pL15EK]]*
CB1370 *daf-2(e1370) III*
OAR-2 *tdc-1(n3420) II; daf-2(e1370) III*
OAR-1 *daf-2(e1370) III; tyra-3(ok325) X*
QW495 *tyra-3(ok325) X; lin-15(n765ts) X; zfEx121[Ptyra-3$_{short}$::TYRA-3 + pL15EK*]
QW1582 *tyra-3(ok325) X; lin-15(n765ts)X; zfEx743[Pelt-2::TYRA-3 + pL15EK*]
QW2029 *tyra-3(ok325) X; lin-15(n765ts)X; zfEx962[Prgef-1::TYRA-3 + pL15EK*]
OAR94 *tyra-3(ok325) X; lin-15(n765ts)X; nbaEx21[Ptyra-3$_{long}$::TYRA-3 + pL15EK]]*
QW1649 *zfIs144[Pmec-4::Chrimson::wCherry, pL15EK]*
QW1046 *lite-1(ce314) X; zfIs100[Pcex-1::ChR2::GFP]*

QW1602 *lin-15(n765ts) X; zfEx758[Pcex-1::NLSwCherry::SL2::GCaMP6, pL15EK]*
GR1307 *daf-16(mgDf50) I*
OAR3 *daf-16(mgDf50) I; tdc-1(n3420) II*
OAR4 *daf-16(mgDf50) I; tyra-3(ok325) X*
TJ356 *zIs356[Pdaf-16::DAF-16a/b::GFP + pRF4]*
OAR5 *tyra-3(ok325) X; zIs356[Pdaf-16::DAF-16a/b::GFP + pRF4]*
OAR6 *tdc-1(n3420) II; zIs356[Pdaf-16::DAF-16a/b::GFP + pRF4]*
OAR62 *tyra-3(ok325) lin-15(n765ts) X; nbaEx1[pelt-2::TYRA-3 + pL15EK];zIs356[Pdaf-16::DAF-16a/b::GFP + pRF4]*
CF1553 *muIs84[(pAD76) Psod-3::GFP + pRF4]*
OAR13 *tdc-1(n3420) II ; muIs84[(pAD76) Psod-3::GFP + pRF4]*
OAR14 *tyra-3(ok325) X ; muIs84[(pAD76) Psod-3::GFP + pRF4]*
OAR92 *tyra-3(ok325) lin-15(n765ts) X; nbaEx1[Pelt-2::TYRA-3 + pL15EK]]; [muIs84 [(pAD76) Psod-3::GFP + pRF4]*
CL2070 *dvIs70[Phsp-16.2::GFP + pRF4]*
OAR63 *tdc-1(n3420) II, dvIs70[Phsp-16.2::GFP + pRF4]*
OAR64 *tyra-3(ok325) X, dvIs70[Phsp-16.2::GFP + pRF4]*
OAR65 tyra-3(ok325) lin-15(n765ts) X; dvIs70[Phsp-16.2::GFP + pRF4]; nbaEx1[Pelt-2::tyra-3;pL15EK]
CL2166 *dvIs19[(pAF15)Pgst-4::GFP::NLS] III*
OAR80*dvIs19[(pAF15) Pgst-4::GFP::NLS] III; tyra-3(ok325) X*
OAR93*; tdc-1(n3420) II; dvIs19[(pAF15) Pgst-4::GFP::NLS] III*
OAR81 tyra-3(ok325) lin-15(n765ts) X;dvIs19[(pAF15) gst-4p::GFP::NLS] III; nbaEx1 [Pelt-2::tyra-3;pL15EK]
NM2761 *hid-1(sa722) X*
NM3067 *hid-1(sa722) lin-15(n765ts) X; jsEx896[Phid-1-HID-1-GFP]*
NM3139 *hid-1(sa722) lin-15(n765ts) X; jsEx909[Pges-1-HID-1-GFP + pL15EK]*
NM3154 *hid-1(sa722) lin-15(n765ts) X; jsEx897[Prab-3-HID-1-GFP + pL15EK]*
QW2027 *hid-1(sa722) X; zIs356[Pdaf-16::DAF-16a/b::GFP + pRF4]*
QW2045 *lin-15(n765ts) X; zfEx969[Ptyra-3$_{long}$::mCherry; + pL15EK]*

Stress resistance assays

***Heat Stress*:** Thermotolerance assays were performed as described (Prahlad, Cornelius and Morimoto, 2008) with some modifications. For each strain, four 35 mm NGM agar plates containing 20 animals (with or without 10 mM exogenous tyramine) were incubated at 35˚C for 4 h. To ensure proper heat transfer, 6 mm

thick NGM agar plates were used. Animals were synchronized as L4s and used 14 h later. Plates were sealed with Parafilm in zip-lock bags, and immersed in a water bath equilibrated to the appropriated temperature. Surviving animals were counted after 20 h at 20˚C. For all assays, animals were scored as dead if they failed to respond to prodding with a platinum-wire pick to the nose. For longitudinal thermotolerance assays, we used a room at 35˚C and survival was quantified every 20 min on NGM plates containing 30-40 young adults.

Oxidative stress: Iron sulfate ($FeSO_4$) was used as an oxidative stressor. For Fe^{2+} treatment, 20 L4 worms were transferred to 35 mm agar plates containing $FeSO_4$ at the indicated concentration and time (1 mM, 1 h for mild stress and 15 mM, 1 h for strong stress). For longitudinal assays we scored the survival every 20 minutes in agar plates containing 3 mM Fe^{2+}.

Food deprivation**:** L4 animals were rinsed off the plate and washed with M9 buffer and then were seeded in a 96 multiwell plate (one worm per well) containing M9 with or without tyramine (10 mM). Survival was monitored every day until no living animals were observed. Animals with larvae in their uterus ("bag of worms") were only occasionally observed, and those animals were discarded from the assay.

Flight response: To induce the flight response a vibrational stimulus (Tap) was applied to the plate every 5 minutes for 2.5 hours. Tap stimuli were delivered using custom Matlab script for Arduino Uno microcontroller to drive a linear push solenoid (Saia-Burgess195205-127 / STA / 75L STA 0˚ PUSH). This tap protocol

was chosen because, this inter stimulus interval results in repeated induction of the flight response with minimal habituation (Wicks and Rankin, 1995) (see velocity trace in Figure III-6, b). The number of inductions of the flight response (30 in 2.5 hours) was selected after analyzing the effects of number of taps (from 1 to 40 elicited every 5 minutes) on the animal resistance to subsequent oxidative or heat stress (see Figure III-3, b). Tyramine release leads to the suppression of head movements through the activation of LGC-55, a tyramine-gated chloride channel (Alkema *et al.*, 2005; Pirri *et al.*, 2009). Animals that were subjected to 30 successive taps every 5 minutes, still suppressed their head movements in response to anterior touch (Figure III-6, f). This indicates that the RIM is activated and tyramine is released upon during the repeated mechanical stimulation of this tapping protocol. All the custom software created and used in this work are available upon request.

Hormesis assays

Young adult worms were exposed to mild oxidation (1 mM Fe^{2+}, 1 h), fasting (8 h without food), heat (35˚C, 20 min), or transient activation of the flight response (tapping plates every 5 min during 2.5 h (30 taps)). All the pre-treatments were performed both in the presence or absence of exogenous tyramine (10 mM). After recovery (1 h on NGM agar plates seeded with OP50) the animals were exposed either to high Fe^{+} concentration (3 mM) or heat (35˚C). Animal survival was evaluated every 20 min. The survival index (SI) was calculated as follows: SI

= (number of surviving pre-treated worms/ total number of pre-treated animals) minus (number of naive surviving animals/total number of naive animals). The SI was calculated, by scoring the number of survivors after 2 h of exposure to 3 mM Fe^{2+} or 4 h of exposure to 35˚C. Positive values indicate an improved stress resistance while negative values indicate an impairment of stress resistance compared to naive animals.

Lifespan assays

Lifespan studies were performed at 20˚C on NGM plates (BactoAgar: BritaniaLab, Argentina or Becton Dickinson, USA) with OP50 as a food source as described previously (Kenyon *et al.*, 1993; Dorman *et al.*, 1995; Lionaki and Tavernarakis, 2013). Briefly, gravid hermaphrodites were placed on fresh plates and allowed to lay eggs overnight (day 0 post-hatch). The following day, gravid animals were withdrawn. This time point represents day 1 after hatching. On day 3 post-hatch, worm were re-synchronized by picking L4 animals and transferred into individual plates (10-15 worms per plate (7-8 plates per condition)). To avoid food depletion, animals were transferred to fresh Petri dishes about every two days until the cessation of progeny production. Animals were scored everyday as dead if they displayed no spontaneous movement or response when prodded. Worms that displayed internally hatched progeny, an extruded gonad or desiccation due to crawling off the agar were excluded from the analysis. We found lifespan extension and increased resistance for both *tdc-1* alleles: *n3419*

and *n3420*. These results differ from those reported by Chun (Chun *et al.*, 2015), where no differences were observed between lifespan of wild-type and *tdc-1(n3419)* mutant animals. This could be due to slight difference in growth conditions (*e.g.* different agar sources) or differences in the wild-type strain used for comparison in lifespan experiments. The *tdc-1(n3420)* and *tdc-1(n3419)* alleles were backcrossed >10 x into wild-type strain that was used as a control in the lifespan experiments (obtained from the Horvitz lab, approximately 5x refreezes from the original N2 strain described by Brenner (Brenner, 1974)).

For studying the effect of flight response in lifespan,100 -120 animals were transferred to a single 60mm NGM plate for each condition. A vibrational stimulus (Tap) was applied to the plate every 5 minutes using an Arduino controlled linear push solenoid. To avoid any potential effect of vibrational stimulus on development, tap treatment was started on day 1 after L4-stage (day 4 post hatching). Vibrational stimulus was applied either transiently, tap every 5 min for 2.5 hours, same protocol as used in the hormesis experiments) or during the entire animal life. Kaplan Meier survival curves were generated using SigmaPlot 12.0 and compared by Log-Rank test.

Locomotion assays

Mobility was assessed at days 4, 7 and 10 of adulthood. To evaluate mobility, 10 worms were transferred to an unseeded NMG plate into a drop of M9 buffer. Once the drop was dried-up, worms were left to acclimate for 2-3 minutes. 30 - 60 seconds videos were acquired by a camera controlled by Fire-i^{TM} software

(Unibrain) at 15 fps. The average speed (µm/sec) was calculated by dividing the total distance travelled by each worm as a function of the elapsed time using wrMTrck plugin from ImageJ software.

Simultaneous acute and long-term stress assays

Young adult worms were exposed to oxidative stress or heat stress and to a repeated acute stress (tapping plates or light pulse) simultaneously. Survival was evaluated and a survival curve or SI was calculated for each condition.

Oxidative stress: L4 worms expressing *Pmec-4::ChRimson (for TRN activation) or* P*cex-1*::ChR2 (channelrhodopsin (ChR2) in the tyraminergic RIM neurons) were placed on 3 mM Fe^{2+} plates, seeded with a thin lawn of 3 mM Fe^{2+} OP50, and subjected to either a plate tap or a 5 sec light pulse every 5 min for 2.5 h. Light stimuli were delivered using custom Matlab script to an Arduino Uno microcontroller driving a Mightex compact universal LED controller (Mightex SLC-MA02-U). Tap stimuli were delivered using an Arduino controlled linear push solenoid. Light pulses for optogenetic experiments (617 nm for ChRimson activation and 470 nm for ChannelRhodopsin) were delivered using Mightex High-Power LED Collimator Sources (Mightex, LCS-0617-03-11, LCS-0470-03-11). Animals were tracked using Multi-Worm Tracker software (Swierczek *et al.*, 2011) and single frames were captured every minute to score survival. Survival curves were generated by examining the captured frames, and marking worm

deaths using a custom MATLAB script (Mathworks). Animals were considered dead when they were completely motionless for extended period (till the end of the experiment). Velocity was analyzed using Choreography (Swierczek *et al.*, 2011; Yemini, Kerr and Schafer, 2011) and custom MATLAB scripts. Custom software used are available upon request.

Heat stress: 40 young adult *Pmec-4::ChRimson* transgenic animals, that were grown in darkness in the presence (+ATR) or absence (-ATR) of *all-trans* retinal, were placed on NGM plates seeded with a thin lawn of OP50. A copper ring was placed in the center of the plate to prevent animals from crawling off the plate during the assay. Plates were placed on a transparent plastic chamber connected to a recirculating heated water bath (Hoefer Scientific Instruments, HSI RCB-300 Refrigerated Circulating Bath). A digital thermocouple (Fluke 52 II Dual Input Digital Thermometer) was inserted into the agar to maintain a constant temperature of 35ºC. Images of animals were captured every 5 min for 7 h to assess survival. 5 s light pulses of 617 nm were delivered every 5 min for the duration of the experiment. Survival curves were generated as described for the oxidative stress experiment (see above).

RIM activity measurements

Microfluidic devices used for imaging Ca^{2+} dynamics in freely moving animals were prepared using soft lithography courtesy of D. Albrecht (Worcester

Polytechnic Institute). L4 animals that expressed GCaMP in the RIM (*lin-15(n765ts); zfEx758[pcex-1::NLSwCherry::SL2::GCaMP6])* were grown overnight. Young adults animals were placed in S Basal buffer and loaded into the microfluidic chamber. Imaging was performed at 2.5 x magnification using an AxioObserver A1 inverted microscope (Zeiss) connected to a Sola SE Light Engine (Lumencor) and an ORCA-Flash 4.0 digital CMOS camera (Hamamatsu). Micromanager Software (Edelstein *et al.*, 2014) was used to control fluorescence timing and image capture. Animals were loaded into the microfluidic device and exposed to either oxidative stress (6 mM Fe^{2+}) or food deprivation. After an initial 20-40 min acclimation period, fluorescent images were captured at a rate of 1 frame/5 s. For the fight response images were captured at 1 frame/500 ms. RIM GCaMP 6.0 fluorescence values were analyzed using ImageJ software. The traces for the flight response shown in Fig. III-5, d represent the average RIM GCaMP6 Ca^{2+} activity ($\Delta F/F$) 5 seconds before and 20 seconds after a tap stimulus. Shaded areas around the traces represent SEM for the averaged traces. A region of interest (ROI) was drawn around the RIM neuron, as well as for a background region. The integrated density was calculated for the background area and subtracted from the image, followed by calculation of integrated density for each ROI. These values were extracted for 6 consecutive image captures starting at the indicated time points. The ROI values for each condition were pooled and averaged. The averaged integrated density values for each capture were normalized to the average of the first time point.

RIM responses to aversive heat were performed using a similar approach as described previously (Hawk *et al.*, 2018). Briefly, animals were maintained at 20°C and immobilized with 10 mM levamisole on a 5% agarose pad between two coverslips for imaging. Samples were placed on a Peltier device, which allowed precise temperature control via custom LabView (National Instruments) software. GCaMP6 and mCherry fluorescence were simultaneously recorded with a 250 ms exposure time under 10 x magnification using a Hammamatsu ORCA-Flash4.0 camera equipped with a Photometrics Dual-View 2 optical splitter, Image acquisition was controlled using Micromanager software with a capture rate of 1 frame per second. Prior to recording, the coverslips containing the immobilized animals were placed on the Peltier device, which was held at 20°C. Image acquisition began when the temperature protocol was started. This protocol consisted of an initial 5 minute baseline period at 20°C followed by a 5 minute ramp to 35°C. The temperature was held at 35°C for 3 minutes, then decreased over 5 minutes back to 20°C and held at 20°C for a further 5 minutes. Three independent experiments were performed resulting in recordings.of RIM calcium responses of 30 animals. Calcium responses were measured by drawing a 300 px^2 oval ROI around the RIM soma to measure mean fluorescent intensity. Since both GCaMP and mCherry signals were projected onto the same imaging sensor, the ROI could be translated to measure the corresponding mCherry fluorescence in the same animal. This ROI was also moved to a portion of an animal devoid of fluorescence to measure background signal in the green and

red channels. The background was subtracted from the respective fluorescent measurements. The ratio of GCaMP to mCherry signal within an animal was determined and normalized to baseline by dividing by the average ratio during the first minute of recording for each animal. Traces in Fig 2e-g represent the mean of the 30 animals recorded and shaded regions indicate SEM. Custom software used is available upon request.

Confocal microscopy and image analysis

Animals were mounted in M9 with levamisole (10 mM) onto slides with 2% agarose pads. Images were acquired on confocal microscopy (LSCM; Leica DMIRE2) with 20 x and 63 x objectives, processed by Image J FIJI software.

Subcellular DAF-16 localization

DAF-16 translocation was analyzed using strains containing the translational *Pdaf-16::DAF-16a/b::GFP* reporter in a wild-type or tyramine signaling mutant background (*Pdaf-16::DAF-16a/b::GFP*; *tdc-1*; *Pdaf-16*::*DAF-16a/b::GFP*; *tyra-3,* Pdaf-16::DAF-16a/b::GFP; *tyra-3*; *Pelt-2::*TYRA-3). Young adult animals in basal conditions or exposed to either mild (35ºC, 10 min) or strong heat stress (35ºC, 30 min), with or without exogenous tyramine, were mounted to analyze DAF-16 cellular distribution under a fluorescence microscope. To analyze the effects of flight response triggering in heat-mediated DAF-16 nuclearization, animals were exposed simultaneously to heat (37 C, 1 h) and either a vibrational stimulus

(plate tap every 5 minutes during the heat exposure) or optogenetic activation of the RIM (5 second pulse of 470 nm light every 5 minutes in animals expressing ChR2 in the RIM, grown in the presence or absence of *all-trans* retinal). The number of GFP labeled nuclei per animal was quantified using Image J FIJI software and normalized to the naïve condition within the day.

Expression analysis of DAF-2/IIs target genes

hsp-16.2, sod-3 and gst-4 expression levels were analyzed in transgenic strains containing transcriptional reporters, in wild-type or tyramine signaling mutant backgrounds (see strain list). Animals were imaged using an epifluorescence microscope (Nikon Eclipse E-600) coupled to a CCD camera (Nikon K2E Apogee) and a laser spectral confocal microscope (Leica TCS SP2). Fluorescence intensity was quantified using Image J FIJI software.

H_2O_2-induced oxidative stress resistance

The H_2O_2 stress assays were performed as described (Ayyadevara *et al.*, 2005). Briefly, 50 adult worms were transferred to 35-mm plates containing 3 ml S basal supplemented with cholesterol (5 µg/ml), *E. coli* OP50 (2×10^9 cells/ml), and freshly added H_2O_2 (5 mM). After 3 h of exposure to H_2O_2 dead animals were quantified.

Histamine and tyramine supplementation

The assays were performed as described (Pokala *et al.*, 2014). Histamine-dihydrochloride (Alfa Aesar) or tyramine hydrochloride (Alfa Aesar) stocks were made with MilliQ sterile water, and diluted to 10 mM into NGM agar before pouring. Plates were stored at 4°C and used within one week after pouring. For histamine-dependent neuronal silencing, young-adult animals expressing the *Drosophila* histamine-gated chloride channel, HisCl, in the RIM neuron (RIM::HisCl) were exposed to 10 mM histamine 8 h prior and during the oxidation or heat stress protocol.

Molecular Biology

Standard molecular biology techniques were used. *Ptyra-3*::mCherry transcriptional reporter constructs were made by cloning a 3.4 kb (*Ptyra-3*$_{long}$) or 1.8 kb (*Ptyra-3*$_{short}$) promoter fragment upstream of the *tyra-3* start site into the pPD95.75 mCherry plasmid. These promoter fragments were also subcloned in front of the *tyra-3* cDNA followed by the *unc-54* 3´UTR to rescue the endogenous (Neurons and intestine, *Ptyra-3*$_{long}$ promoter) or partial (Neuronal *Ptyra-3* $_{short}$ promoter) *tyra-3* expression pattern. For intestinal rescue constructs, the *tyra-3* cDNA was cloned behind the intestinal *elt-2* promoter. For pan-neuronal rescue constructs*, tyra-3* cDNA was cloned behind the pan-neuronal *rgef-1* promoter. Transgenic strains were obtained by microinjection of plasmid DNA at 20 ng/µl into the germline with co-injection marker *lin-15* rescuing plasmid pL15EK (80

ng/µl) into *lin-15(n765ts)* mutant animals unless otherwise noted. At least three independent transgenic lines were obtained. Data are shown from a single representative line.

Pharyngeal pumping rate

Young adult worms were transferred to NMG plates seeded with *E. coli* OP50. The number of contractions in the terminal bulb of the pharynx was counted for 1 min using a stereomicroscope at 75 x magnification.

Data collection, availability and statistics

All the data are publicly available in Open Science Framework: https://osf.io/mj3n9/?view_only=b6c7ff8697544e71b725767f17e19628. All data are represented in a format that shows the distribution (Dot plots) and all the graph elements (median, error bars, etc) are defined in each figure legend. We did not use any software to determine sample size. For most of our experiments, and in accordance to most reports using *C. elegans*, we used a large number of animals per condition in each assay (typically more than 40-50 animals). This number of animals is large enough to ensure appropriate statistical power in the test used. All the statistical tests were performed after checking normality. Grubbs´test was used for outliers analysis ($p<0.05$). We performed the experiments at least 3-4 times to ensure reproducibility. All the animals were grown in similar conditions and the experiments were performed in different days,

with different animal batches. In general, replicates were performed by different researchers. Drugs were previously controlled by analyzing a known phenotype (*e.g.* worm paralysis and head relaxation on 30mM tyramine). Animals used were age-synchronized (L4 or 24h past L4).

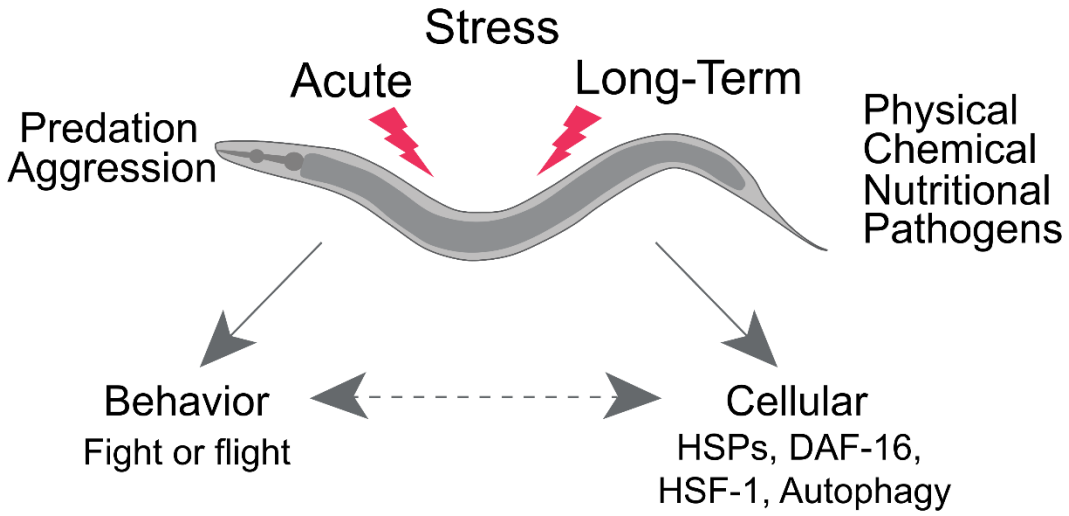

Figure III-1. *C. elegans* faces different types of environmental stressors. Like other animals *C. elegans* is exposed to different forms of stress in its environment that occur either abruptly (e.g. predation) or more progressively (food shortage, osmotic stress, oxidation, high or low environmental temperatures). Stress can induce behavioral and/or cellular responses. Stress response to environmental stressors such as heat, starvation and oxidative stress features a central role for the DAF-2/Insulin/IGF-1 signaling (IIS) pathway and the activation of DAF-16/FOXO, SKN-1/NRF and HSF-1 transcription factors. In response to acute challenges, such as touch *C. elegans* can engage in an escape-response where it rapidly moves away from a life-threatening stimulus.

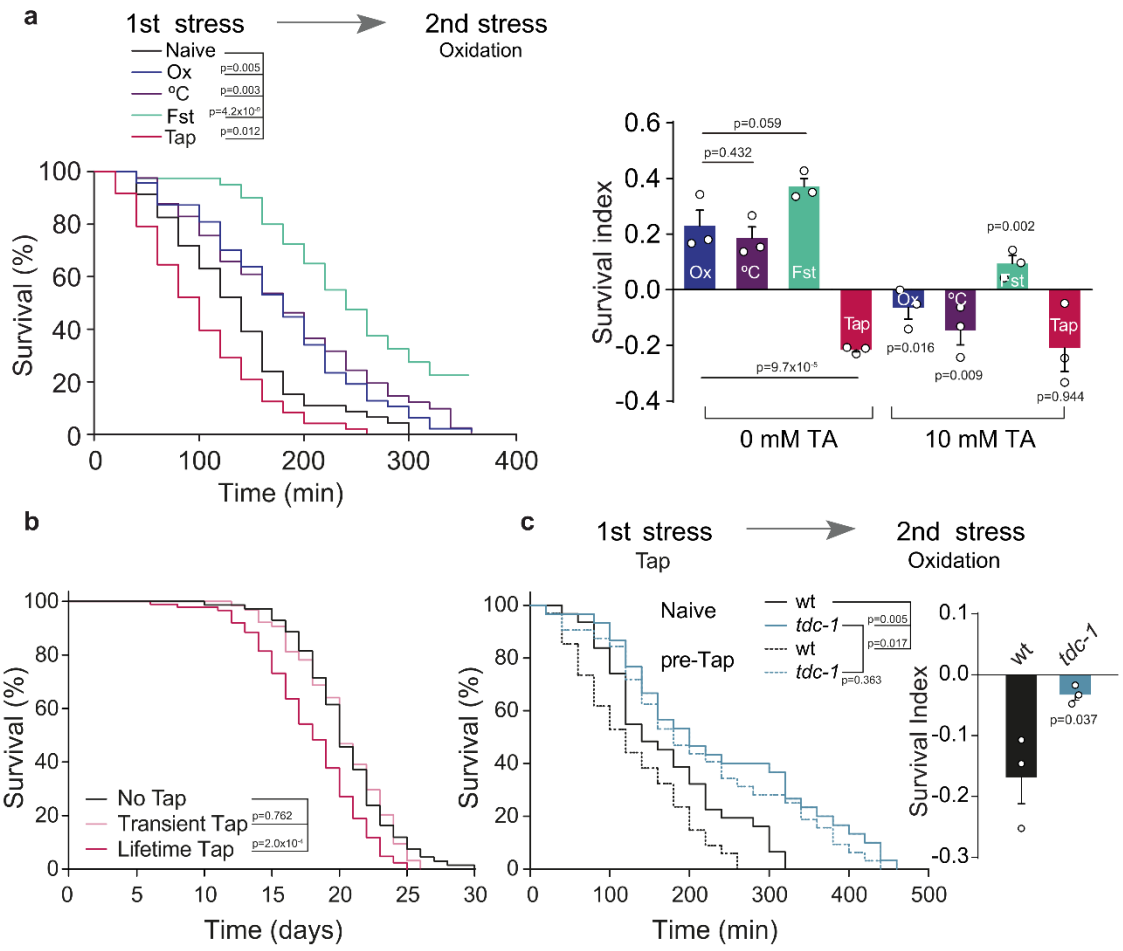

Figure III-2. The flight response and tyramine impair the resistance to subsequent stressors. a, Representative survival curves of pre-stressed nematodes exposed to subsequent oxidation. Pre-stressors: Ox: Oxidation, ºC: Heat, Fst: Fasting and Tap. Right, Survival Index (SI = fraction of surviving pre-treated animals minus fraction of surviving naïve animals) compare to naïve animals, in the absence or presence of tyramine (TA) during pre-treatment. Data represented as mean ± SEM. For 0 mM TA conditions, One-way ANOVA followed by Holm-Sidak's test was used. For 10 mM TA conditions, a two-tailed t

test (no TA vs TA) was used. **b,** Representative survival curves of animals subjected to activation of the flight response (every 5 min) for either 2.5 hours (Transient) or throughout life (Lifetime) (two-sided log-rank) **c,** Oxidation survival curves and SI (mean ± SEM, two-tailed t test, n=3) of *tdc-1* mutants pre-exposed to mechanical stimulus (tap).

For survival curves (a-c), a two-sided log-rank test was used and the experiments were independently repeated three times (n=3) with similar results. 60-120 worms per condition per experiment were used.

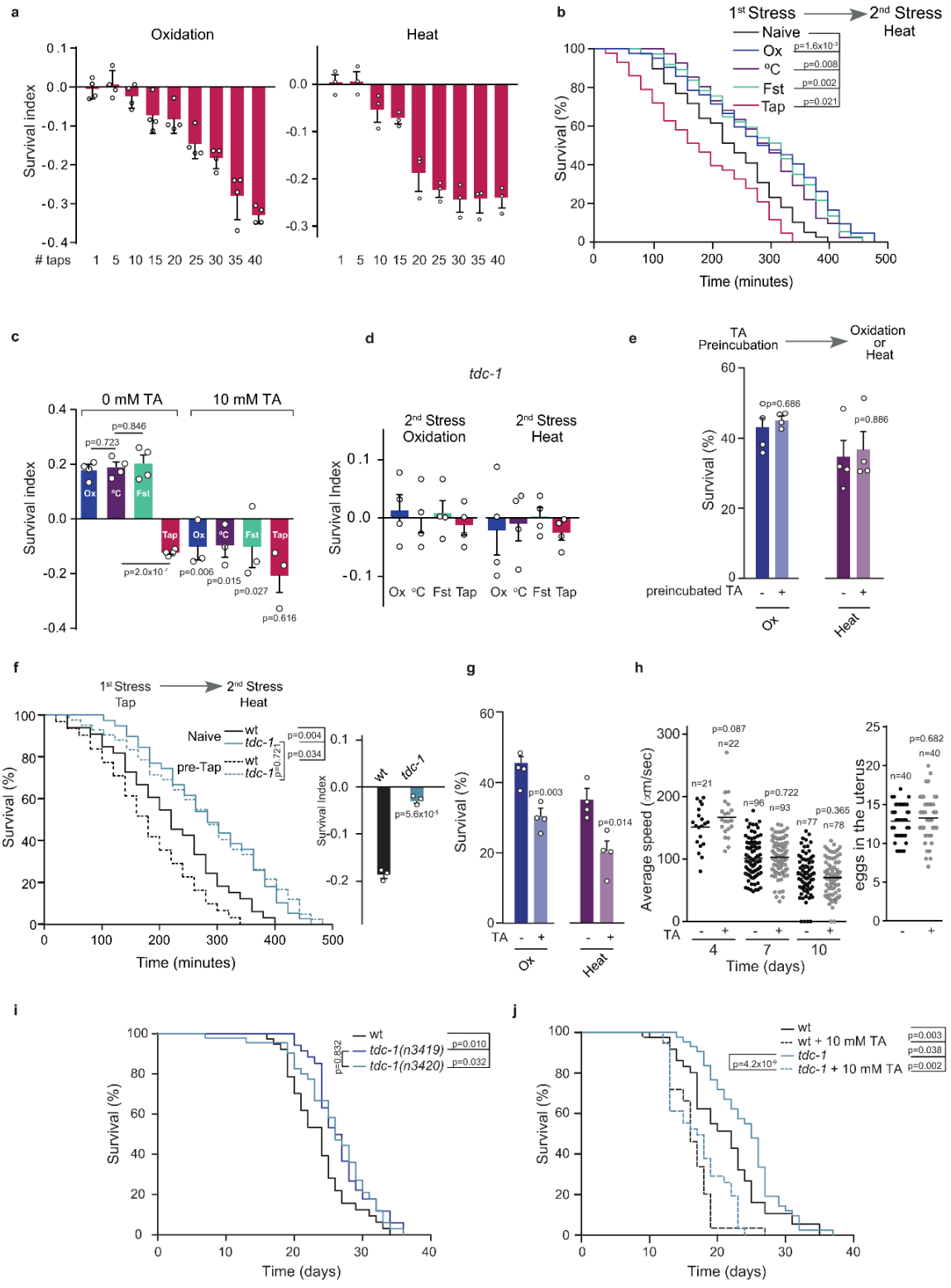
a
Oxidation
Heat
Survival index
taps
1 5 10 15 20 25 30 35 40
b
1st Stress
2nd Stress
Heat
Naive
Ox
°C
Fst
Tap
p=1.6x10-3
p=0.008
p=0.002
p=0.021
Survival (%)
Time (minutes)
c
0 mM TA
10 mM TA
p=0.846
p=0.723
p=2.0x10-7
p=0.006
p=0.015
p=0.027
p=0.616
d
tdc-1
2nd Stress
Oxidation
2nd Stress
Heat
e
TA
Preincubation
Oxidation
or
Heat
p=0.686
p=0.886
preincubated TA
f
1st Stress
Tap
2nd Stress
Heat
Naive
pre-Tap
wt
tdc-1
p=0.004
p=0.034
p=0.72
p=5.6x10-5
g
p=0.003
p=0.014
h
p=0.087
p=0.722
p=0.365
p=0.682
n=21
n=22
n=96
n=93
n=77
n=78
n=40
n=40
Average speed (cm/sec)
eggs in the uterus
Time (days)
i
wt
tdc-1(n3419)
tdc-1(n3420)
p=0.832
p=0.010
p=0.032
j
wt
wt + 10 mM TA
tdc-1
tdc-1 + 10 mM TA
p=4.2x10-9
p=0.003
p=0.038
p=0.002

Figure III-3. The flight response and tyramine decrease lifespan and impair resistance to stressors. a, Oxidation and heat survival index of animals pre-exposed to different tap stimulus protocols (from 1 to 40 plate taps every 5 minutes). Data represent mean ± SEM of independent experiments. n=4 and n=3 for oxidation and heat, respectively. At least 40 animals were analyzed in each independent experiment. Repeated triggering of the flight response (>20-25 times) prior to the exposure to oxidative or heat stress reduced animal survival **b, Top**, Scheme for the sequential stress experiments. Pre-stressors: 1 h 1 mM Fe^{2+} (Oxidation: Ox), 0.5 h 35ºC (Heat: ºC), 8 h food deprivation (Fasting: Fst), or tap stimulus every 5 min for 2.5 h (Tap). After 1 h of recovery, survival to heat stress (4 h 35ºC) was evaluated. **Bottom,** Representative Kaplan-Meier survival curves of pre-stressed nematodes exposed to subsequent thermal stress (heat), two sided log-rank test was used for statistical comparison. The curves are representative of three independent replicates with similar results (n=3). 40-80 animals were used per condition per experiment. **c,** Heat survival index in the absence and presence of exogenous tyramine (TA) during pre-exposure to the mild stressor followed by 1 h recovery and exposure to the second strong stressor in the absence of TA after pre-treatment. Data represent mean ± SEM. For 0 mM TA conditions, One-way ANOVA followed by Holm-Sidak post-hoc test versus pre-heat was used, n=4, 40-80 animals/condition. For 10 mM TA conditions, two-tailed Student´s t test (versus same condition without TA) was used, n=3, 40-80 animals/condition. Exogenous tyramine during mild stressor

exposure inhibits hormesis. **d**, Oxidation and heat survival index of *tdc-1(n3420)* mutant animals pre-exposed to the same stressors detailed in b. Data represent mean ± SEM, n=4, 40-80 animals/condition. Unlike wild-type animals, *tdc-1* mutants displayed no hormetic effects after pre-treatment with mild environmental stressors **e,** Pre-incubation with exogenous tyramine (TA) in the absence of environmental pre-stressors did not produce significant differences in subsequent oxidative stress and thermal resistance. Animals were exposed to 10 mM of exogenous TA for 3 h. After 1 h of recovery, the resistance to heat- (4 h at 35ºC) and oxidative- (2 h, 3 mM Fe^{2+}) stress was evaluated. Bars represent the mean ± SEM of independent experiments. n=4, 80-100 animals per condition per experiment. Two-tailed Student´s t-test (versus same condition without pre-exposure to TA) was used. **f**, **Left,** Representative Kaplan-Meier survival curves of naïve and pre-stressed (tap) animals exposed to heat (35ºC). The experiment was independently repeated 3 times (n=3) with similar results (35-50 animals per condition per experiment), two tailed log-rank test. **Right**, Survival index of naïve and pre-stressed, wild-type and *tdc-1* mutant upon exposure to heat stress. Bars represent mean ± SEM, n=3, 35-50 animals/condition, two-tailed Student´s t-test. The flight response impairs survival to heat exposure in wild-type but not in tyramine-deficient mutants. **g,** Resistance of wild-type animals exposed to oxidation or heat in the absence and presence of exogenous tyramine (10 mM). Bars represent mean ± SEM, n=4, 60-80 animals/condition. Two-tailed Student´s t-test (versus same condition without TA) was used. Exogenous tyramine

reduces oxidation and heat resistance **h,** Scatter dot plots (line at the mean) for: **Left,** Average locomotion rate of animals grown in the presence of exogenous tyramine (10 mM) for 4, 7 and 10 days. **Right**, Average numbers of eggs in the adult uterus (36 h post-L4s) in the presence of exogenous tyramine (10 mM, 36 h of exposure). n for each condition is indicated in figure. Two-tailed Student´s t-test (versus same condition without TA) was used. Exogenous tyramine does not significantly affect neither the locomotion nor the egg-laying, even upon extended exposure. **i,** Representative Kaplan-Meier lifespan curves of wild-type and *tdc-1* mutant animals. Two tailed log-rank test was used. The experiment was independently repeated 3 times (n=3) with similar results (40-80 animals per condition per experiment). Tyramine-deficient animals have an increased lifespan compared to wild-type. **j**, Representative Kaplan-Meier lifespan curves in the absence or presence of 10 mM exogenous TA. Two tailed log-rank test was used. The curves are representative of three independent replicates with similar results (n=3). 40-80 animals were used per condition per experiment. Exogenous tyramine reduces animal´s lifespan.

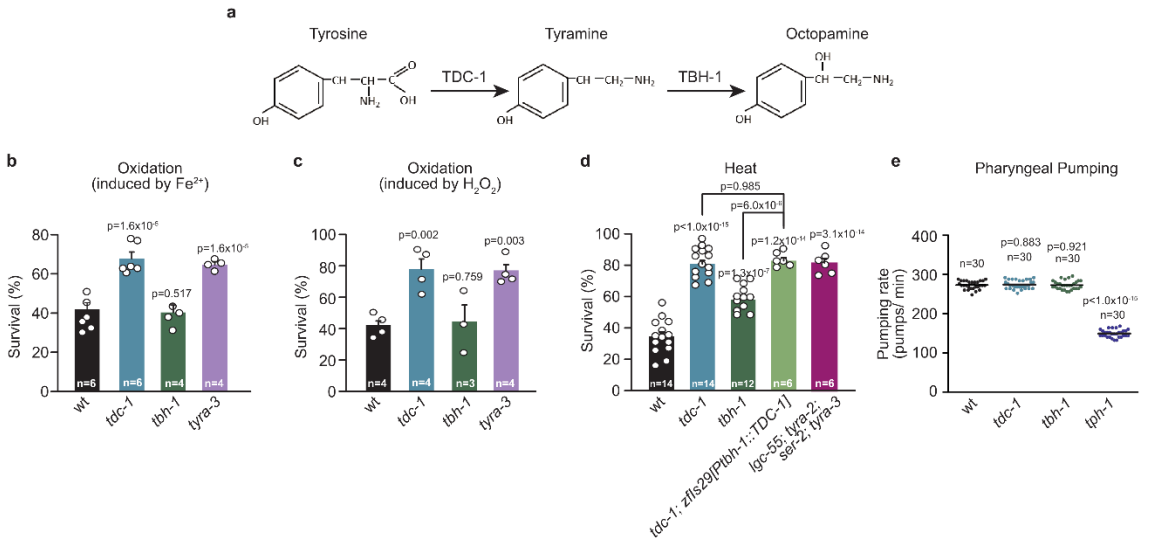

Figure III-4. Tyramine-deficient animals are resistant to environmental stress. a, Tyramine and octopamine biosynthesis pathway. Tyramine is synthesized from tyrosine by tyrosine decarboxylase (TDC-1) in the RIM and RIC neurons; octopamine is synthesized from tyramine by tyramine β-hydroxylase (TBH-1) in the RIC neurons[13]While *tdc-1* null mutants are deficient in both tyramine and octopamine, *tbh-1* null mutants are deficient only in octopamine. **b-c,** Survival percentages of wild-type, tyramine/octopamine deficient (*tdc-1*), octopamine deficient (*tbh-1)* and tyramine receptor (*tyra-3)* null mutants exposed to oxidation induced by **b,** $Fe^{2+}SO_4$ (1 h, 15 mM) and **c,** H_2O_2 (3 h, 5 mM). Bars represent the mean ± SEM. The number of independent experiments (n) is shown in the figure. 60-80 animals per condition per experiment were used. One-way ANOVA followed by Holm-Sidak post-hoc test for multiple comparisons versus wild-type was used. **d,** Survival to heat (4h at 35°C) of wild-type, *tdc-1*,

tbh-1, *tdc-1; zfIs29*[P*tbh-1::*TDC-*1*] (tyramine but not octopamine deficient) and the quadruple tyramine-receptor mutant QW833 (*lgc-55; ser-2; tyra-2; tyra-3)*. Bars represent the mean ± SEM. The number of independent experiments (n) is shown in the figure. 60-80 animals were used per condition per experiment. One-way ANOVA followed by Holm-Sidak post-hoc test for multiple comparisons was used. *tdc-1* mutants have an improved survival to thermal stress. Octopamine-deficient mutants (*tbh-1*) were slightly more heat resistant than wild-type animals, albeit not at the level of tyramine/octopamine deficient *tdc-1* mutants. Moreover, rescue of *tdc-1* expression in only the octopaminergic neurons (*tdc-1*; *Ptbh-1*::TDC -1) failed to reduce thermoresistance of *tdc-1* mutants. In addition, the quadruple mutants of all tyramine receptors show heat resistance levels similar to that of *tdc-1.* These results indicate that the lack of tyramine underlies the oxidative and thermal resistant phenotype of *tdc-1* mutants. **e,** Scatter dot plot (line at the mean) showing pharyngeal pumping rates (pumps per minute) of wild-type, *tdc-1*, *tbh-1* and *tph-1* null mutants. *tph-1* (tryptophan hydroxylase) mutant animals, which lack serotonin, have a reduced pharyngeal pumping and were used as a control. Since *tdc-1* mutants have no obvious defects in pharyngeal pumping, dietary restriction is not likely to be the cause of the enhanced stress resistance and increased longevity. n=30 animals per condition. One-way ANOVA followed by Holm-Sidak post-hoc test versus wild type was used.

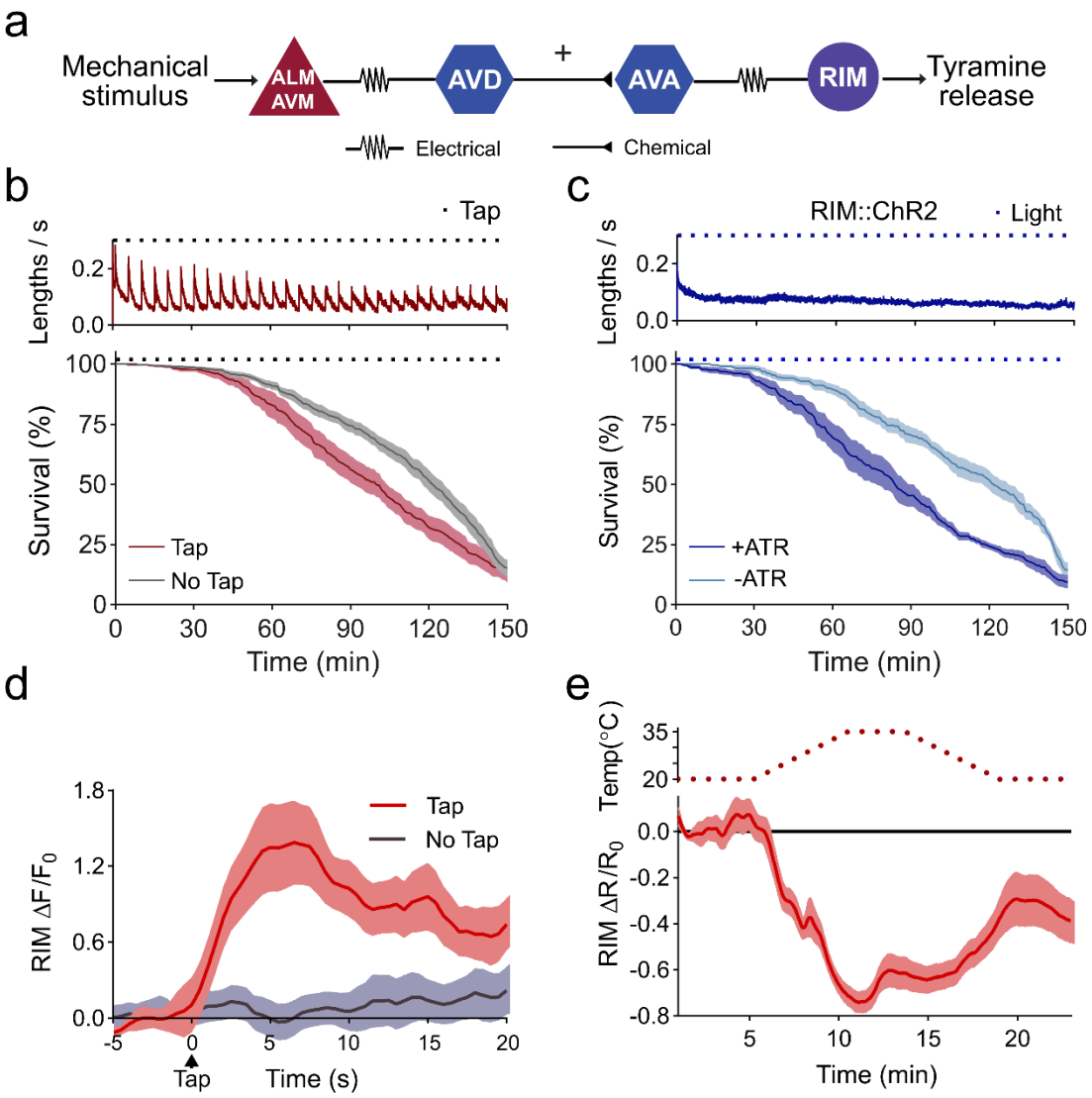

Figure III-5. The RIM neuron exhibits opposing activity patterns during the flight response *vs* exposure to environmental stressors. a, Circuit for *C. elegans* flight response triggered by mechanical stimulation. **b,** Velocity traces (top, n=10 independent experiments) and survival curves (bottom) during oxidative stress for wild-type animals in the absence (n=13 independent experiments) or presence (n=10 independent experiments) of a mechanical

stimulus (black squares). **c,** Velocity (n=7 independent experiments) and survival curves of animals exposed to oxidative stress and RIM optogenetic activation with (+ ATR) or without all-trans retinal (- ATR) (n=6 independent experiments per condition). Blue squares indicate light stimulus. **d,** Ca^{2+} dynamics of RIM::GCaMP6 ($\Delta F/F_0$) upon a mechanical stimulus t=0, tap: n=13 animals (red), no tap: n=14 animals (grey). **e,** Ca^{2+} responses upon heat stress (n=29 animals). Central lines indicate mean; shaded regions indicate SEM.

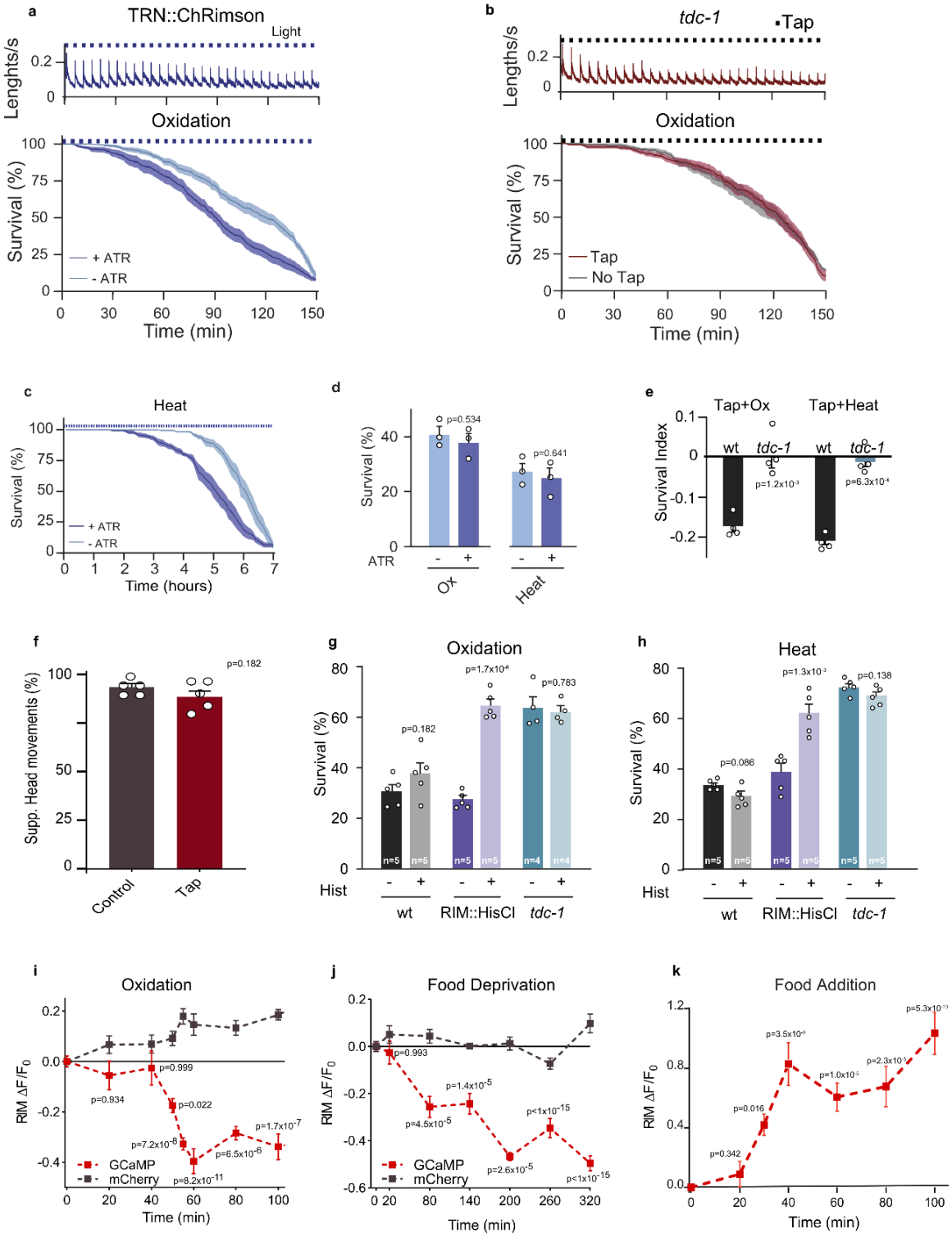
a
TRN::ChRimson
Light
Lenghts/s
0.2
0
Oxidation
100
75
50
25
0
Survival (%)
+ ATR
- ATR
0 30 60 90 120 150
Time (min)
b
tdc-1
Tap
Lengths/s
0.2
0
Oxidation
100
75
50
25
0
Survival (%)
Tap
No Tap
0 30 60 90 120 150
Time (min)
c
Heat
100
75
50
25
0
Survival (%)
+ ATR
- ATR
0 1 2 3 4 5 6 7
Time (hours)
d
Survival (%)
40
20
0
p=0.534
p=0.641
ATR
- + - +
Ox
Heat
e
Tap+Ox
Tap+Heat
Survival Index
0.1
0
-0.1
-0.2
wt
tdc-1
wt
tdc-1
p=1.2x10-3
p=6.3x10-4
f
Supp. Head movements (%)
100
50
25
0
p=0.182
Control
Tap
g
Oxidation
Survival (%)
80
60
40
20
0
p=0.182
p=1.7x10-4
p=0.783
n=5 n=5 n=5 n=5 n=4 n=4
Hist
- + - + - +
wt
RIM::HisCl
tdc-1
h
Heat
Survival (%)
80
60
40
20
0
p=0.086
p=1.3x10-3
p=0.138
n=5 n=5 n=5 n=5 n=5 n=5
Hist
- + - + - +
wt
RIM::HisCl
tdc-1
i
Oxidation
RIM ΔF/F0
0.2
0.0
-0.2
-0.4
p=0.999
p=0.934
p=0.022
p=1.7x10-7
p=7.2x10-8
p=6.5x10-6
GCaMP
mCherry
p=8.2x10-11
0 20 40 60 80 100
Time (min)
j
Food Deprivation
RIM ΔF/F0
0.2
0.0
-0.2
-0.4
-0.6
p=0.993
p=1.4x10-5
p=4.5x10-5
p<1x10-15
p=2.6x10-5
GCaMP
mCherry
p<1x10-15
0 20 80 140 200 260 320
Time (min)
k
Food Addition
RIM ΔF/F0
1.2
0.8
0.4
0.0
p=0.342
p=0.016
p=3.5x10-5
p=1.0x10-5
p=2.3x10-5
p=5.3x10-13
0 20 40 60 80 100
Time (min)

Figure III-6. Optogenetic activation of the flight response reduces the resistance to environmental stressors. a, Velocity traces and survival curves during strong oxidative stress (3 mM Fe^{2+}) for *tdc-1* mutants in the absence (grey) or presence (red) of a mechanical stimulus (tap), n=7 independent experiments of 40 animals were used for each condition. Velocity remains constant over the 2.5 h duration of recording in the absence of a stimulus, but increases rapidly in response to a mechanical plate tap (top). Tap delivery does not reduce stress resistance in *tdc-1* mutants (bottom) to oxidative stress. Black squares indicate timing of tap delivery. Red line: tap, grey line: no tap, shaded regions indicate SEM. **b,** Optogenetic activation of the mechanosensory neurons induces a flight response that results in velocity increases. Animals are exposed to 5 second pulses of 617nm light every 5 minutes (top), n=8 independent experiments. Optogenetic induction of the flight response reduces stress resistance to strong oxidation (3 mM Fe^{2+}) (bottom). Dark blue line: survival curve of animals raised with all-trans retinal (ATR) n=10 independent experiments; Light blue line: animals raised without ATR, n=9 independent experiments, 40 animals were used for each experiment. Central lines indicate mean, shaded regions indicate SEM, blue squares indicate timing of light delivery. Strain used: QW1649 *zfIs144[Pmec-4::Chrimson::wCherry, pL15EK].* **c,** Survival index of animals, with or without vibrational stimulus (plate tapping every 5 minutes) while being exposed to oxidative (1 h, 3 mM Fe^{2+}) or heat stress (4 h at 35°C). Tap impaired environmental stress resistance in the wild type, but

not in *tdc-1* mutant animals. Bars represent the mean ± SEM from 4 independent experiments (n=4). 60-90 animals per condition per experiment. Two-tailed Student´s test was used for statistical comparison versus the wild type. **d,** Percentage of animals suppressing head movements in response to anterior touch in unstressed animals and animals that have been subjected to a tap stimulus every 5 minutes for 2.5 hours. Tyramine release in response to mechanical stimulation induces a fast reversal and the suppression of head movements[13-14] Animals that were subjected to 30 taps administered every 5 minutes still suppress their head movements in response to anterior touch. This indicates that tyramine continues to be released during the tapping protocol and that RIM neuronal activity is not affected. Bars represent the mean ± SEM from 5 independent experiments (n =5). 20 animals per condition per experiment were used. Two tailed Student's t-test. **e,** Survival curves of animals exposed to heat stress (7 h at 35°C) with simultaneous optogenetic activation of mechanosensory neurons (QW1649: *zfis144[Pmec-4::Chrimson::wCherry +pL15EK])*. Animals expressing Chrimson in mechanosensory neurons were cultivated in the presence or absence of all-*trans* retinal (ATR) and subjected to 5 second 617 nm light pulses every 5 minutes at 35°C. Blue squares indicate timing of light delivery. Central lines indicate mean, shaded regions indicate SEM. Optogenetic activation of mechanosensory neurons reduced heat resistance in animals raised on ATR (n=6 independent experiments) compared to animals raised without ATR (n=5 independent experiments), 40 animals were used for each experiment. **f,**

Stress survival analysis of animals grown in the presence or absence of ATR without light stimulation. Oxidative stress: (Ox,1 h, 3 mM Fe^{2+}); Heat (4 h at 35°C). ATR does not modify animal resistance to these environmental stressors. Bars represent the mean ± SEM from 3 independent experiments (n=3). 40-50 animals per condition per experiment. No significant differences were observed indicating that ATR does not affect stress resistance, two-tailed Student's t-test. **g-h,** Stress survival of animals expressing the histamine-gated chloride channel HisCl in the RIM neuron (RIM::HisCl). Animals were exposed to 10 mM histamine (Hist) prior and during oxidation (1 h, 15 mM Fe^{2+}, **g**) or heat (4 h, 35°C **h**). Specific silencing of the RIM neuron leads to increased animal resistance to environmental stress. Bars represent mean ± SEM. The numbers of independent experiments performed for each condition (n) are indicated in the figure. 80-100 animals per condition per experiment were used. Statistical comparison versus same strain in the absence of histamine was calculated using two-tailed Student's t-test. **i-j,** Ca^{2+} responses upon oxidative-stress (**i**, GCaMP: n=36 animals, mCherry: n=15 animals) and food deprivation (**j**, GCaMP: n=30 animals, mCherry: n=6 animals). Grey trace: mCherry fluorescence insensitive to calcium. Central lines and dots indicate mean, shaded regions and error bars indicate SEM (One-way ANOVA, compared to initial time point, Dunnett's multiple comparison). **k,** Overall RIM Ca^{2+} levels (ΔF/F) increase upon refeeding (with *E. coli)* of animals that have been starved overnight. Data are represented as mean ± SEM. n=36 for each data point, 6 independent experiments. Fluorescence

increase is initiated within 10 minutes after food addition indicating that RIM activity quickly recovers and is likely not due to GCaMP expression changes. One-way ANOVA, compared to initial time point, Dunnett's multiple comparison.

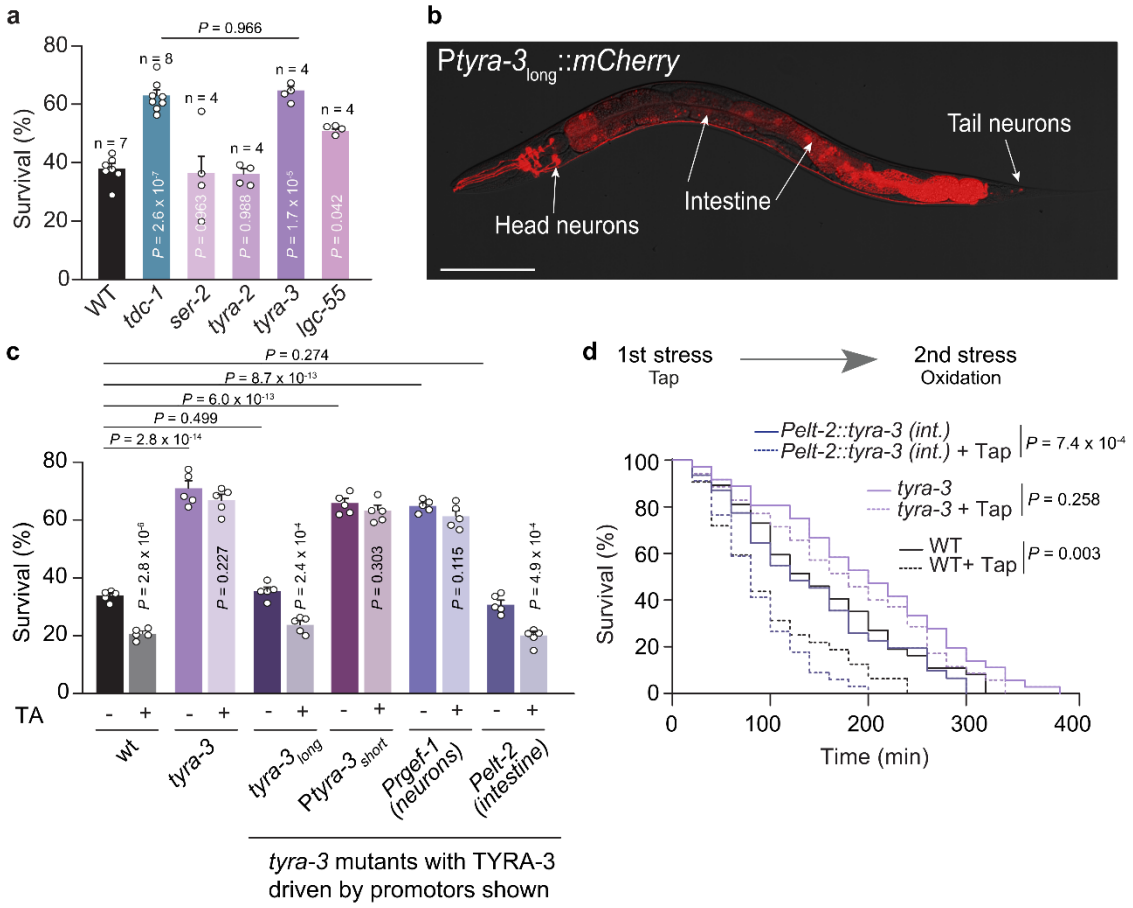

Figure III-7. The GPCR TYRA-3 is required in the intestine for tyraminergic modulation of the stress response.

a, Resistance of tyramine receptor mutants exposed to oxidation (mean ± SEM, for each condition n is indicated in the figure, 40-60 worms per condition per experiment). One-way ANOVA, Holm-Sidak's post-hoc test for multiple comparisons was used. **b,** Expression of a 3.4 kb *Ptyra-3*$_{long}$::mCherry reporter. Scale bar: 150 µm. **c,** Survival percentages (mean ± SEM, n=5) of *tyra-3* mutant animals expressing a *tyra-3* cDNA driven by P*tyra-3*$_{long}$ (Endogenous), P*tyra-3*$_{short}$ (Neuronal subset), P*rgef-1* (Pan-neuronal) or P*elt-2* (Intestinal) promoter

upon exposure to oxidative stress, with or without tyramine (10 mM). For conditions without TA, One-way ANOVA, Holm-Sidak's post-hoc test versus wild type was used. Two-tailed t test was used for comparison within each strain (no TA vs TA). **d,** Representative survival curves of naïve (solid line) or pre-tapped animals (dashed line) exposed to oxidation (two-sided log-rank). The experiment was independently repeated 3 times (n=3) with similar results.

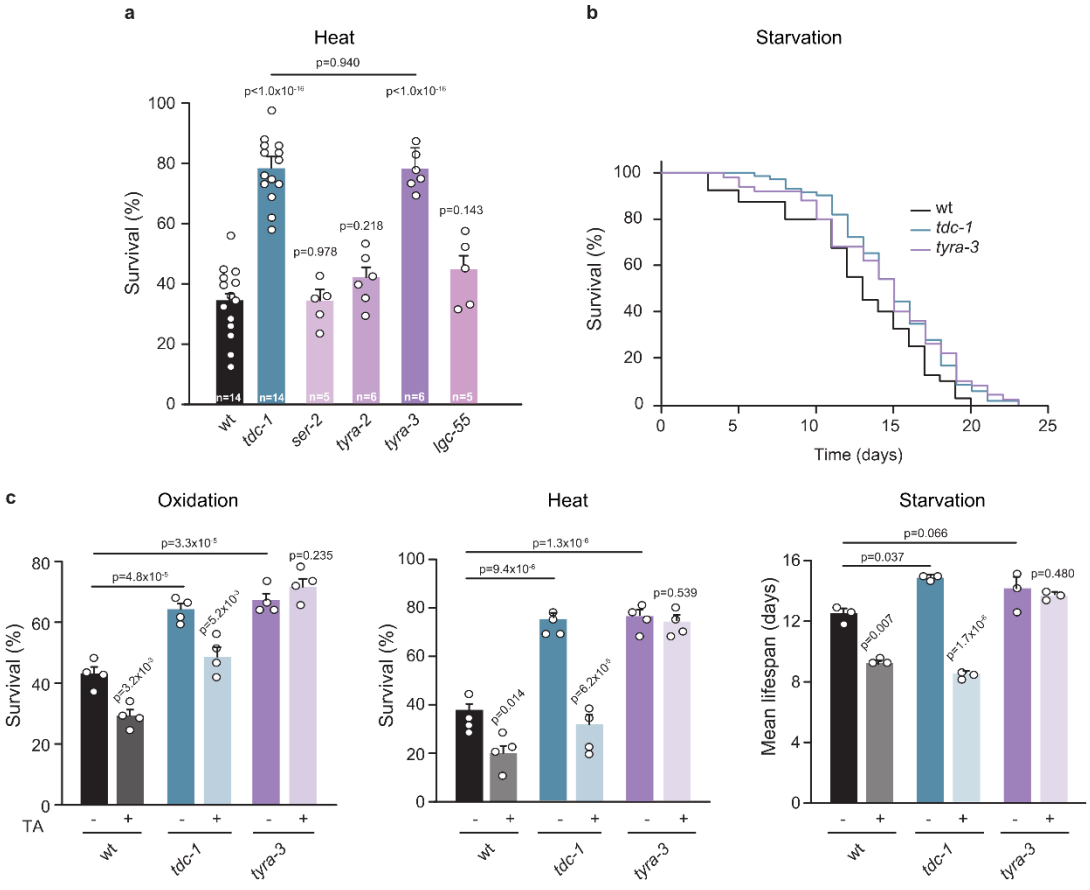

Figure III-8. Tyramine modulates the stress response through the activation of the GPCR TYRA-3. a, Resistance of wild-type and tyramine receptor mutant animals exposed to heat (4 h, 35 ºC). Only *tyra-3* mutant animals are as resistant as *tdc-1* mutant animals to heat stress. The numbers of independent experiments performed for each condition (n) are indicated in the figure. 80-100 animals per condition per experiment were used. One-way ANOVA followed by Holm-Sidak post-hoc test for multiple comparisons. **b,** Representative survival curves of wild-type, *tdc-1* and *tyra-3* mutants exposed to starvation. Animals were removed from food at the L4 stage. The curves are representative of three

independent replicates with similar results (n=3). 40-80 animals were used per condition per experiment **c,** Resistance of wild-type, *tdc-1* and *tyra-3* mutant animals exposed to oxidation, heat or starvation in the absence or presence of exogenous TA (10 mM). Detrimental effects of exogenous TA on stress resistance are abolished in *tyra-3* mutant animals. Bars represent mean ± SEM, n = 4 for oxidation and heat and n=3 for starvation, 60-80 animals/condition. For conditions without TA, One-way ANOVA followed by Holm-Sidak post-hoc test versus wild-type was used. For conditions with TA, two-tailed Student´s t test (versus same strain without TA) was used.

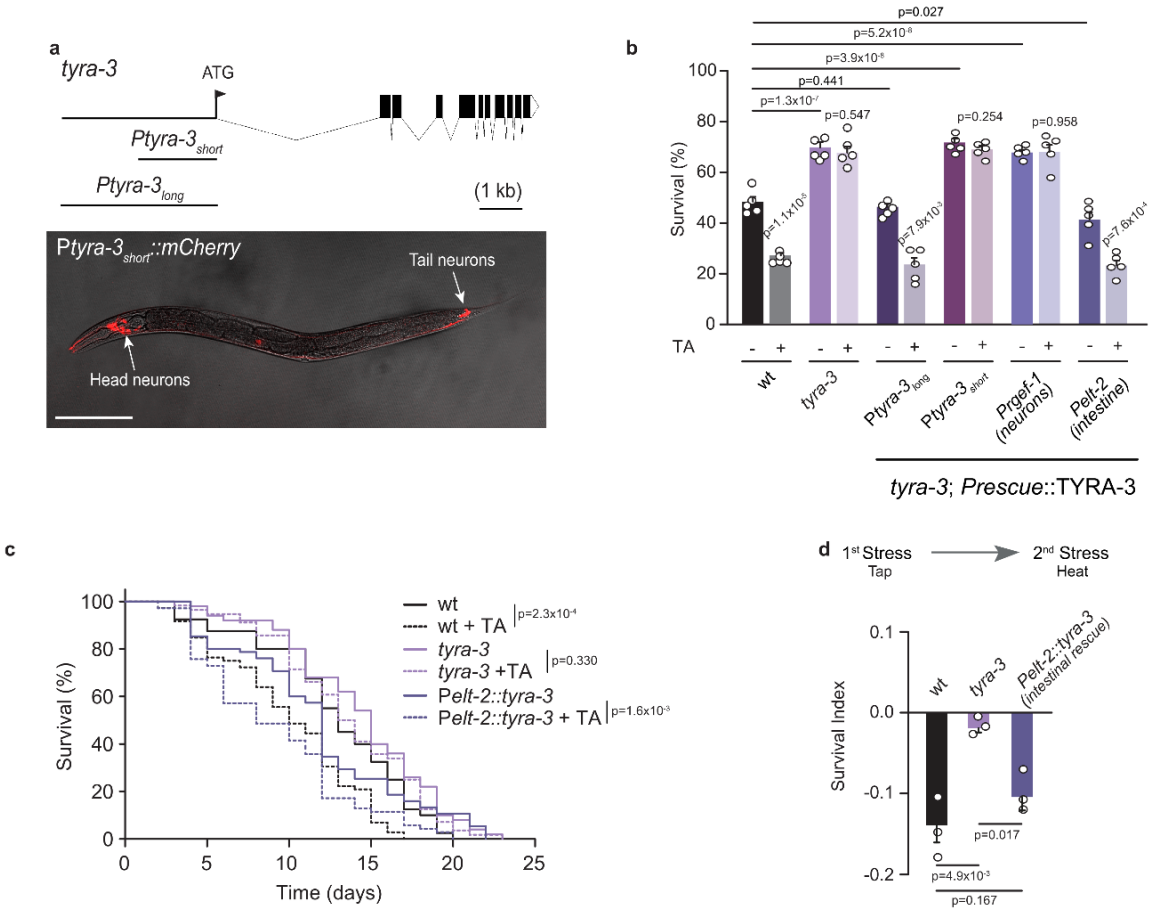

Figure III-9. *tyra-3* acts in the intestine to inhibit stress resistance. a, Top, Gene structure of *tyra-3*. Coding sequences are represented by black boxes. **Bottom,** Confocal images of transgenic animals expressing mCherry driven by a short fragment of *tyra-3* promoter (short promoter, 1.8 kb upstream of start codon). mCherry expression is limited to a subset of head and tail neurons (and vulval cells). Scale bar: 200 µM. A mCherry reporter driven by a long 3.4 kb promoter (*Ptyra-3*$_{long}$) show expression in both, neurons and intestine (see manuscript Fig 3b). **b,** Survival percentages of *tyra-3* mutant animals expressing

tyra-3 cDNA driven by P*tyra-3*$_{long}$ (Endogenous expression), P*tyra-3*$_{short}$ (Expression in a subset of neurons), P*rgef-1* (Pan-neuronal) or P*elt-2* (Intestinal) promoter upon exposure to heat stress with or without tyramine (10 mM). Bars represent mean ± SEM, n=5, 80-100 animals/condition. For conditions without TA, One-way ANOVA followed by Holm-Sidak post-hoc test versus wild-type was used. For conditions with TA, two-tailed Student´s t test (versus same strain without TA) was used. Expression of *tyra-3* in the intestine, but not in neurons, was sufficient to restore the stress sensitivity and the negative impact of exogenous tyramine on heat. **c,** Representative Kaplan-Meier survival curves of the wild-type, *tyra-3* null mutants and animals expressing *tyra-3* solely in the intestine(P*elt-2::tyra-3*). Animals were food deprived as L4s in the absence or presence of 10 mM TA. The curves are representative of three independent replicates with similar results (n=3). 40-80 animals were used per condition per experiment. Two-tailed log-rank test was used for statistical comparison. Expression of *tyra-3* in the intestine restores the negative impact of exogenous tyramine lifespan upon starvation **d,** SI to heat exposure (4 h, 35ºC) of animals pre-exposed to vibrational stimulus (tapping). Intestinal expression of *tyra-3* restores the detrimental effect of tapping on the stress response. Bars represent mean ± SEM, n = 3, 30-40 animals/condition. One-way ANOVA followed by Holm-Sidak post-hoc test for multiple comparisons.

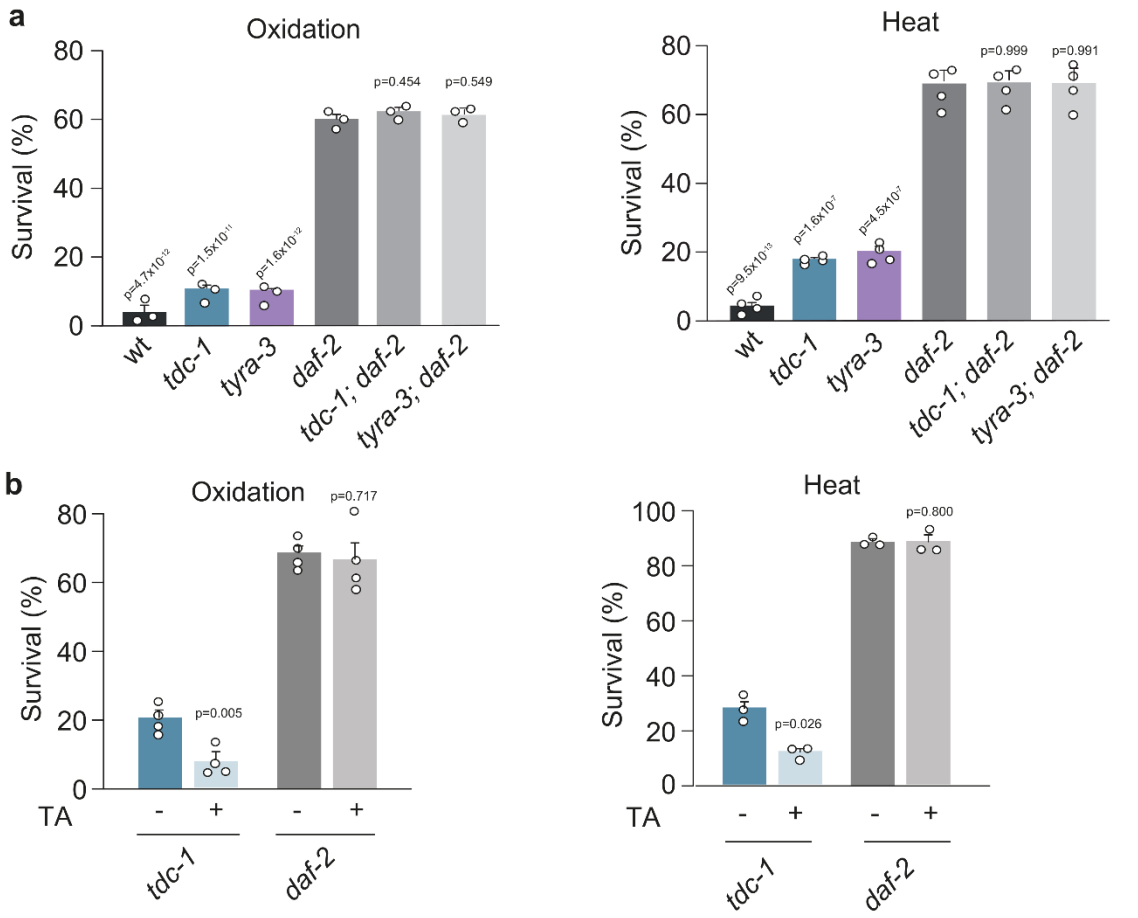

Figure III-10. Tyraminergic inhibition of stress response depends on the DAF-2 insulin receptor. a, Survival percentage of animals exposed to oxidative stress (3 h, 15 mM Fe^{2+}) or heat (7 h, 35ºC,). *tdc-1; daf-2* and *tyra-3; daf-2* double mutants are as resistant as *daf-2* single mutant animals. Bars represent mean ± SEM, n = 3 (heat) and n=4 (oxidation), 80-100 animals per condition per experiment. One-way ANOVA followed by Holm-Sidak's test for multiple comparisons compared to *daf-2* mutants. **b,** Survival percentage of animals exposed to oxidative stress (3 h, 15 mM $Fe^{2+,}$ top) or heat (7 h, 35ºC, bottom) in

the absence and presence of exogenous TA (10 mM). Detrimental effect of exogenous TA heat or oxidative stress resistance is not observed in *daf-2* mutant animals. Bars represent the mean ± SEM, n = 3 (heat) and n=4 (oxidation). 80-100 animals per condition per experiment. Two-tailed Student's t-test versus each strain without TA. This indicates that tyraminergic regulation of environmental stress response depends on *daf-2*.

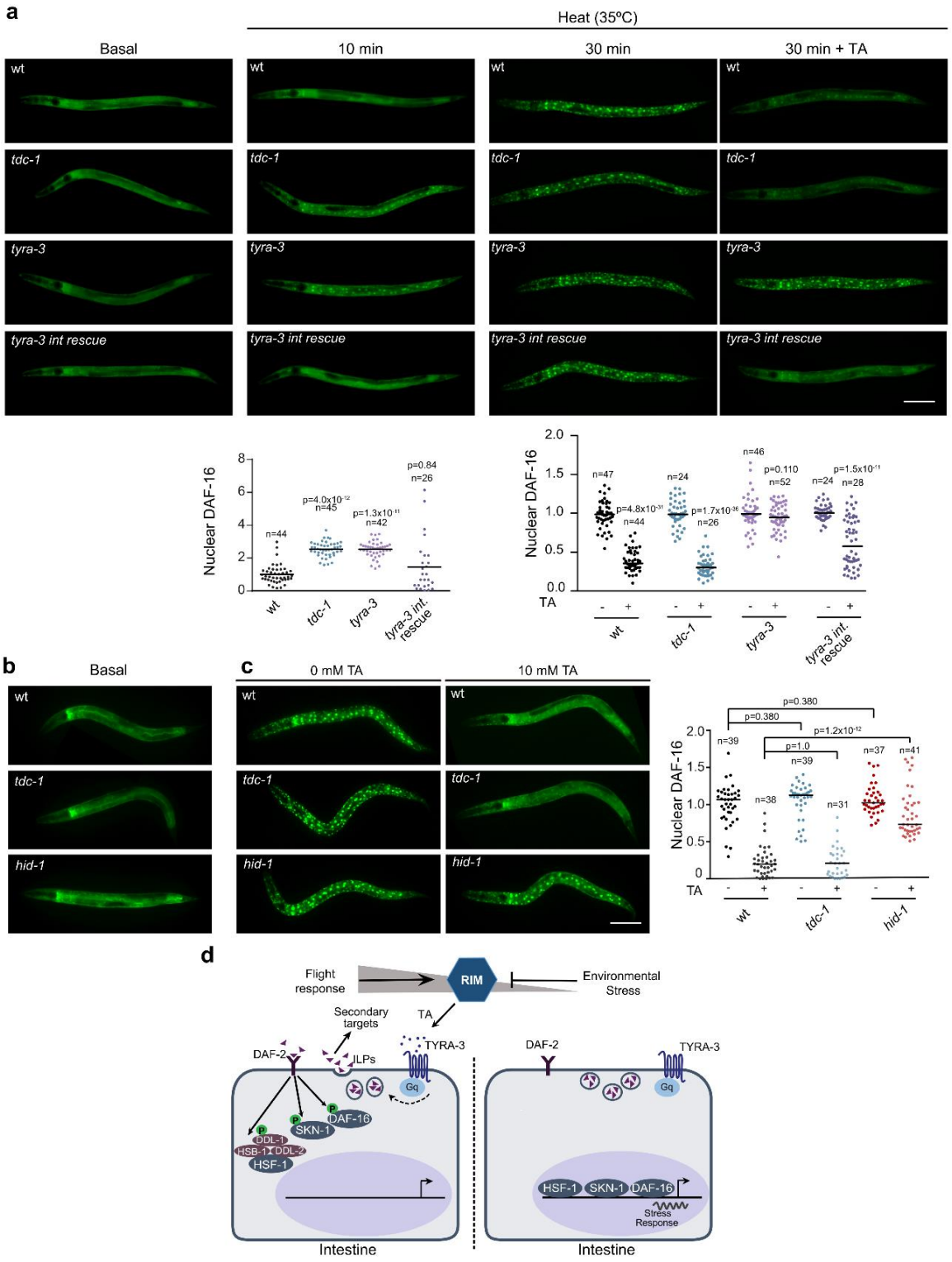
a
Heat (35ºC)
Basal
10 min
30 min
30 min + TA
wt
tdc-1
tyra-3
tyra-3 int rescue
Nuclear DAF-16
p=4.0x10-12
n=45
p=1.3x10-11
n=42
p=0.84
n=26
n=44
wt
tdc-1
tyra-3
tyra-3 int. rescue
p=4.8x10-31
p=1.7x10-36
p=0.110
p=1.5x10-11
n=47
n=24
n=46
n=52
n=28
TA
b
Basal
hid-1
c
0 mM TA
10 mM TA
p=0.380
p=1.2x10-12
p=1.0
n=39
n=38
n=31
n=37
n=41
d
Flight response
RIM
Environmental Stress
Secondary targets
TA
DAF-2
ILPs
TYRA-3
Gq
DAF-16
SKN-1
DDL-1
HSB-1
DDL-2
HSF-1
Intestine
Stress Response

Figure III-11. Tyramine signaling inhibits stress-dependent nuclear translocation of DAF-16. a, DAF-16a/b::GFP localization in basal condition and upon exposure to heat (35ºC) for 10 min and 30 min in the absence or presence of tyramine (10 mM TA, 30 min). Scale bar: 150 µm. Bottom, Corresponding scatter dot plot with the number of cells with nuclear DAF-16 per animal (normalized to naïve animals, line at the mean). For 10 min heat conditions, One-way ANOVA Holm-Sidak's post-hoc test versus wild-type was used. For 35 min heat conditions, a two-tailed t-test (no TA vs TA) was used. The experiment was repeated 4 times (n=4). For each condition n is indicated in the figure. **b-c,** DAF-16a/b::GFP localization in *hid-1* mutants in basal conditions (b) and upon exposure to heat (35ºC, 30 min) in the absence or presence of tyramine (c) . Right, scatter dot plot with nuclear DAF-16 expression normalized to naïve animals (line at the mean). One-way ANOVA (Kruskal-Wallis test) and Dunn´s post-hoc test were used. The experiment was repeated 3 times (n=3). For each condition, n is indicated in the figure. **d,** Model: Tyraminergic modulation of the DAF-2/IIs pathway.

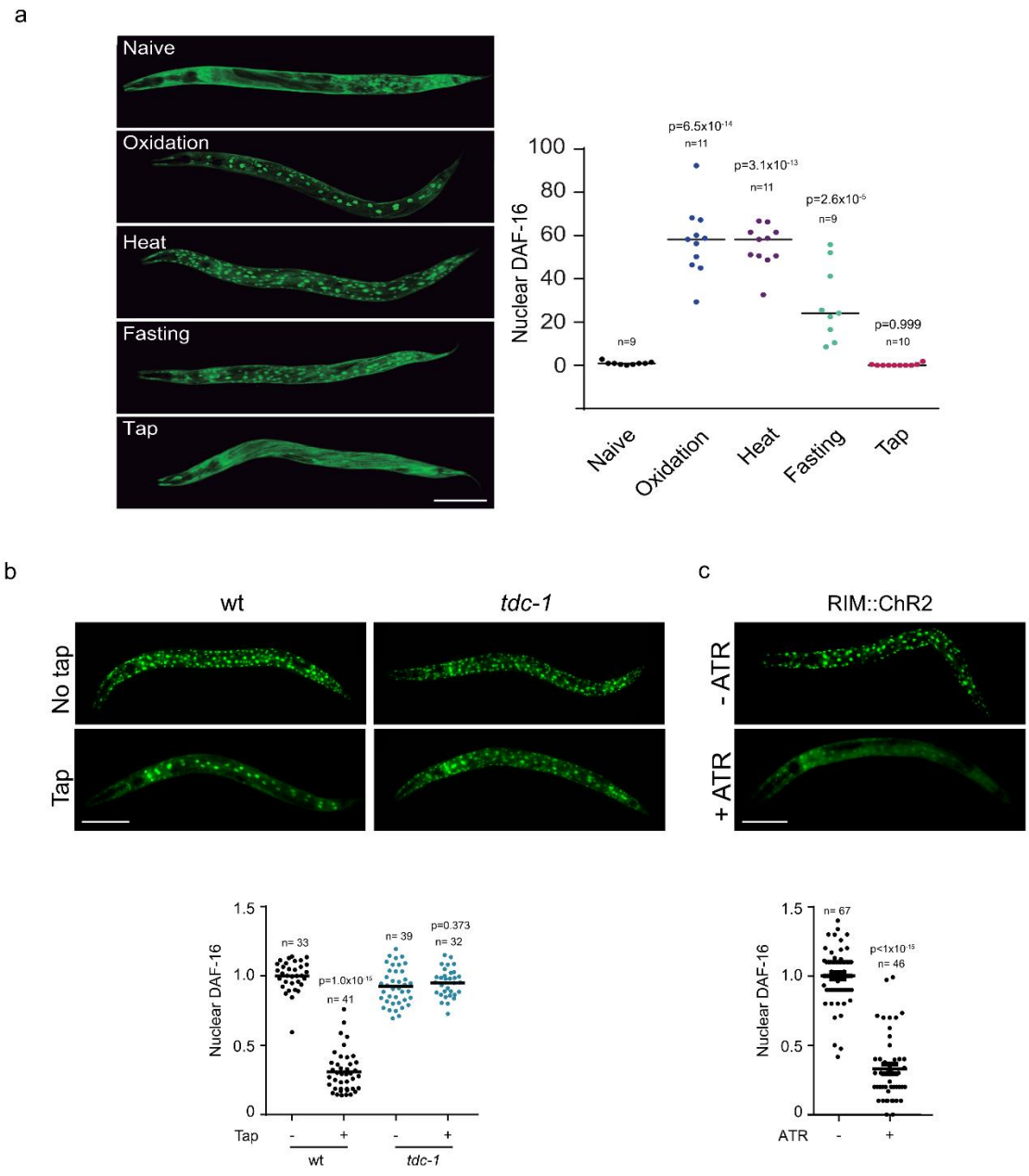

Figure III-12. The flight response inhibits stress-dependent nuclear translocation of DAF-16. a, L**eft,** Fluorescence images of young adults expressing the translational reporter *Pdaf-16*::*DAF-16a/b::GFP* upon exposure to mild stressors as described in Fig. III-1: 1 h 1 mM Fe^{2+} (Oxidation: Ox), 0.5 h

35ºC (Heat: ºC), 8 h food deprivation (Fasting: Fst), or tap stimulus every 5 min for 2.5 h (Tap). Fluorescence images of young adults expressing the translational reporter *Pdaf-16*::*DAF-16a/b::GFP*. Right, Scatter dot plot (line at the mean) with the number of cells with nuclear DAF-16 per animal. n for each condition is indicated in the figure. One-way ANOVA, Dunnett´s post-hoc test were used compared to naïve. Scale bar: 150 µm. **b**, Top, DAF-16 localization in wild-type and *tdc-1* mutant animals exposed to vibrational stimulus (tap every 5 minutes) upon heat exposure (37ºC, 1 h). Bottom, Scatter dot plot (line at the mean) with the number of cells with nuclear DAF-16 per animal (normalized to naïve animals (left). n for each condition is indicated in the figure. Two-tailed Student´s t-test was used versus same strain without tapping. Scale bar: 150 µm. Repetitive induction of the flight response impairs DAF-16 localization to the nucleus in wild-type, but not in *tdc-1* mutant animals. **c,** Top, DAF-16 localization upon heat exposure (37ºC, 1 h) of RIM::ChR2 transgenic animals raised with or without all-trans retinal (ATR) subjected to 5 second 617 nm light pulses every 5 minutes. Bottom, Scatter dot plot (line at the mean) with the number of cells with nuclear DAF-16 per animal (normalized to ATR-treated animals). n for each condition is indicated in the figure. Two-tailed Student´s t-test was used. Scale bar: 150 µm. Repetitive optogenetic activation of the tyraminergic neuron RIM impairs DAF-16 nuclear translocation.

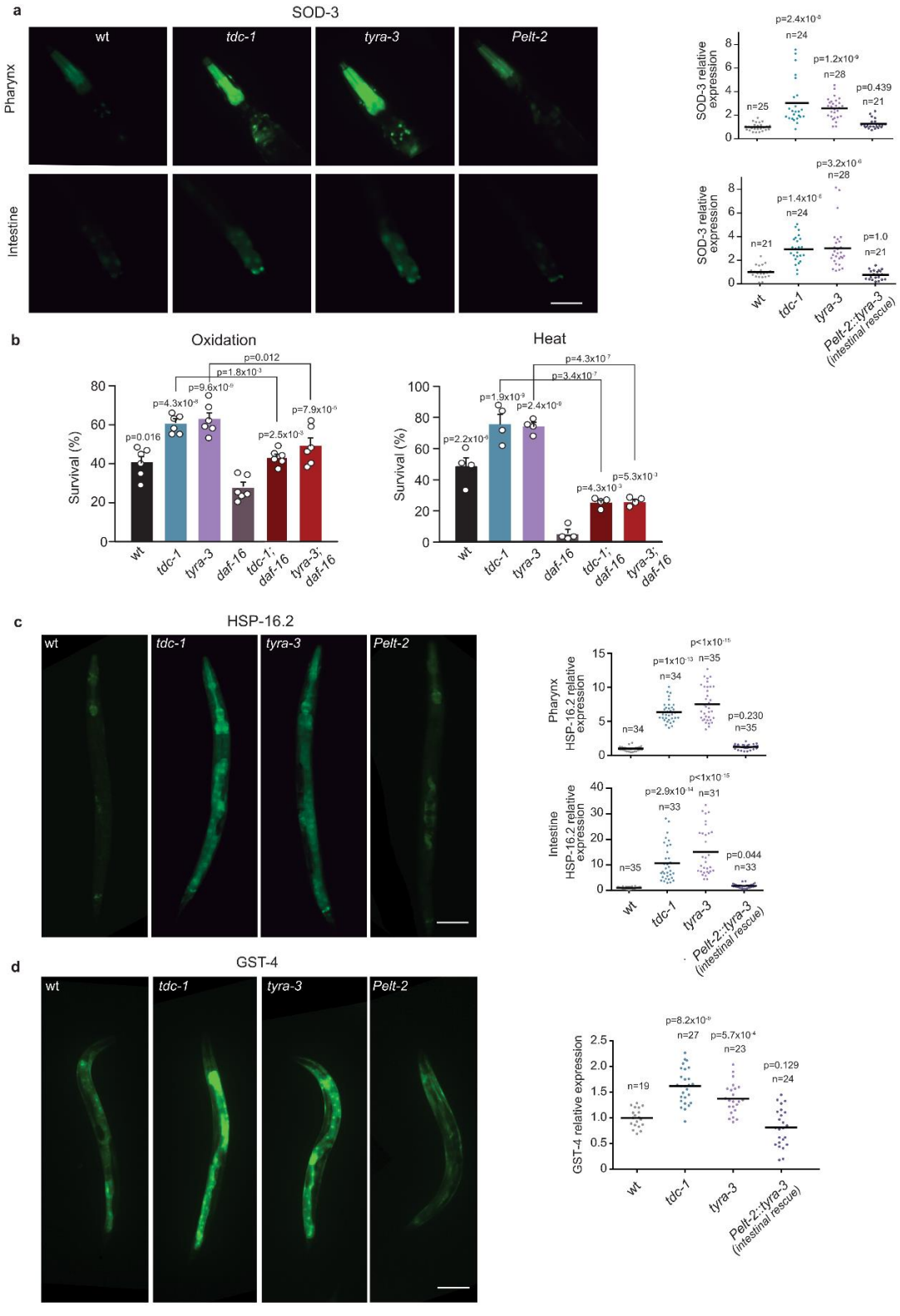
a
SOD-3
wt
tdc-1
tyra-3
Pelt-2
Pharynx
Intestine
SOD-3 relative expression
p=2.4x10-8
n=24
p=1.2x10-9
n=28
p=0.439
n=21
n=25
p=3.2x10-6
n=28
p=1.4x10-8
n=24
p=1.0
n=21
n=21
wt
tdc-1
tyra-3
Pelt-2::tyra-3 (intestinal rescue)
b
Oxidation
Heat
Survival (%)
p=0.012
p=1.8x10-3
p=9.6x10-5
p=4.3x10-8
p=7.9x10-6
p=2.5x10-3
p=0.016
p=4.3x10-7
p=3.4x10-7
p=1.9x10-9
p=2.4x10-8
p=2.2x10-6
p=4.3x10-3
p=5.3x10-3
wt
tdc-1
tyra-3
daf-16
tdc-1; daf-16
tyra-3; daf-16
c
HSP-16.2
wt
tdc-1
tyra-3
Pelt-2
Pharynx HSP-16.2 relative expression
p<1x10-15
p=1x10-13
n=35
n=34
p=0.230
n=35
n=34
Intestine HSP-16.2 relative expression
p<1x10-15
p=2.9x10-14
n=31
n=33
p=0.044
n=33
n=35
wt
tdc-1
tyra-3
Pelt-2::tyra-3 (intestinal rescue)
d
GST-4
wt
tdc-1
tyra-3
Pelt-2
GST-4 relative expression
p=8.2x10-9
n=27
p=5.7x10-4
n=23
p=0.129
n=24
n=19
wt
tdc-1
tyra-3
Pelt-2::tyra-3 (intestinal rescue)

Figure III-13. Tyramine signaling mutants display an ectopic activation of stress response genes. a, Left**,** Representative Fluorescence images (40 x magnification) of the pharynx and intestine of animals expressing *Psod-3::GFP* in different genetic backgrounds after 20 min of exposure to 5 mM Fe^{++}. Scale bar: 100 µm. Right, Corresponding quantification of the fluorescence level per animal in the pharynx and intestine. Scatter dot plot (line at the mean) with the relative expression of *sod-3* normalized to naïve animals. n for each condition is indicated in the figure. One-way ANOVA (Kruskal-Wallis test) and Dunn´s post-hoc test were used **b,** Survival percentage of animals exposed to oxidative stress (1 h, 15 mM Fe^{2+}) or heat (4 h, 35ºC). *tdc-1; daf-16* and *tyra-3; daf-16* double mutants were compared to the corresponding single mutants. Bars represent mean ± SEM. For oxidation resistance experiments n=6. For heat resistance experiments n=4. 80 animals per condition, per experiment. One-way ANOVA, Holm-Sidak post-hoc test was used to compare against *daf-16* mutants. Two-tailed Student´s t-test was used to compare *tdc-1; daf-16* and *tyra-3; daf-16* double mutants with *tdc-1* and *tyra-3* single null mutants, respectively. *tdc-1; daf-16* and *tyra-3; daf-16* double mutants display intermediate resistance phenotypes. This indicates that tyraminergic control of the stress response does not depend exclusively on *daf-16*. **c,** Left**,** Representative Fluorescence images (20 x magnification) of young adult animals expressing *Phsp16.2::GFP* in different genetic backgrounds after 15 min of heat (35ºC). Scale bar: 150 µm. Right, Corresponding quantification of the fluorescence level per animal in

pharynx and intestine. Scatter dot plot (line at the mean) with the relative expression of *Phsp16.2::GFP* normalized to naïve animals. n for each condition is indicated in the figure. One-way ANOVA (Kruskal-Wallis test) and Dunn´s post-hoc test were used compared to naïve. **d,** Left**,** Representative Fluorescence images (20 x magnification) of young adult animals expressing *Pgst-4::GFP* in different genetic backgrounds in basal conditions (20°C on NGM plates seeded with OP50 as a food source). Scale bar: 100 µm. Right, Corresponding quantification of the fluorescence level per worm. Scatter dot plot (line at the mean) with the relative expression of *Pgst-4::GFP* normalized to naïve animals. n for each condition is indicated in the figure. One-way ANOVA and Dunnett´s post-hoc test were used compared to naïve. These experiments indicate that distinct DAF-2 dependent transcription factors are activated in *tdc-1* and *tyra-3* mutants: DAF-16/*sod-3* HSF-1/*hsp16.2* and SKN-1/*gst-4.*

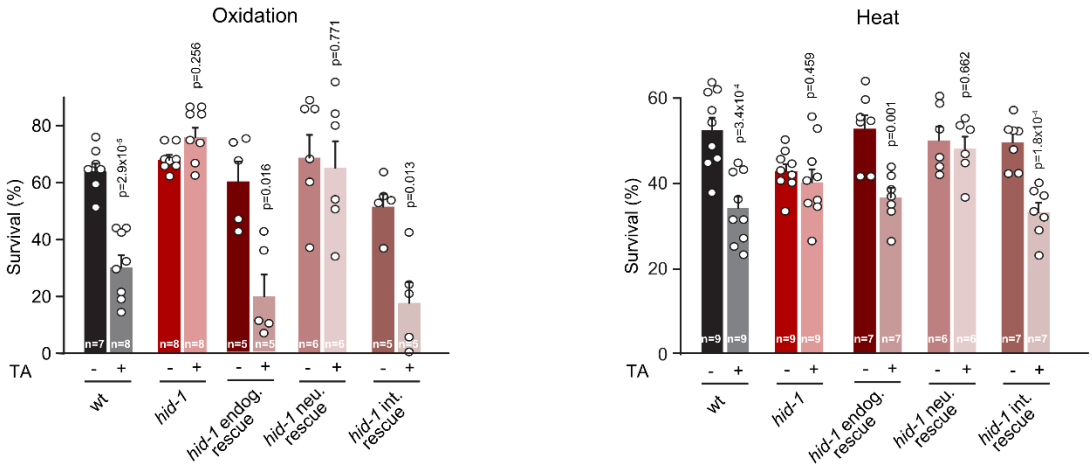

Figure III-14. Tyramine's inhibition of stress resistance requires intestinal *hid-1*

Survival percentages of young adult *hid-1* mutant animals expressing either the endogenous (endog. rescue), the neuronal (neu. rescue) or the intestinal (int. rescue) rescue constructs exposed to oxidation (left) or heat (4 h, 35ºC) (right) in the absence or presence of 10 mM TA. Bars represent mean ± SEM from independent experiments. The number of independent experiments for each condition (n) is shown in the figure. 80-100 animals per condition per experiment were used. A Two-tailed Student´s t test (versus same strain without TA) was used. *hid-1* expression in the intestine in *hid*-1 mutants restores the negative impact of tyramine on oxidative and heat stress resistance.

Chapter IV: Discussion

Neuromodulatory control of stress responses

The work presented in this thesis has explored how neuromodulators shift the internal state of an animal in order to respond to a specific type of stressor. A key biological problem is that different stressors impose distinct challenges to an organism, and the nature of the stressor dictates the appropriate response. Ideally, an animal would be simultaneously prepared for, or protected against, all threats, however energetic limitations make this unpractical. Therefore, an animal must prioritize certain physiological and behavioral processes over others but be able to change priorities in response to internal or environmental conditions. Volume transmission of peptides and other neuromodulators is an ideal mechanism to affect such changes as signaling molecules can diffuse over large areas and alter the output of neural circuits (Jan and Jan, 1982).

In chapter II we show how the neuropeptide FLP-18, in conjunction with the monoamine tyramine, shift the behavioral state of *C. elegans* and elicit an escape response to a predatory threat. This escape response shares many features with reorientations during foraging behavior, from the order of motor programs (reversal-omega turn-forward locomotion) to the neuronal circuit that generates the behavior (Chalfie *et al.*, 1985; Gray, Hill and Bargmann, 2005). Despite the similarity, we show in appendix I that the escape response is distinct from reorientations during foraging, with much faster and longer reversals, and a prolonged period of rapid forward movement following the omega turn.

How does the *C. elegans* nervous system generate this behavioral flexibility? The difference in behavioral output between spontaneous reversals and stimulated reversals comes in part from the recruitment of at least one pair of additional neurons, the AVD, which are not active during spontaneous reversals (Kawano *et al.*, 2011). The AVD are pre-motor interneurons which synapse on A-type motor neurons that drive backward locomotion. It is possible that the additional excitatory input from the AVD acts to increase the velocity of reversals during the escape response. In Chapter II we show that FLP-18 modulates muscle activity by raising calcium levels. In addition to increased neuronal input, peptidergic modulation may account for the differences observed between reversals in foraging behavior and during the escape response.

Interestingly, FLP-18 plays a role in the foraging strategy known as area restricted search (ARS) but has an opposite impact on reversals and turning to what we find during the escape response. *C. elegans* employ ARS when removed from food by varying the frequency of reorientations (reversals and turns) as a function of time. Immediately after removal from food reorientations are elevated in an attempt to identify the previously encountered food, after 10-15 minutes if no food is encountered animals will reduce reorientations and switch to a dispersal mode where they make long forward runs to find locate a new food source (Hills, Brockie and Maricq, 2004; Wakabayashi, Kitagawa and Shingai, 2004; Gray, Hill and Bargmann, 2005). Cohen *et al.* (2009) found that *flp-18* mutants do not upregulate reversals and omega turns as much as wild

type animals in the first minutes following removal from food, and furthermore they fail to suppress reversals and turns during the dispersal phase. The effects of FLP-18 on foraging were found to be mediated through the G-protein coupled receptor (GPCR) NPR-4. These results indicate that during foraging, FLP-18 has a context specific role in regulating reversals and omega turning, first increasing then later decreasing their frequency as time off food grows.

Our results from chapter II point to a different but related role of FLP-18 in reversal and omega turning during the escape response, where FLP-18 acts through NPR-5 to increase omega turning and reversal frequency. These findings most closely resemble the role of FLP-18 during the ARS foraging strategy where reversals and turns are increased but are opposite to dispersal where FLP-18 acts to suppress reversals and omega turns.

How does the same neuromodulator differentially regulate a common behavior in these different contexts? One possibility is that the site of release is different in foraging behavior versus during the escape response. The AIY interneurons receive significant input from sensory neurons that respond to food odors, and restoring FLP-18 expression specifically in the AIY rescued *flp-18* mutant foraging defects (Cohen *et al.*, 2009). Whereas our results indicate that triggering the escape response causes FLP-18 release from the AVA and RIM neurons (Figure II-7) which are downstream of mechanosensory neurons. FLP-18 signaling from the AIY is likely extrasynaptic (Cohen *et al.*, 2009), and tyramine, a putative co-transmitter with FLP-18 in the RIM, activates the GPCR

SER-2 in VD motor neurons through extrasynaptic diffusion (Donnelly *et al.*, 2013). If FLP-18 from the AIY or the RIM and AVA can diffuse to affect distant targets during either foraging or the escape response, how does the circuit distinguish between these two signals to appropriately increase or decrease reversals and turns? The extent of diffusion for peptides can be limited by the action of extracellular peptidases which inactivate neuropeptides. Peptidase activity has been shown to allow two neurons using the same peptide to elicit different behavioral effects in the stomatogastric ganglion of the crab *Cancer borealis* (Wood and Nusbaum, 2002).

The *C. elegans* genome encodes 22 members of the neprilysin metallopeptidase family, referred to as NEP-1 through NEP-22, however the impact of most of these proteins on behavior has not been thoroughly investigated. NEP-1 has been shown to affect peptide induced enhancement of pharyngeal pumping rate and locomotion (Spanier *et al.*, 2005), suggesting NEP genes do play a role in regulating neuropeptide signaling in *C. elegans*. It is unknown whether any NEP proteins spatially regulate FLP-18 signaling regarding foraging and escape behavior, however NEP-2 is expressed in body wall muscle (Yamada *et al.*, 2010), the site of action of FLP-18 in escape behavior, and NEP-11 is expressed in several head neurons including the AVA (Khraiwesh and Salehi-Ashtiani, 2017) where FLP-18 functions in foraging behavior (Cohen *et al.*, 2009). It would be interesting to see whether mutations in these genes affect the behavioral specificity of FLP-18 release from AIY or escape circuit neurons.

Another aspect of neuropeptide signaling that could account for differential effects is that many neuropeptide genes encode more than one biologically active peptide which are cleaved to produce mature peptides (Li and Kim, 2008). While putative neuropeptides can be predicted from sequence analysis of neuropeptide genes, it does not guarantee that all peptides are equally expressed. For example, the neuropeptide gene *flp-1* encodes 8 putative neuropeptides, only 6 of which have been biochemically isolated (Rosoff *et al.*, 1993). Interestingly, the *flp-1* gene is subject to alternative splicing that produces two transcripts, each of which encode a different subset of peptides (Rosoff, Burglin and Li, 1992; Rosoff *et al.*, 1993). This raises the possibility that a single gene can produce differential peptide signaling between cell types, developmental stages, or sexes. The *flp-18* gene has two alternate promotors and encodes 6 distinct putative peptides (Li *et al.*, 1999). While all 6 *flp-18* peptides have been biochemically identified from whole animal lysate (Husson *et al.*, 2005), cell specific differential expression of specific *flp-18* peptides could still occur as a result of alternative splicing, as with *flp-1,* or through differences in the expression of peptide processing enzymes such as the proprotein convertase *egl-3* which is involved in peptide maturation.

Peptidergic signaling from the AIY and RIM could result in differential behavioral effects through the selective activation of different receptor types in different target tissues. It was demonstrated *in vitro* that the FLP-18 receptors NPR-4 and NPR-5 have different affinities for the individual FLP-18 peptides

(Cohen *et al.*, 2009). Whether the AIY and RIM release different subsets of FLP-18 peptides or not, the spatial distribution of receptor subtypes relative to the site of release could result in differential effects. For example, if a low affinity receptor is close to the site of release, it may be activated by the high concentration of peptide. Whereas if the releasing neuron is further away, diffusion may dilute peptide concentration enough to render a low affinity receptor insensitive to the same peptide. Expression of rescuing constructs containing or lacking individual FLP-18 peptide coding sequences in *flp-18* could shed light on their function in specific behaviors, however disruption of the structure of the neuropeptide precursor protein could lead to problems in neuropeptide maturation and make results difficult to interpret.

NPR-5 signaling pathway in muscle

In chapter II we show that FLP-18 coordinates bending and omega turning behavior during the escape response by activating NPR-5 in neck and body wall muscle which results in an increase in intracellular calcium. Kubiak *et al.* (2008), showed that in Chinese hamster ovary (CHO) cells, NPR-5 activation by FLP-18 peptides induces an increase in intracellular calcium that can be blocked by incubation with the phospholipase inhibitor U-73122, suggesting a $G\alpha_q$ coupled signaling pathway (Kubiak *et al.*, 2008). However, pretreatment with pertussis toxin enhanced the calcium response and a slight increase in cyclic AMP was

also detected following FLP-18 application which indicates NPR-5 may signal through $G\alpha_{i/o}$ and $G\alpha_s$ pathways, respectively (Kubiak *et al.*, 2008).

It is unknown what signaling pathway NPR-5 couples to *in vivo* but based on *in vitro* experiments (Kubiak *et al.*, 2008; Cohen *et al.*, 2009) we hypothesized that NPR-5 may function through the $G\alpha_q$ pathway in body wall muscle. In vertebrates, $G\alpha_q$ signaling contributes to excitation-contraction coupling in both striated and smooth muscle through activation of phospholipase Cβ (Wu *et al.*, 1992), which leads to Inositol 1,4,5-trisphosphate (IP_3) mediated calcium release from the sarcoplasmic reticulum (Vergara, Tsien and Delay, 1985; Volpe *et al.*, 1985; Domeier *et al.*, 2008). The EGL-30/$G\alpha_q$ signaling pathway is conserved between *C. elegans* and humans (Brundage *et al.*, 1996), and EGL-30/$G\alpha_q$ - IP_3 mediated intracellular calcium release is important for the regulation of rhythmic muscle contractions during the defecation motor program in *C. elegans* (Dal Santo *et al.*, 1999). However, the role of EGL-30/$G\alpha_q$ - IP_3 is less well studied in the coordination of excitation contraction coupling in body-wall muscle during locomotion. EGL-30 expression has been detected in body-wall muscle (Bastiani *et al.*, 2003), and *egl-30* mutation severely disrupts locomotion (Brundage *et al.*, 1996). However, this may be due to impaired acetylcholine release caused by loss of *egl-30* in motor-neurons (Lackner, Nurrish and Kaplan, 1999). Furthermore, loss of the IP_3 receptor gene *itr-1* in *C. elegans* has a minimal effect on locomotion (Maryon, Saari and Anderson, 1998), suggesting that IP_3 is not the major source of calcium driving muscle contraction during locomotion.

Nonetheless, our evidence supports a role for EGL-30/$G\alpha_q$ acting downstream of FLP-18 and NPR-5 to increase calcium levels in muscle. It is possible that increased calcium levels result from other the activity of EGL-30/$G\alpha_q$ effectors other than IP_3 such as protein kinase C (PKC). In vertebrate muscle, PKC phosphorylation of voltage gated calcium channels enhances conductance increasing muscle calcium (Huster *et al.*, 2010; Weiss *et al.*, 2012). The *C. elegans* gene *pkc-2* encodes an ortholog of vertebrate PKCα and is expressed in body wall muscle and neurons (Islas-Trejo *et al.*, 1997) raising the possibility of its role as an NPR-5 downstream effector.

Ultimately, more work is needed to determine if the NPR-5 mediated increase in muscle calcium is dependent on $G\alpha_q$ signaling. The suppression of muscle calcium signal we observed in *egl-30* mutations could very well be caused by a reduction in presynaptic transmitter release at the neuromuscular junction (NMJ), as EGL-30 function is important for cholinergic transmission (Lackner, Nurrish and Kaplan, 1999; Miller, Emerson and Rand, 1999). Tissue specific expression of EGL-30 in neurons or muscle of *egl-30* mutant animals could help to distinguish a presynaptic versus postsynaptic role for EGL-30, however, *C. elegans* are highly sensitive to expression levels of EGL-30 (Brundage *et al.*, 1996; Bastiani *et al.*, 2003) making rescue experiments challenging to interpret. Alternately, knocking down EGL-30 in using RNA interference (RNAi) (Fire *et al.*, 1998), might be a more effective approach as neurons are generally less sensitive to RNAi than other tissues (Asikainen *et al.*,

2005). This would allow examination of the effect of muscle specific knockdown of EGL-30 on calcium levels, while potentially leaving neuronal EGL-30 function intact and avoiding overexpression effects of rescue.

If NPR-5 were found to couple to EGL-30/$G\alpha_q$ it would be the first example of such a pathway affecting body wall muscle calcium dynamics in *C. elegans.* However, given the rise in cyclic AMP levels observed after FLP-18 application to CHO cells expressing NPR-5 (Kubiak *et al.*, 2008) an alternative model is that FLP-18 activation of NPR-5 induces a $G\alpha_s$ mediated signaling cascade that results in increased muscle calcium levels. In vertebrates, β-adrenergic receptor activation by catecholamines occurs during the fight or flight response and leads to the enhancement of cardiac and skeletal muscle calcium current and contractility through a $G\alpha_s$ / cyclic AMP mediated signaling cascade (Osterrieder *et al.*, 1982; Bean, Nowycky and Tsien, 1984; Fuller *et al.*, 2010). Protein kinase A (PKA) is activated by increased cyclic AMP and increases intracellular calcium in muscle through phosphorylation of ion channels, including L-type voltage gated calcium channels (Kamp and Hell, 2000; Fuller *et al.*, 2010; Sassone-Corsi, 2012).

FLP-18 could play a similar role during the escape response in *C. elegans* as catecholamines do in vertebrates, by enhancing muscle function through activation of a $G\alpha_s$ coupled NPR-5. The *C. elegans* $G\alpha_s$ protein GSA-1 is broadly expressed in neurons and muscle (Korswagen *et al.*, 1997; Park *et al.*, 1997; Berger, Hart and Kaplan, 1998) and in body wall muscle GSA-1 localizes to

dense bodies, as does NPR-5 (Fig. II-6; Korswagen *et al.*, 1997). Similarly, the *C. elegans* PKA catalytic subunit KIN-1 is highly expressed in muscle (Lee *et al.*, 2016) raising the possibility that activated KIN-1 could increase calcium levels through phosphorylation of the L-type voltage gated calcium channel EGL-19 in muscle in response to NPR-5 activation by FLP-18.

Behavioral significance of FLP-18 and tyraminergic co-transmission.

Many neurons across animal species signal using both classical neurotransmitters and additional peptides or other neuromodulators. Co-transmission is an important feature of neuronal communication but our understanding of the behavioral impact of co-transmission remains limited. In chapter II I introduced signaling from the RIM interneurons as a model to understand the function of co-transmission on the coordination of complex behavior, with a comparison to the role vertebrate sympathetic neurons. Both systems rely on the co-release of a neuropeptide and monoamine transmitter to coordinate behavioral and physiological responses to danger. In vertebrates these are neuropeptide Y (NPY) and noradrenaline (NA), whereas in *C. elegans* the transmitters are the RFamide FLP-18 and tyramine. Co-transmission of neuropeptides and small molecule transmitters increases the complexity of signaling in a number of ways. Packaging of transmitters into different vesicle types can allows neurons to respond to changes in stimulation intensity with different transmitter exocytosis due to varying release properties of vesicles. This

is the case for sympathetic neurons where NA is found in both small dense core vesicles and co-packaged with NPY in large dense core vesicles (Fried *et al.*, 1985; Fried, Lundberg and Theodorsson-Norheim, 1985), the latter of which are preferentially released under high frequency stimulation (Lundberg *et al.*, 1986). It is thought that under periods of high sympathetic drive, the potentiating effects of NPY help supplement NA action and maintain transmitter homeostasis.

FLP-18 like other peptides is packaged into dense core vesicles (Li and Kim, 2008) and the results from chapter II suggest that strong mechanosensory stimulation may be required for FLP-18 release in the context of the escape response. *flp-18* mutants resemble wild type animals in response to a 3-tap burst but do not enhance reversal or forward run velocity in response to a 20-tap burst (Fig. II-1). However, we also observed defects in ventral head bending and omega turning in *flp-18* mutants in response to gentle anterior touch (Fig. II-3) suggesting that single mechanosensory stimuli are sufficient for *flp-18* release rather than high frequency bursts. While it is unknown whether tyramine is packaged into dense core vesicles with FLP-18 or if it is stored separately, it is clear that tyramine release is triggered by identical stimuli to FLP-18, as gentle anterior touch triggers suppression of head oscillations during reversals, a tyramine dependent behavior (Alkema *et al.*, 2005). Mutations in *unc-31,* the *C. elegans* calcium dependent activator for protein secretion (CAPS), are defective in dense-core but not synaptic vesicle exocytosis (Speese *et al.*, 2007). If tyramine were stored in dense-core vesicles then *unc-31* mutants should fail to

suppress head oscillations in response to anterior touch, as tyramine release would be impaired.

Co-release of peptides and neurotransmitters further increases flexibility of signaling by acting with distinct temporal dynamics on target tissues. Tyramine and FLP-18 are released onto neck muscle during the escape response and exert opposite effects but the different time course of each transmitter functions in a complementary manner to coordinate the transition from reversal to omega turn. Tyramine activates the fast acting ionotropic chloride channel LGC-55 to inhibit muscle and suppress head oscillations during the reversal (Alkema *et al.*, 2005; Pirri *et al.*, 2009), while FLP-18 activates the GPCR NPR-5, which depolarizes neck muscle (Fig. II-11). In addition to suppressing neck movements, tyramine promotes long reversals by suppressing the forward locomotion AVB interneurons (Pirri *et al.*, 2009). We hypothesize that the slow but persistent excitation from second messenger activity keeps neck muscle primed to initiate the ventral turn once tyraminergic hyperpolarization ceases and forward locomotion resumes. Thus, by releasing two transmitters with different kinetics, RIM effectively couples two linked motor programs, the reversal and the omega turn, in the escape response.

Energy balance during fight or flight.

In chapter II and appendix I, we show how monoamine and neuropeptide signaling function in the coordination of a complex behavior. That behavior, the

C. elegans escape response, like fight or flight reactions in other species, allows the animal to survive encounters with a natural predator, nematophagous fungi (Maguire *et al.*, 2011). Fight or flight behavior is physically demanding and is accompanied by metabolic changes that increase nutrient availability to provide adequate energy to muscles and other tissues. Insulin/ insulin-like growth factor-1 (IGF-1) signaling (IIS) is a major regulator of metabolic function, and in chapter III we show that the *C. elegans* insulin receptor DAF-2 is activated as a result of tyramine released during the escape response (Figure III-10). Tyramine does not bind to DAF-2 directly but instead activates the GPCR TYRA-3 in the intestine, which we hypothesize triggers the release of the DAF-2 ligands, insulin like peptides (ILPs). DAF-2 activation promotes energy utilization while reduction in DAF-2 function results in lower metabolic rate and increased fat accumulation (Kimura *et al.*, 1997; Ogg *et al.*, 1997; Van Voorhies and Ward, 1999). Interestingly FLP-18 also functions to promote energy utilization as *flp-18* mutants accumulate more fat and have reduced oxygen consumption compared to wild type (Cohen *et al.*, 2009). The effect of FLP-18 on fat accumulation is mediated by the receptors NPR-5 in ciliated sensory neurons and NPR-4 in the intestine (Cohen *et al.*, 2009), tissues which also express ILPs, suggesting that FLP-18 may interact with the DAF-2 /IIS signaling pathway as well. Thus, FLP-18 signaling may prepare an animal for vigorous activity during the escape response in multiple ways: by enhancing muscle calcium, which could drive strong contraction (Figure II-11), and by more generally increasing metabolic rate

to allow for prolonged physical exertion. This is supported by our finding that animals lacking *flp-18* are unable to maintain elevated locomotion rate after the escape response, whereas wild type animals will execute a forward run, moving at high speeds for up to three minutes after the reversal (Figures II-1, II-2). Together these results indicate that in addition to coordinating distinct motor programs, FLP-18 and tyramine also alter the metabolic state of the animal to provide a systemic response to a predatory threat.

Neural encoding of the nature of a stressor.

One of the most striking findings from our work in chapter III is that in *C. elegans*, the response to acute stress, like predation, is antagonistic to the response to long-term environmental stressors like oxidation or heat (Figures III-1,III-2, III-3). The neuroendocrine signaling that coordinates anti-predator behavior inhibits cellular defensive pathways. In animals from worms to humans, the damaging effects of environmental stressors are mitigated by the action of conserved transcription factors DAF-16/FOXO, SKN-1/Nrf2, HSF-1. DAF-2/IIS signaling phosphorylates these proteins and prevents their translocation to the nucleus, leaving cells susceptible to damage. As tyramine released during the escape response results in DAF-2 activation, RIM activity must be tightly regulated for animals to mount a proper response to environmental (i.e. heat, oxidation starvation) versus acute (i.e. predation, aggression) stressors.

Mechanical stimuli that trigger the escape response are detected by mechanosensory AVM and ALM neurons and relayed to the RIM through excitatory chemical and electrical synapses from the AVD and AVA interneurons (Chalfie *et al.*, 1985), resulting in increased RIM activity (Figure III-5, a,d). Exposure to oxidation, starvation and heat all result in suppression of RIM activity (Figures III-5, e, III-6, i-k) but the circuit mechanisms that mediate this suppression are unknown. Noxious heat is sensed by the AFD neurons which are also required for the systemic heat-shock response (Prahlad, Cornelius and Morimoto, 2008; Liu, Schulze and Baumeister, 2012). Output from the AFD converges on the first layer interneurons AIY, AIB and AIZ. The AIY and AIB also mediate the systemic starvation response and may directly sense amino acids as nutrient signals (Kang and Avery, 2009). The neural mechanisms for sensing oxidative stress are not fully understood, however there is evidence that *C. elegans* can detect the presence of reactive oxygen species (ROS). Animals will suppress feeding behavior in the presence of ROS sources like hydrogen peroxide or UV light and this suppression requires the gustatory receptor homologs LITE-1 and GUR-3 (Bhatla and Horvitz, 2015). If these receptors are indeed ROS sensors, they could provide a mechanism by which information about oxidative stress could be relayed to the RIM. However more work will need to be done to identify the specific mechanisms that mediate the suppression of RIM activity in response to oxidation.

We hypothesize that the AIB interneurons are likely candidates for downregulating RIM activity in response to environmental stressors as they receive and integrate diverse sensory inputs and have chemical and electrical synapses with the RIM. The AIB are glutamatergic and the glutamate gated chloride channel AVR-14 is expressed in the RIM. Moreover, optogenetic activation of the AIB causes an inhibitory post synaptic potential in the RIM which is abolished in glutamate deficient *eat-4* mutants (Piggott *et al.*, 2011). More work will need to be done to determine the precise neural coding of environmental stressors but we suggest a model in which the first layer interneurons (AIB, AIY, AIZ) integrate sensory information and act to suppress RIM activity, possibly through glutamatergic signaling from the AIB, which results in termination of tyramine release and allows the transcriptional stress response pathways to become active to promote survival. If this were the case, mutations that disrupt glutamate signaling, such as *avr-14* or *eat-4*, would be expected to render animals more susceptible to environmental stressors as RIM activity and tyramine release would become dysregulated.

Future directions

C. elegans has proven to be a powerful model system to study basic biological questions and due to the conservation of core molecular pathways findings in *C. elegans* can guide our understanding of human disease states (Hashmi *et al.*,

2013; Rodriguez *et al.*, 2013). The work presented in chapter III elucidates the mechanism by which chronic activation of the fight-or-flight response reduces resilience to stress in *C. elegans.* In humans, diseases such as post-traumatic stress disorder (PTSD) and panic disorder are characterized by hyperarousal and are associated with dysregulation of catecholamine signaling (Yehuda *et al.*, 1998; Strawn and Geracioti, 2008; Daskalakis, Lehrner and Yehuda, 2013; Oh *et al.*, 2015). Interestingly, similar to what we observed in *C. elegans* subjected to repeated activation of the flight response, PTSD patients display decreased stress resistance, increased oxidative stress, susceptibility to disease and premature aging (Danese *et al.*, 2009; Yaffe *et al.*, 2010; Borovac Štefanović *et al.*, 2015; Wolf *et al.*, 2016). In chapter III we show that tyramine signaling leads to activation of the *C. elegans* insulin receptor DAF-2, which prevents the cytoprotective transcriptional activity of DAF-16/FOXO. A similar pathway may underlie the cluster of stress related symptoms associated with PTSD. However, in mammals catecholamine signaling inhibits insulin secretion (Gilliam, Palmer and Taborsky, 2007; Sharp and Straub, 2012) rather than stimulating ILP release as we suggest tyramine does in *C. elegans*. Despite these differences, the complexity of neuroendocrine responses in the vertebrate fight or flight response leave open the possibility of indirect modulation of downstream insulin signaling pathways in PTSD and related disorders.

In mammals, activation of the fight-or-flight response and sympathetic nervous system can be triggered not just by physical harm but through visual,

olfactory or other sensory modalities (Dielenberg, Hunt and McGregor, 2001; Curtis *et al.*, 2012). Our work in *C. elegans* indicates that mechanical stimuli, which mimic encounters with a predator, cause the release of tyramine and the suppression of stress resistance, however it is unknown whether escape responses triggered by other sensory modalities such as aversive odors, high temperature or osmotic shock affect tyramine release. The neural circuit for generating escape responses to these cues differs from the touch response circuit but the outputs may converge on the same neurons, including the RIM, suggesting tyramine may be involved. If so, repeated activation of these escape responses should have the same negative impact on stress resistance as mechanical tap, but this remains to be determined.

Finally, what impact does the timing of a traumatic event have on the fitness of an animal later in development? Our work in chapter III focused primarily on activating the flight response in young adult animals that had fully developed nervous systems, however there is evidence that trauma in early development has pronounced and lasting effects on metabolism, disease susceptibility and premature aging (Danese *et al.*, 2009; Miller, Chen and Parker, 2011; Huffhines, Noser and Patton, 2016). Preliminary evidence in *C. elegans* indicates that activation of the flight response during the first larval (L1) stage renders animals more susceptible to other stressors as adults (Diego Rayes, personal communication). The preclusion of DAF-16/FOXO from the nucleus by tyramine signaling is unlikely to persist for days, suggesting a more complex

explanation for the persistence of impaired stress resistance. The nervous system is still developing during the L1 stage and it is possible that early trauma rewires neural circuits or alters RIM activity in a permanent manner. Interestingly, exposure to pathogenic bacteria during the L1 stage causes behavioral aversion that persists far longer than if the animal were exposed during any other developmental stage, and this aversion depends on tyramine release during that critical window (Jin, Pokala and Bargmann, 2016). This suggests that tyramine signaling has the capacity to induce long lasting changes in nervous system function but more needs to be done to uncover the mechanisms behind these effects.

This thesis demonstrates the dynamic role that neuromodulators have in shaping the behavioral and physiological state of an animal to meet the challenges posed by its environment. In chapter II, we demonstrated how neuropeptide signaling acts in concert with monoaminergic transmission to coordinate a complex behavior. Using behavioral analysis of mutant and transgenic animals we identified a role for the neuropeptide FLP-18 in promoting reversals, bending and omega turning and forward run behavior during the escape response. Using fluorescence imaging we showed that FLP-18 is released from the AVA and RIM neurons in response to mechanical stimulation and identified its site of action, the GPCR NPR-5 in the muscle where FLP-18 functions to enhance calcium levels. FLP-18 is a co-transmitter with tyramine and this work shows that these two molecules act in synergistically and

antagonistically in multiple tissues to coordinate the escape response. In chapter III, we demonstrated the consequences of chronic activation of the escape response and how this form of repeated acute stress renders animals vulnerable to a host of environmental stressors. Using calcium imaging we uncovered how the RIM responds to acute stressors differently than environmental stressors, and thereby increases or decreases tyramine release accordingly. We traced the molecular pathway downstream of tyramine release to activation of GPCR TYRA-3 in the intestine, which leads to DAF-2/ IIS receptor activation and subsequent preclusion of the FOXO transcription factor, DAF-16, from the nucleus, thereby inhibiting cytoprotective gene transcription. The genetic tractability, relatively simple and completely defined nervous system of *C. elegans* allowed us to address major questions in neurobiology that would be impossible in more complex systems, and the answers uncovered in *C. elegans* have broad relevance due to the high level of conservation of basic molecular pathways from nematodes to humans.

PREFACE TO APPENDIX I

The work presented in Appendix I addresses the question of how a nervous system encodes and coordinates a complex behavior using the *C. elegans* escape response as a model compound motor sequence. Using behavioral analysis of tyramine signaling mutants, optogenetics and laser ablation studies we show that feed-forward inhibition from the tyraminergic RIM interneurons coordinates the transition from reversal to omega turn during the *C. elegans* escape response through hyperpolarization of the RIV motor neurons. Furthermore, simultaneous calcium imaging of the neurons that make up the escape circuit reveal the dynamics of cellular activity in freely behaving animals. Mutations in tyramine biosynthesis alter the pattern of neuronal activity and show how tyramine signaling modulates circuit function to orchestrate a complex behavior.

Jeremy Florman preformed the behavioral, worm tracking, optogenetic and laser ablation experiments and analyzed the data. Vladislav Susoy performed the calcium imaging experiments in the lab of Aravinthan Samuel and analyzed the data. Chris Clark and Jeremy Florman generated the transgenic strains used in the experiments. Christopher Clark, Andrew Leifer, Aravinthan Samuel, Mark Alkema and Jeremy Florman co-wrote the manuscript. Portions of this manuscript and figure AI-1 were published as part of the dissertation of Christopher Clark. This work was prepared for publication at the time of this writing.

APPENDIX I: TEMPORAL COORDINATION OF A MOTOR CIRCUIT BY MONOAMINERGIC SIGNALING IN *C. ELEGANS*

Christopher M Clark[*1], Andrew M Leifer[*2], Jeremy T Florman*[1], Vladislav Susoy[3]
Aravinthan D Samuel[+3], Mark J Alkema[+1]

(1) Department of Neurobiology, University of Massachusetts Medical School,
364 Plantation Street, Worcester, MA 01605, USA
(2) Princeton University, Lewis Sigler Institute for Integrative Genomics,
170 Carl C. Icahn Laboratory, Princeton, NJ, 08544 USA
(3) Department of Physics & Center for Brain Science, Harvard University,
17 Oxford Street Cambridge, MA 02138, USA

* authors contributed equally
+ Corresponding authors

Aravi Samuel: samuel@physics.harvard.edu
Mark Alkema: mark.alkema@umassmed.edu

Key words: C. elegans, neural circuits, navigation, sensorimotor processing, motor programs, synaptic chains, complex behavior, optogenetics, calcium imaging

Abstract:

Compound behaviors are thought to arise through the sequential activity of synaptically connected neurons. Synaptic chain models have long been proposed to encode such temporal sequences. However, it has been difficult to demonstrate the existence or dynamics of these chains, or connect a synaptic chain to upstream sensory neurons or downstream motor neurons. The *C. elegans* escape response is a compound motor sequence that allows the animal to reverse and turn away from a threatening stimulus. Using calcium imaging throughout the escape response circuit in behaving animals, we elucidate how an elaborate progression of motor programs emanates from the connectome. Using optogenetics and targeted cell killing we define neuronal requirements of the motor subprograms of the escape response. We find that a chain of chemical and electrical synapses organize synchronization and sequence in the dynamics of the escape response circuit. Our study provides new insights into the orchestration of compound behaviors by complex synaptic networks.

Sensorimotor circuits can generate compound behaviors requiring the temporal orchestration of multiple motor programs in response to an initiating stimulus. While the complete path from sensory input to motor output has been defined in a few reflexive responses (Edwards, Heitler and Krasne, 1999; Eve Marder and Dirk Bucher, 2001; Nusbaum and Beenhakker, 2002; Korn and Faber, 2005), it remains unclear how the sequential motor activities of compound behaviors are

encoded by synaptically connected neurons. Synaptic chain models have long been proposed to explain how neurons produce sequential patterns of activity (Lashley, 1951). In the forebrain of the zebra finch, for example, studies suggest that an excitatory feed forward chain of chemical synapses structures the temporal sequence of song (Li and Greenside, 2006; Jin, Ramazanoğlu and Seung, 2007; Long, Jin and Fee, 2010). However, it has been difficult to directly demonstrate the existence or dynamics of multi-neuron chains in birds or any other animal, or connect a synaptic chain to upstream sensory neurons or downstream motor neurons.

Fixed action patterns are robust and instinctive motor sequences that are executed to completion following a sensory trigger (Camhi, 1984). Even animals with simple undulatory movement and small nervous systems like *C. elegans* are capable of fixed action patterns and a temporal unfolding of motor programs that cannot be understood as single reflexes. The complete wiring diagram of the *C. elegans* nervous system consists of 302 neurons that are connected through 8000 chemical synapses and 900 gap junctions (White *et al.*, 1986; Varshney *et al.*, 2011). The worm wiring diagram provides an opportunity to define complete neuronal paths from sensory stimulus to behavioral sequence. While chemical synapses provide a clear temporal directionality, gap junctions are thought to synchronize neuronal activity. Strikingly, almost 90% of all neurons are interconnected through gap junctions, suggesting one extensive electrical

syncytium. The abundance of electrical synapses in the worm nervous system poses a puzzle and indicates that mechanisms beyond feed forward excitatory chains are needed to generate the distinct phases of a compound motor sequences. To determine how complex behaviors are encoded in a connectome we analyzed the neuronal coding of a fixed action pattern of *C. elegans*.

The *C. elegans* escape response is a compound motor sequence

C. elegans moves forward or backward by propagating bending waves in the anterior or posterior direction along the muscle cells lining its ventral and dorsal sides. Forward movement is accompanied by exploratory head movements. When subjected to gentle anterior touch or mechanical vibration, *C. elegans* induces rapid backward movement while suppressing lateral head movements (Figure AI-1, a) (Chalfie *et al.*, 1985). The reversal is followed by a deep ventral bend of the head, and a subsequent slide of the head along the ventral side of the body, a maneuver called an omega turn. After the omega turn, the animal moves forward in the opposite direction and head movements resume. The entire escape response lasts approximately 10 seconds and requires the temporal coordination of several motor programs. This fixed action pattern increases the nematode's chances to escape entrapment by the constricting hyphal rings of nematophageous fungi (Maguire *et al.*, 2011). A similar motor sequence – backward, turn, forward – can occur spontaneously in navigating worms (Gray, Hill and Bargmann, 2005). We found that the spontaneous motor sequence has

markedly different dynamics than the stimulus-evoked escape response. Reversals induced by anterior touch or mechanical vibration were longer and approximately twice as fast as spontaneous reversals (Figure AI-1, b,c). Forward movement following a stimulus-evoked reversal had a transiently elevated speed whereas forward movement following a spontaneous reversal is resumed at basal speed (Figure AI-1, b). The probability of initiating an omega turn following a reversal increases with the length of reversal. We found that escape response reversals are longer than spontaneous reversals (Figure AI-1, d), but, for any given duration length, omega turns are initiated more frequently during stimulus-evoked than spontaneous reversals (Figure AI-1, e). Omega turns are initiated almost exclusively following reversals, and thus constitute a context specific behavior (Huang, Cosman and Schafer, 2006; Swierczek *et al.*, 2011).

Anterior touch activates the ALM and AVM mechanosensory neurons (Suzuki *et al.*, 2003; O'Hagan, Chalfie and Goodman, 2005). The *C. elegans* neural wiring diagram has provided potential neural paths for the initial backward movement reflex following anterior touch stimulation (Chalfie *et al.*, 1985). Laser ablation studies indicate direct pathways from the mechanosensory neurons to premotor interneurons (AVA and AVD) to motor circuits for backward movement. However, the neural dynamics within this circuit, which neurons generate the omega turn, and how the reversal and the turn are linked in the execution of the escape response is unknown.

Ablation of the RIM reduces reversal duration and omega turning

Synaptic chains temporally couple motor programs through feed-forward excitation. Removal of a neuron from that chain would preclude the activation of subsequent cells and terminate behavioral output at a specific stage in the compound motor sequence. Using laser ablation, we removed individual pairs of upstream interneurons (AVD, RIM and AIB) and quantified the effect on escape behavior. Elimination of AVD, RIM or AIB interneurons alone was insufficient to prevent the execution of the escape response, suggesting that the circuit mediating the escape response is more complex than a simple synaptic chain. Indeed, the wiring diagram indicates that multiple pathways exist to link mechanosensory AVM and ALM neurons to downstream motor neurons. We did however observe specific changes in the escape response that differed between ablated neurons. Ablation of the AVD reduced the velocity of the reversal but had no impact on the duration of reversal (figure AI-2, a). Ablation of the RIM also decreased reversal velocity but in contrast to AVD ablation, animals lacking the RIM displayed reduced reversal duration (figure AI-2, b). Ablation of the AIB interneurons did not affect the reversal velocity or duration (figure AI-2, c). Turning behavior was reduced by ablation of any of the interneurons compared to wild type. AVD (figure AI-2, a. omega = 19.7%, ventral turn = 12.1%, no response = 68.1%, n=66), RIM (figure AI-2, b. omega = 14.2%, ventral turn = 19.0%, no response = 66.6%, n=42), AIB (figure AI-2, c. omega = 17.6%, ventral

turn = 17.6%, no response = 64.7%, n=34), mock ablation (figure AI-2, d. omega = 37.5%, ventral turn = 19.4%, no response = 43.0%, n=72). Together these results indicate that the escape circuit is not a simple synaptic chain, but individual interneuron, play specific roles in regulating motor programs in the escape response.

Tyramine signaling regulates the duration of reversals.

Tyraminergic signaling from the RIM impacts head movements and reversals (Alkema *et al.*, 2005; Pirri *et al.*, 2009; Donnelly *et al.*, 2013). To determine whether tyramine was involved in coordinating the reversal-to-turn transition we analyzed escape behavior in tyramine signaling mutants. In response to mechanical stimuli, wild type animals exhibited a characteristic escape response with a mean reversal duration of 4.5±0.1 seconds (figure AI-3, a & c). *tdc-1* mutants, which lack tyramine biosynthesis, reversed for a shorter duration compared to wild type, with a mean reversal lasting 3.6±0.2 seconds (figure AI-3, a & c).

The tyramine gated chloride channel LGC-55 is expressed in the forward locomotion interneuron AVB and could increase reversal duration by suppressing forward locomotion (Pirri *et al.*, 2009). We found that *lgc-55* mutants had reversal defects that were nearly identical to *tdc-1* mutants, with a mean duration of 3.5±0.1 seconds (figure AI-3, b & c). Reversal duration could be rescued in *lgc-55* mutants by transgenic expression of *lgc-55* from the endogenous promotor,

which resulted in a reversal duration of 4.4±0.2 seconds (Figure AI-3, b & c). LGC-55, in its native form, is selective for anions and therefore mediates an inhibitory hyperpolarizing effect when activated by tyramine. Modification of residues that regulate ion selectivity cause LGC-55 to be selective for cations rather than anions resulting in an excitatory tyramine gated ion channel, referred to as LGC-55 Cation (Pirri, Rayes and Alkema, 2015). Expression of LGC-55 Cation under the endogenous promoter in *lgc-55* mutants resulted in rapid termination of reversals with a mean duration of 2.1±0.2 seconds (Figure AI-3, b & c). Together, these results indicate that the role of the RIM in coordinating reversal behavior is mediated by tyraminergic inhibitory signaling through LGC-55 which functions to prolong the reversal.

The timing of the ventral turn is coordinated by tyramine

The head bend that initiates the omega turn is exclusively ventral and is tightly coupled to the termination of backward movement. How is this coordination achieved? Tyramine and LGC-55 are required to suppress head oscillations during reversals and LGC-55 is expressed in neck muscle, as well as in the SMD and RMD motor neurons that innervate neck muscle (Alkema *et al.*, 2005; Pirri *et al.*, 2009). However, the omega turn is exclusively ventral and there is no dorsal or ventral bias in the expression pattern of LGC-55 that would induce turning asymmetry. The RIV motor neurons innervate ventral neck muscle and are electrically coupled to the SMDs. We assessed the role of LGC-55 in ventral

turn bias by exposing tyramine signaling mutants to exogenous tyramine. When wild type (LGC-55 anion) animals were placed on 30mM exogenous tyramine plates they initiated long reversals and paralyzed with relaxed relatively straight necks (Figure AI-4, a. Mean angle ± SEM = 1.6±1.1 degrees ventral). *lgc-55* mutants on the other hand did not exhibit long reversals and continue moving their heads freely after their body became paralyzed (Figure AI-4, b. Mean angle ± SEM = 4.9±6.8 degrees ventral). When animals expressing the LGC-55 Cation a *lgc-55* mutant background were placed on exogenous tyramine, they failed to paralyze and instead crawled forward in a path that curved ventrally and hypercontracted their necks with a pronounced ventral kink (Figure AI-4, c. Mean angle ± SEM = 31.8±1.7 degrees ventral). These results indicate that tyramine signaling through LGC-55 can indeed induce ventral asymmetry in head bending which could contribute to the initiation of the omega turn.

Mutations in tyramine signaling genes modulate timing of the ventral turn.

We next asked how the activation of individual neurons in the escape circuit contribute to the generation of the ventral turn and the role that tyramine plays in coordinating timing. The RIV motor neurons are downstream of escape circuit neurons and exclusively innervate ventral neck muscle, thus they represent a likely candidate for initiating the ventral turn. We expressed the light gated cation channel Channelrhodopsin-2 (ChR2) (Nagel *et al.*, 2003) under the *lim-4* promotor [*Plim-4::*ChR2::GFP] to drive ChR2 expression in the RIV among other

neurons. Depolarization of RIV by exposure to blue light induced a rapid ventral turn with a mean latency of 0.9±0.1s (Figure AI-5 a,h).

We next tested the role of the AIB and RIM interneurons in ventral turning. The AIB is electrically coupled to the RIM and optogenetic activation of the AIB or RIM is likely to induce the release of tyramine which modulates reversal length. As reversal behavior and ventral turning are tightly coupled we conducted optogenetic experiments in an *unc-3* mutant background in which head movements are normal but animals are unable to reverse, allowing us to separate the role of RIM in ventral turning from its role in reversal modulation. Activation of AIB using the transgene [*Pnpr-9::*ChR2::GFP] resulted in a ventral turn with a mean latency of 6.3±0.3s (Figure AI-5 b,h), while activation of RIM using the transgene [*Ptdc-1*::ChR2::GFP] caused a longer delay during which animals relaxed their necks and then initiated a ventral turn after a mean latency of 10.2±0.4s (Figure AI-5 c,h).

To assess the role of tyramine in the timing of the ventral turn we crossed tyramine signaling mutants into the *unc-3*; *Ptdc-1*::ChR2::GFP background and activated the RIM with blue light stimulation. In both *tdc-1 and lgc-55* mutants the latency to ventral turning was reduced compared to wild type (7.3±0.4s and 5.9±0.3s respectively, Figure AI-5, d,e,h). In contrast, activation of the RIM in *lgc-55* mutants expressing LGC-55 Cation resulted in a more rapid ventral turn than wild type or *lgc-55* mutants (4.7±0.2s, Figure AI-5, f,h). Blue light stimulation of the RIM resulted in no ventral turn in 66% of animals raised in the absence of *all-*

trans retinal (Figure AI-5, g), a co-factor required for ChR2 function. Together these results support the hypothesis that tyramine signaling from the RIM delays the initiation of the ventral turn through activation of the LGC-55 chloride channel, while expression of the LGC-55 Cation channel results in a rapid ventral turn.

Tyramine affects calcium activity in the AVB and RIV neurons during the escape response.

The results of our behavioral and optogenetic experiments suggest that tyramine plays a key role in coordinating the timing of both the reversal and the ventral turn. To determine the impact of tyramine signaling on neuronal activity during the escape response we generated a transgenic strain expressing the genetically encoded calcium indicator GCaMP6 (Chen, 2013) in 7 pairs of neurons in the escape circuit (AVD,AVE,AVA,AVB,RIM,AIB and RIV) as well as in mechanosensory neurons (Figure AI-6, a). Behavior and neuronal responses were monitored in freely moving animals using a dual camera system. One camera monitored behavioral dynamics while another camera simultaneously monitored neuron fluorescence at higher magnification. To induce escape response, we subjected individual worms to short vibrations of the assay plate during periods of basal forward movement.

We first characterized neuronal activity patterns during the escape response in wild type animals. The mechanosensory ALM neurons transduce touch to the anterior portion of the body. The vibrational stimulus caused an

immediate rise in ALM calcium levels that declined towards baseline shortly after cessation of the stimulus while animals were still in the process of reversing (Figure AI-6, b). The AVA are typically characterized as premotor interneurons that control backward locomotion (Chronis, Zimmer and Bargmann, 2007; Husson *et al.*, 2007; Kawano *et al.*, 2011). AVA calcium levels rise rapidly at the onset of the stimulus-evoked reversal, remained elevated, and returned to pre-stimulus levels when forward locomotion resumed (Figure AI-6, c). The RIM neurons are electrically coupled to the AVA neurons and have been shown to inhibit forward locomotion and head movements through the release of tyramine (Pirri *et al.*, 2009). RIM calcium levels paralleled those in the AVA, rising rapidly at the onset of the reversal and decreasing to baseline when forward locomotion and head movements began (Fig. AI-6, d). Although the AIB neurons had not previously been implicated in the escape response, AIB are electrically coupled to the RIM and have been shown to be active during reversals in navigating worms (Chalasani *et al.*, 2007; Piggott *et al.*, 2011). AIB also has synaptic outputs onto the AVA, AVB premotor interneurons and RIM. Similarly to RIM, AIB calcium levels began to rise at the onset of the reversal and fell after the omega turn (Figure AI-6, e). The synchronization of AVA, RIM, and AIB is consistent with their extensive coupling by electrical synapses. The AVB neurons are characterized as premotor interneurons that control forward movement (Chalfie *et al.*, 1985). AVB calcium levels dropped during reversals but increased after the omega turn when the animal resumed forward movement (Figure AI-6, f). The

increased AVB activity correlates with the increase in the forward locomotion rate following the omega turn. The RIV motor neurons have previously been implicated in the initiation of omega turns (Gray, Hill and Bargmann, 2005) and optogenetic activation of RIV causes an immediate ventral turn (Figure AI-5, a). Consistent with these results we observed that calcium levels in the RIV remain relatively low during the reversal and rise sharply when the ventral turn begins (Figure AI-6, g).

We next asked how loss of tyramine affected the neuronal dynamics during the escape response by crossing *tdc-1* mutants into the escape circuit GCaMP strain. Activity in the electrically coupled AVA, RIM and AIB neurons followed a similar pattern to what was observed in wild type animals, with calcium levels in all three pairs of neurons rising sharply at the onset of the reversal and subsiding as forward movement resumed (Figure AI-6, h-j). Unlike wild type animals, *tdc-1* mutants failed to suppress activity in the AVB during reversals and instead show a transient increase in calcium levels immediately following the vibrational stimulus (Figure AI-6, k). The pattern of RIV activity was similar between wild type and *tdc-1* mutants with peak fluorescence spiking at the initiation of the ventral turn, however in *tdc-1* mutants this peak occurred earlier than in wild type (Figure AI-6, l). These results support the hypothesis that tyramine is a key modulator of neuronal activity that acts through inhibition to delay the activation of the AVB and RIV during the escape response, thereby

promoting long reversals and ensuring that the ventral turn occurs synchronously with the resumption of forward locomotion.

Discussion

Our results provide direct functional and structural mapping of a neural circuit organizing multiple phases of a complex motor sequence. The escape response circuit of *C. elegans* has been characterized as feed-forward reflex arcs where stimulation of anterior or posterior touch receptors trigger backward or forward movement, respectively. We have found that the complex motor sequence following anterior touch – backward movement, turning, and followed by forward movement – is carried out by a progression of neuronal activity across synaptically connected neurons (Figure AI-7). Strikingly, many neurons of the escape circuit, ALM-AVM-AVD and AVA-RIM-AIB-RIV-SMD, are connected in chains of electrical synapses. Our data indicate that electrical synapses can synchronize ensemble activity of neurons within the escape circuit. However, our data also shows that neurons connected by electrical synapses can also display distinct activity patterns. This indicates that chemical synapses within this circuit are required for shaping the temporal dynamics of the circuit. For example, excitatory chemical synapses from the AVD neurons provide a feedforward mechanism to the subsequent activation of the AVA-RIM-AIB-RIV-SMD cluster. The subsequent activity of the ALM-AVM-AVD and AVA-RIM-AIB clusters are

consistent with synfire models in which synchronous activity of one group of neurons is required to activate the next group (Hayon, Abeles and Lehmann, 2005). However, the results of our laser ablation studies indicate that there is functional redundancy in the circuit, as removal of individual neurons disrupts but does not prevent execution of behavior (Figure AI-2). Chemical synapses can also provide an inhibitory feedforward and feedback mechanism. For example, tyramine signaling from RIM provides inhibitory feedforward inputs onto SMD and electrically coupled RIV (Pirri *et al.*, 2009), thereby delaying the onset of SMD/RIV activity during the reversal. We have previously shown that extra-synaptic tyramine signaling inhibits GABA release on the ventral body wall muscles thus facilitating the ventral body bend during the omega turn (Donnelly *et al.*, 2013). Feedback inhibitory output of AIB onto RIM (Piggott *et al.*, 2011) may reset the activity of the RIM, terminating the release of tyramine and disinhibiting the AVA and SMD, allowing forward movement and head bending to resume simultaneously (Fig. AI-7).

Electrical synapses are known for their ability to synchronize neural activity patterns. Nevertheless, distinct activity patterns can also occur among electrically coupled neurons, for example in the GABAergic neurons of the neocortex and cerebellum (Merriam, Netoff and Banks, 2005; Vervaeke *et al.*, 2010). We have shown that synaptic chains of neurons that are coupled by both electrical and chemical synapses encodes the distinct phases and transitions of a compound

motor sequence. The neural coding of the fixed action pattern of the nematode escape response is surprisingly complex for a relatively small circuit and provides new insight into the synaptic regulation of compound motor behaviors.

Methods

Behavioral assays

Behavioral assays were performed on young adult animals at room temperature on NGM agar plates seeded with OP50 E.coli as a food source unless otherwise noted (Brenner, 1974). Touch assays were performed on plates seeded with a thin lawn of OP50 to prevent any physical restraint that may occur when the animals move through thick bacteria. To induce escape responses in laser ablated animal, the worms were touched just behind the posterior bulb of the pharynx with a fine hair or eyelash. Escape responses were scored for the number of backwards body bends, suppression of head movements and the execution of an omega turn. Worm tracking experiments were performed using the Multi-Worm Tracker kindly provided by Rex Kerr. Analysis was done using Choreography software and custom designed Matlab (Mathworks) scripts (Swierczek *et al.*, 2011). All behavioral experiments were performed on NGM plates which were seeded with one drop of spread OP50 that was allowed to grow overnight at room temperature to form a thin bacterial lawn. 40 young adult worms were transferred to each assay plate and allowed to rest for 5 min. For

experiments involving a plate tap, the mechanical stimulus was a 20 tap burst with 10ms between each tap. Reversals were considered tap induced if they occurred within 1s of the stimulus. Ventral turns were considered tap induced if they occurred within 10s of the stimulus. Body bending angles for kymographs was measured using WormLab software (MBF Bioscience) and plotted with Matlab's contour function.

Strain generation

Transgenic strains were generated by microinjection of plasmid DNA. The pL15EK (lin-15+) rescue plasmid was co-injected at 80ng/µl with our transgenic plasmids into lin-15(n765ts) mutant animals. Optogenetic plasmids were injected at a concentration of 80-100ng/µl. GFP and mCherry reporter plasmids were injected at 100ng/µl. GCaMP plasmids were injected at 50ng/µl. Integration of extra-chromosomal arrays was done with 10 minutes of 120kV X-ray irradiation. Integrated strains were backcrossed into either the N2 Bristol wild type or lite-1(ce314) mutants that are insensitive to short wavelength light (Edwards *et al.*, 2008).

Cell identification and laser ablations

For laser ablations, animals were anesthetized on an agar pad in a drop of 20 mM sodium azide. Laser ablation of neurons was done on L2 and L3 larva using standard methods (Bargmann and Avery, 1995). The promoters used for

fluorescent reporters used in cell identification were nmr-1 (AVD and RIM) and npr-9 (AIB). Cells were identified using location, morphology, and fluorescent reporter expression. The animals were allowed to recover for 1-2 days following the ablations before they were used for behavioral assays.

Calcium Imaging

Single animals expressing GCaMP3 and mCherry in targeted neurons were imaged while moving freely on a 100mm square NGM agar plate containing a thin lawn of OP50 bacteria. Animals were imaged on a motorized stage with a custom dual image-path spinning disk confocal microscope that allowed for simultaneously recording the animal's behavior and red- and green-channel fluorescence.

Briefly, the microscope employs two imaging paths: the fluorescence imaging path uses a 20x objective to record calcium transients and mCherry fluorescence through a spinning disk confocal microscope while a second low magnification imaging path records the animal's posture and orientation under dark-field illumination. The system is built upon a modified Nikon Eclipse LV 100 upright microscope with a Yokogawa CSU22 Confocal Spinning Disk Unit capable of rotating at 5000rpm. Illumination for fluorescence imaging is provided by blue (445nm) and yellow (561nm) lasers housed in an Andor Technologies Laser Combiner System 5000. The lasers are fiber-coupled into the spinning disk system using a quad-band dichroic. Laser power was set such that the sample

was illuminated with 10mW/mm2 of blue and 3mW/mm2 of yellow laser light. Images were recorded with an Andor iXon+ EMCCD camera fitted with a dual-channel DV2 Dual-View imager by Photometrics. Fluorescent images were acquired using AndoriQ or Nikon Elements software.

To image behavior, a separate imaging path from the bottom of the microscope was used. A custom-made ring of 100 individual infrared LEDs (850nm) illuminate the sample perpendicular to the imaging path to create dark-field illumination. The microscope's condenser lens was removed to make space for the behavior imaging path. A prism located below the sample reflects light from the sample through a telescope and a long-pass filter (Thorlabs, FEL0750) so as to form an image of the sample on a CCD camera (DMK31BU03 from the Imaging Source). The behavior imaging path approximated that of a microscope with a 4x objective. A modified version of the MindControl software (Leifer *et al.*, 2011; Shipley *et al.*, 2014) was used to record the animal's behavior and to implement real-time tracking to control the motorized stage so as to keep the worm's head centered under the high magnification imaging path.

Behavior images were recorded at 30fps (33ms exposure). For the majority of trials, fluorescent images were acquired using a 20x objective at 20fps with an exposure time of 50ms. Dual-channel images were recorded side-by-side simultaneously. In some trials, fluorescent images were instead recorded using a 10x objective for a larger field of view at the cost of spatial resolution. In a small number of trials fluorescence images were acquired with a 20x objective and

temporally alternating laser illumination was used to achieve a greater effective field of view at the cost of temporal resolution. During those trials spectral unmixing was employed to infer relative mCherry and GCaMP fluorescence intensity.

In all trials, a brief vibration was applied to the edge of the plate by either directly vibrating the side of the plate with an electric toothbrush for approximately 0.5s or by hitting the motorized stage with a screwdriver. Neurons coexpressing GCaMP3 and mCherry were imaged before, during and after the mechanosensory stimulus. Due to the nature of the vibration to the entire substrate, animals would either sprint forward or escape backwards. Only animals that executed backwards escape responses that culminated in omega turns were included in analysis. Single animals were stimulated 1-4 times with at least a three-minute interstimulus interval.

Neural activity is reported as normalized deviations from baseline of the ratio between GCaMP3 and mCherry fluorescence, $\Delta R/R0=(R-R0)/R0$ as described in detail in (Shipley *et al.*, 2014). Briefly, the baseline R0 is defined as the mean of R during a time window spanning the start of the recording to the onset of vibration. We have chosen to report fluorescence intensity as a frame-by-frame ratio of green fluorescence from GCaMP3 to red fluorescence from mCherry so as to better account for artifacts from the animal's motion. The ratio is defined as $R= (I_{GCaMP3}- B_{Green}) /(I_{mCherry}- B_{red})$. Where I_{GCaMP3} and $I_{mCherry}$ are the fluorescence intensities of GCaMP3 and mCherry, respectively, calculated by

taking the median intensity value of pixels selected as the 40% brightest red-channel pixel intensities in a circular ROI centered on the neuron of interest. Bgreen and Bred are the background in the green and red, respectively, calculated as the median intensity of the local background defined by an annulus surrounding the neuron of interest. Custom MATLAB scripts were used to calculate the ΔR/R0 for each frame, and the time series was smoothed with a low-pass Gaussian filter (σ = 5 frames).

Occasionally the neuron of interest was obscured through motion artifact, change in z-position, or through tracking failure. If the neuron was obviously obscured or if the mCherry signal fell below an intensity threshold the fluorescence signal was tossed out for those frames. Gaps in fluorescence data of less than 0.5s are interpolated, while larger gaps are shown in the data as whitespace. The 0.5s cutoff was chosen because GCaMP3 has roughly a fall time of half a second.

Optogenetics

Animals were grown on NGM agar plates containing OP50 supplemented with 0.2-0.4nmol of *all-trans* retinal for optogenetic stimulation, or in the absence of *all-trans* retinal for controls. Young adult animals were transferred to a fresh NGM plate containing OP50 with or without retinal supplementation depending on condition and allowed to acclimate for 10 min prior to imaging using a Stereo Discovery.V12 epifluorescence microscope (Carl Zeiss Microscopy GmbH). Animals were illuminated with blue light transmitted light for 5s to activate the

optogenetic proteins expressed in the nervous system. Video recordings were made to quantify ventral turn latency. Animals were considered non-responders if they did not initiate a ventral turn within 35s.

Strains:
N2
QW373: zfIs18[Pmec-4::ChR2::YFP, lin-15+]; lite-1(ce314)
QW912: zfIs46[Pnmr-1::ChR2::GFP, lin-15+]; lite-1(ce314)
QW804: zfIs74[Prig-3::ChR2::mCherry, lin-15+]; lite-1(ce314)
QW910: zfIs9[Ptdc-1::ChR2::GFP, lin-15+]; lite-1(ce314)
QW805: zfIs75[Plgc-55(-120-+773)::ChR2::mCherry, lin-15+]; lite-1(ce314)
QW911: zfIs66[Plim-4(-3328--2174)::ChR2::GFP, lin-15+]; lite-1(ce314)
QW372: zfEx63[Plim-4::ChR2::GFP]; lin-15(n765ts)
QW1097: zfIs112[Pnpr-9::ChR2::GFP]; lite-1(ce314)
QW945: zfIs91[Plgc-55(-120-+773)::Arch::GFP, lin-15+]; lite-1(ce314)
QW973: zfIs74[Prig-3::ChR2::mCherry, lin-15+]; zfIs89[Plgc-55(-120-+773)::Arch::GFP, lin-15+]
QW974: zfIs12[Prig-3::ChR2::GFP, lin-15+]; zfIs76[Plgc-55(-120-+773)::ChR2::mCherry, lin-15+]; lite-1(ce314)
QW972: zfIs18[Pmec-4::ChR2::YFP, lin-15+]; zfIs89[Plgc-55(-120-+773)::Arch::GFP, lin-15+]
QW1110: zfIs18[Pmec-4::ChR2::YFP, lin-15+]; zfIs110[Pnpr-9::Arch::GFP, lin-15+]; lite-1(ce314)
QW971: zfIs18[Pmec-4::ChR2::YFP, lin-15+]; zfIs88[Plim-4(-3328--2174)::Arch::GFP, lin-15+]; lite-1(ce314)
QW625: zfIs42[Prig-3::GCaMP3::SL2::mCherry, lin-15+]

QW743: zfIs64[Pcex-1::GCaMP3::SL2::mCherry, lin-15+]

QW1056: zfEx427[Pnmr-1::mCherry::SL2::GCaMP6, lin-15+]; lin-15(n765ts), lite-1(ce314)

QW697: zfIs53[Plgc-55(-120-+773)::mCherry::SL2::GCaMP3, lin-15+]

QW783: zfIs68[Plim-4(-3328--2174)::mCherry::SL2::GCaMP3, lin-15+]

QW1112: zfIs118[Pnpr-9::mCherry::SL2::GCaMP6s, lin-15+]; lite-1(ce314)

AQ2953: ljIs131[Pmyo-3::GCaMP3::UrSL::RFP]

QW1153: zfIs68[Plim-4(-3328--2174)::mCherry::SL2::GCaMP3]; zfIs4[Plgc-55::mCherry]

QW310: zfIs21[Plim-4::GFP, lin-15+]

QW322: mgIs19[Plim-4::GFP; rol-6]; ufIs53[Punc-17::ChR2::mCherry]

QW775 vsIs48[Punc-17::GFP]; zfis2[Plgc-55::mCherry]

QW2: zfIs1[Ptdc-1::GFP, lin-15+], lin-15(n765ts)

QW1052: zfIs106[Plgc-55::LGC-55::GFP, lin-15+]

VM484: akIs3[Pnmr-1::GFP]

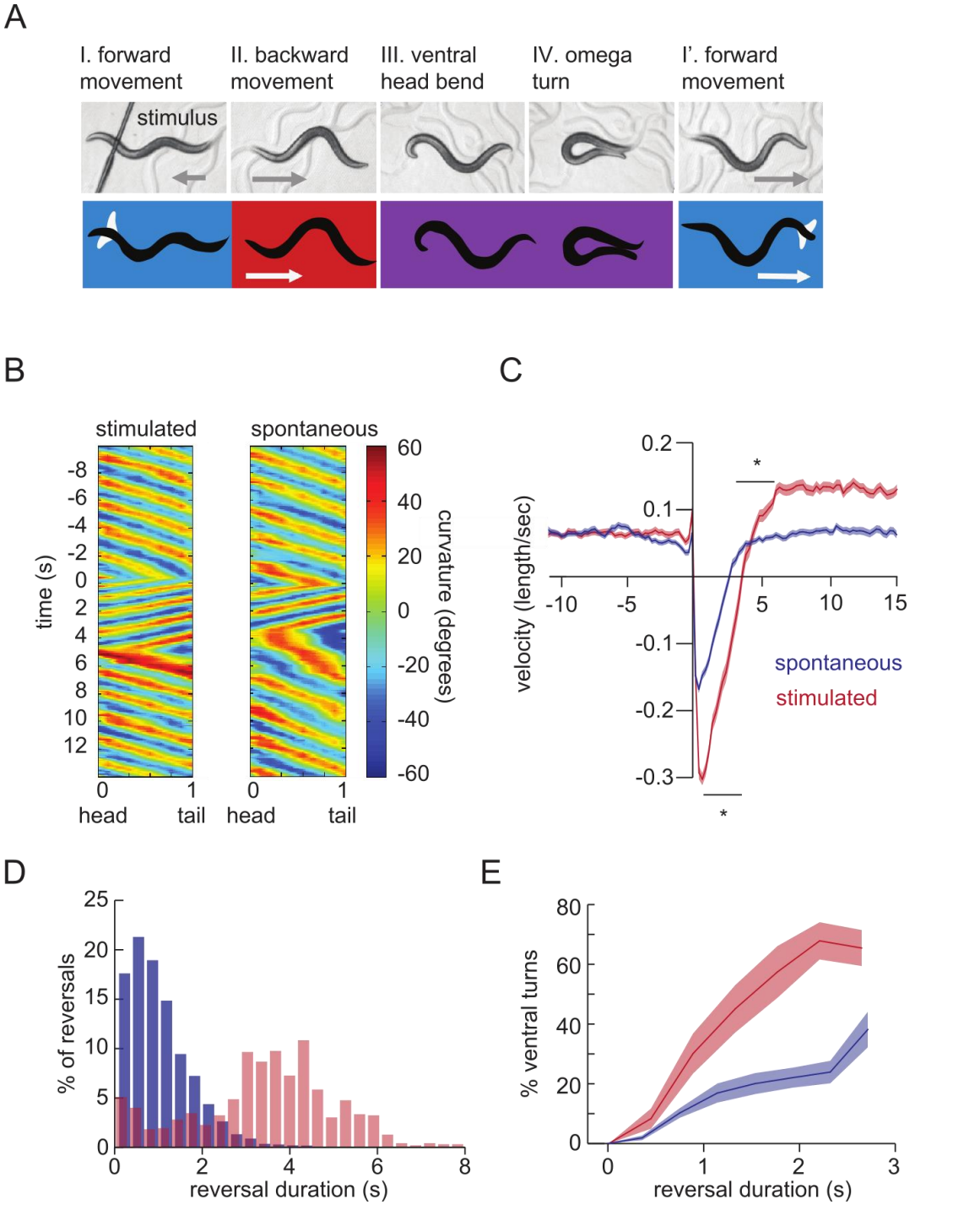

Figure AI-1. The *C. elegans* escape response is a compound motor sequence. (a) C. elegans executes an escape response to mechanical

stimulation. The individual phases (I-IV) of a C. elegans escape response are shown beginning with basal forward locomotion accompanied with exploratory head movements (I). Touch (stimulus) induces a reversal and the suppression of head movements (II), which culminates in a deep ventral bend of the head (III) followed by the deep ventral body bend (omega turn, IV). Forward locomotion and exploratory head movements are reinitiated after the omega turn (I'). Arrows indicate the direction of movement. (b) Kymographs of body curvature during a reversal in response to a tap stimulus delivered at t = 0s and a spontaneous reversal, showing the speed and amplitude of bending activities during forward, reverse, and omega turn movements. (e) Mean (+/- SEM) instantaneous velocity during escape responses to a tap stimulus (red line) and during spontaneous reversals (blue line) (n > 1000). Instantaneous velocity traces were aligned to the onset of the reversal (t = 0s). P values: * <0.05, two-tailed Student's t test. (d) Distribution of reversal duration for tap induced reversals (red bars, n=299) and for spontaneous reversals (blue bars, n=453). (e) Probability (+/- SEM) of a reversal culminating in a ventral omega turn over increasing reversal durations following escape responses to tap stimulus (red line) and following spontaneous reversals (blue line).

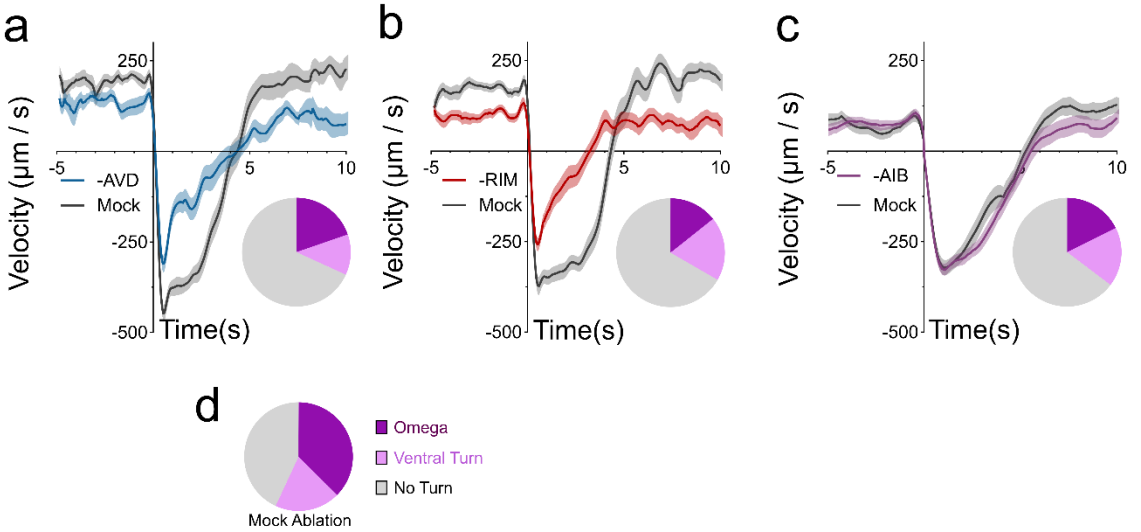

Figure AI-2. Ablation of the RIM affects reversal duration and turning behavior in the escape response. (a-c) Quantification of touch induced escape behavior in animals lacking specific pairs of interneurons versus mock ablated animals. Negative velocity indicates the speed of backward locomotion. Reversal duration is indicated by the time when velocity becomes positive (forward locomotion resumes). Solid lines in graphs indicate mean velocity in µm per second, shaded region indicates SEM. Inset pie charts show the proportion of cell ablated animals responding with an omega turn, ventral turn or resuming forward locomotion without turning (no response). (a) AVD ablation results in slower reversal velocity and reduced omega turning (omega = 19.69%, ventral turn = 12.12% no turn = 68.18%). AVD ablation n= 37, mock ablation n = 45. (b) RIM ablation reduced reversal velocity shortened reversal duration and reduced turning (omega = 14.38%, ventral turn = 19.04%, no turn = 64.7%). RIM ablation n = 44, mock ablation n = 39. AIB ablation did not affect reversals but reduced

turning behavior (omega = 17.64%, ventral turn = 17.64%, no turn = 64.7%). AIB ablation n = 34, mock ablation n = 51. (d) Turning behavior in mock ablated animals (omega = 37.5%, ventral turn = 19.44%, no turn = 43.05%, n = 71).

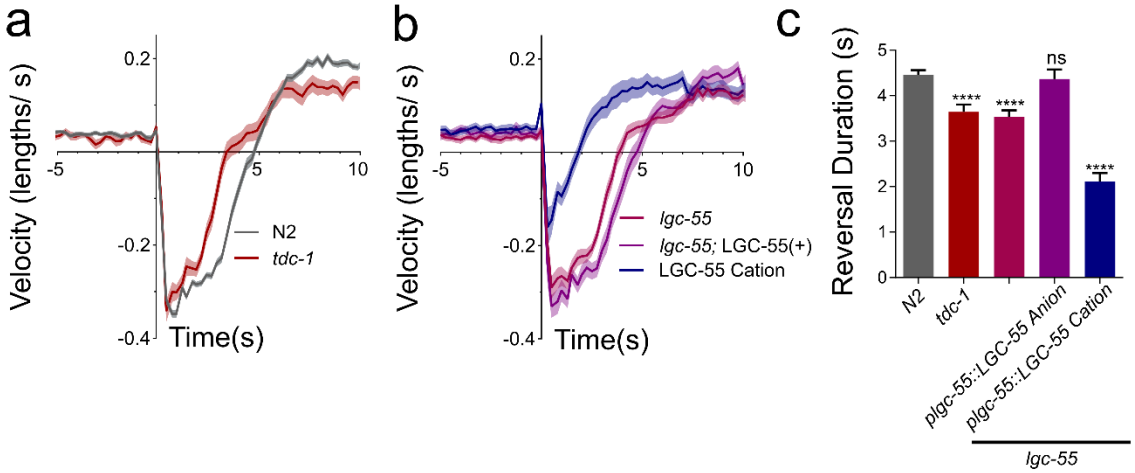

Figure AI-3. Mutations in tyramine signaling shorten reversal duration during the escape response. Quantification of reversal behavior during the escape response triggered by mechanical plate tap. (a-b) Velocity traces aligned relative to the delivery of a tap stimulus at t=0s. The solid lines represent mean velocity in lengths per second and the shaded region indicates SEM. (a) wild type (N2) (n=216), *tdc-1*(n=68). (b) *lgc-55* (n=76), *lgc-55;* +[*Plgc-55*::LGC-55 anion] (n=51), *lgc-55;* +[*Plgc-55*::LGC-55 cation] (n=68). (c) Quantification of the mean duration of tap stimulated reversals. Wild type (N2) mean duration ± SEM = 4.46±0.09 s, n=156. *tdc-1*, mean duration ± SEM = 3.64±0.16 s, n=60. *lgc-55,* mean duration ± SEM = 3.53±0.14 s, n=44. *lgc-55;* +[*Plgc-55::*LGC-55 anion], mean duration ± SEM = 4.36±0.2 s, n=41. *lgc-55;* +[*Plgc-55::*LGC-55 cation], mean duration ± SEM = 2.12±0.18 s, n=32. Statistics were calculated with ordinary one-way ANOVA with Dunnett's multiple comparison test, **** P<0.0001, ns = not significant.

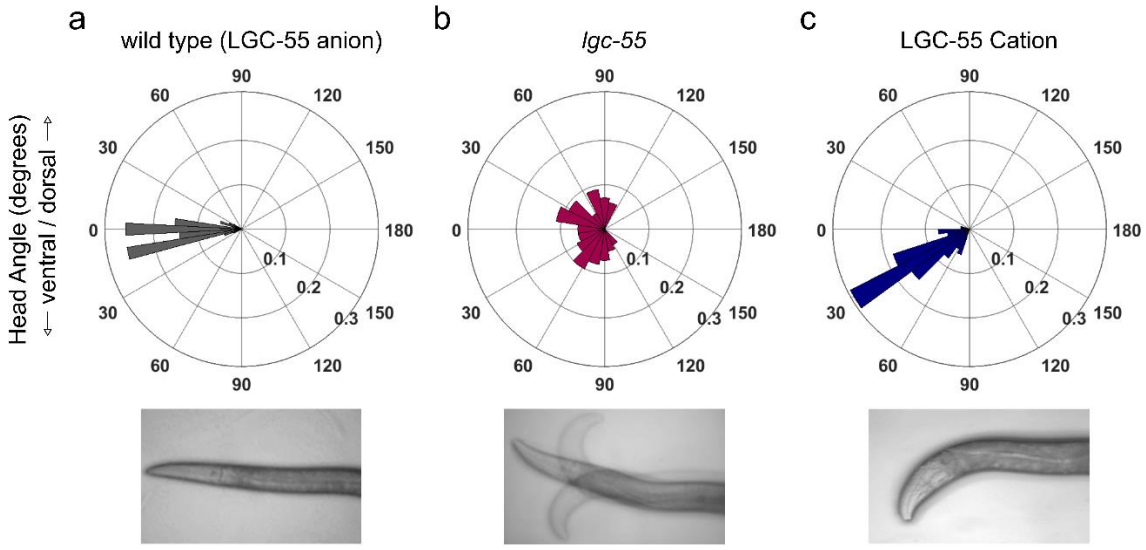

Figure AI-4. Activation of cation-selective LGC-55 imparts a ventral bias.

Polar histogram showing distribution of head angle after 5 min exposure to 30mM tyramine. Bin sizes are 15°, bar heights indicate fraction of responses. Representative images of genotypes are shown below histograms (a) wild type animals paralyze with straight necks. Mean angle ±SEM = 1.63±1.13° ventral, n=98. (b) *lgc-55* mutants continue moving their heads freely. Mean angle ±SEM = 4.92±6.79° ventral, n=99. (c) *lgc-55* mutants expressing the cation selective LGC-55 variant [*lgc-55; Plgc-55*::LGC-55 cation] display a strong ventral head kink. Mean angle ±SEM = 31.84±1.7° ventral, n=98.

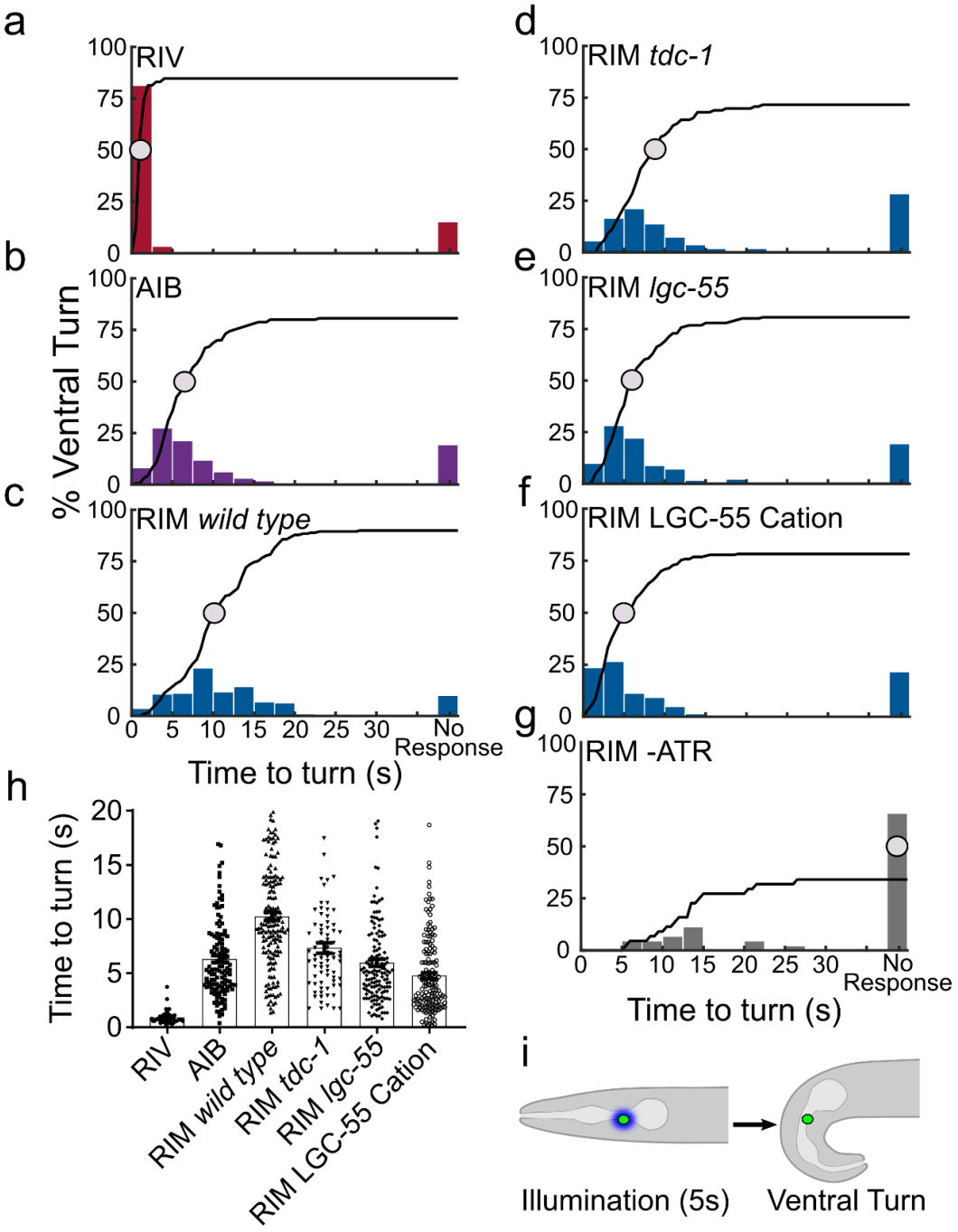

Figure AI-5. The timing of the ventral head bend is delayed by tyramine and LGC-55. Quantification of timing of ventral turn following optogenetic activation of neurons with Channelrhodopsin2 (ChR2). (a-g) Histograms showing the

distribution of ventral turn response times binned in 2.5s incriments. Black line represents the cumulative distribution function with half maximal response indicated with a circle. Animals that do not make a ventral turn within 35s are considered non responders. (a) ChR2 activation of the RIV with *Plim-4::*ChR2::GFP. Response rate = 84.7%, mean latency ±SEM = 0.91±0.08s, n=59. (b-g) Ventral turn response time was measured in *unc-3*(e151) mutant background to eliminate backward locomotion. (b) ChR2 activation of the AIB with *Pnpr-9::*ChR2::GFP. Response rate = 80.6%, mean latency ±SEM = 6.3±0.32s, n=160. (c-g) ChR2 was expressed in the RIM using *Ptdc-1::*ChR2::GFP in different genetic backgrounds. (c) Wild type background. Response rate = 89.9%, mean latency ±SEM = 10.25±0.37s, n=189. (d) *tdc-1* mutant background. Response rate = 71.5%, mean latency ±SEM = 7.33±0.46s, n=109. (e) *lgc-55* mutant background. Response rate = 80.6%, mean latency ±SEM = 5.97±0.32s, n=181. (f) *lgc-55;* +[*Plgc-55*::LGC-55 Cation]. Response rate = 78.3%, mean latency ±SEM = 4.76±0.28s, n=203. (g) *Ptdc-1::*ChR2::GFP wild type worms raised in the absence of *all-trans* retinal. Response rate = 34.1%, mean latency ±SEM = 13.16±1.46s, n=44. (h) Bar graph of the data from a-g depicting mean response time. (i) Schematic depicting approach, animals were stimulated with blue light for 5s and the time required to initate a ventral head bend was recorded.

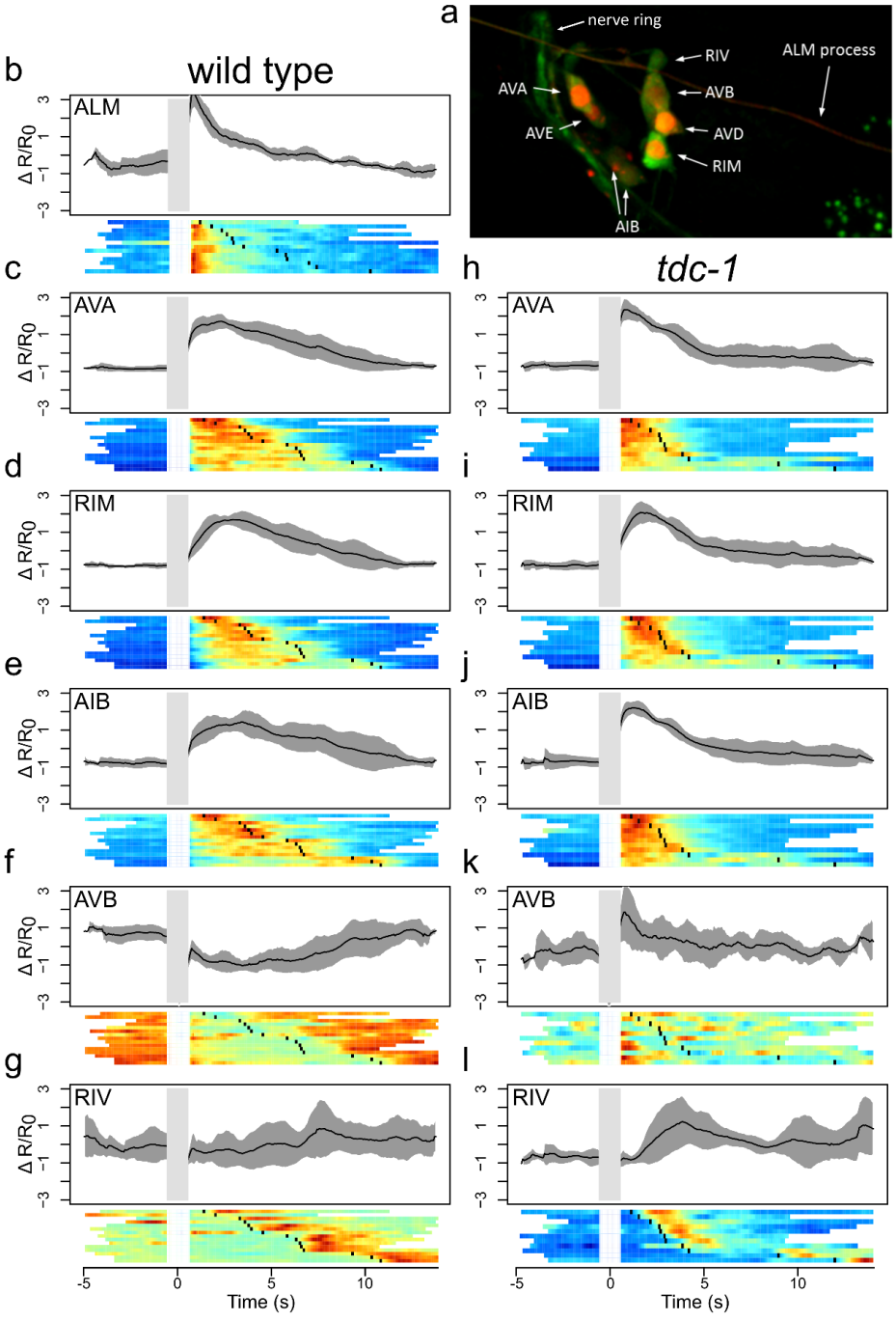

Figure AI-6. Calcium dynamics in a neural network that orchestrates a compound motor sequence. (a) Projection of confocal micrograph showing neurons in the head ganglia expressing GCaMP6s and a nuclear localized

mCherry reporter for cell identification. Individual neurons could be reliably identified based on anatomical position. (b-i) Neural activity was measured as a fluorescence ratio of GCaMP to mCherry in unrestrained behaving animals ($\Delta R/R_0$). Neural activity traces and heat maps are aligned to the onset of reversal from a mechanical stimulus (vertical grey bar), vibration artifacts prevented accurate measurement of fluorescent signal during stimulation. Each heat map row represents a single trial (ALM (b): n=13, wild type (c-g): n=15, *tdc-1* (h-j): n=11). Mean (+/- SEM) instantaneous $\Delta R/R_0$ values over time are plotted above the heat maps, the central black line represents the mean and the shaded grey regions SEM. Reversal duration for individual trials is indicated by a black dot in the heat map which marks the transition from reversal to ventral bend.

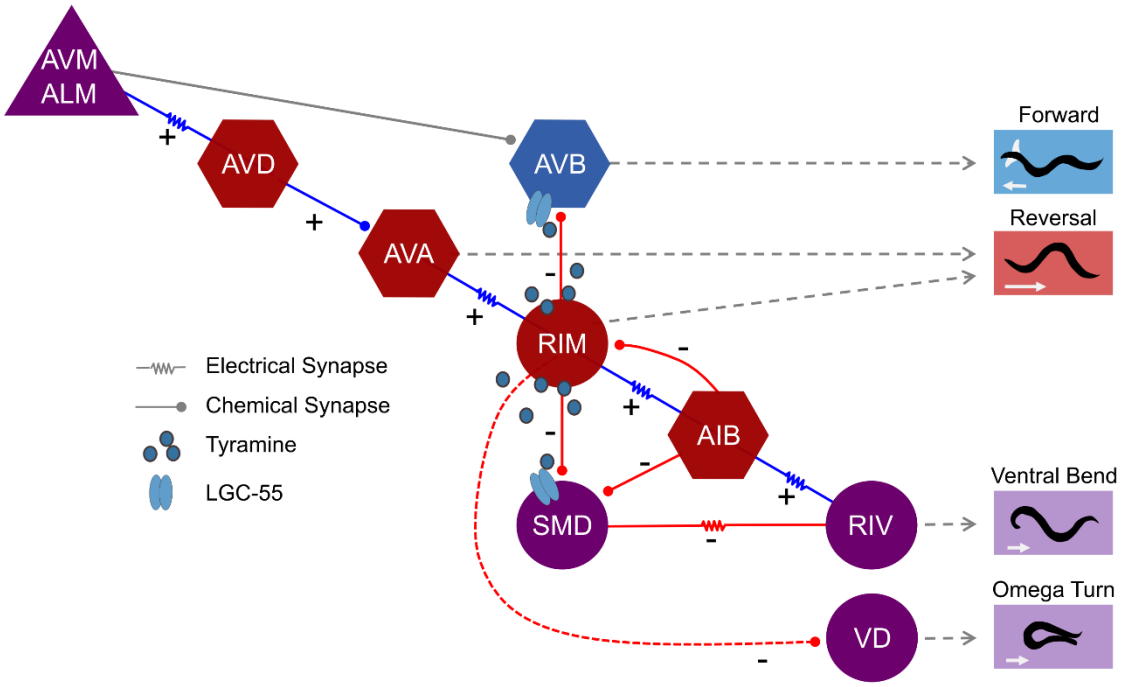

Figure AI-7. Model: A chain of electrical and chemical synapses regulates synchronization and sequence during the C. elegans escape response. Neural activity patterns progress from mechanosensory neurons to motor neurons for backward movement, ventral head bend, and forward movement through a chain of electrical and chemical synapses. Touch activates the ALM/AVM/AVD cluster of electrically connected neurons. Feedforward excitatory signaling from the AVD activates the AVA/RIM/AIB/RIV/SMD cluster. Feedforward inhibitory signaling mediated by tyramine inhibits the AVB, the cholinergic SMD/RIV and the GABAergic VD neurons, prolonging the reversal, delaying the ventral head bend, and facilitating the omega turn, respectively. Feedback inhibitory signaling from the AIB to RIM (Piggott *et al.*, 2011) resets

activity of the RIM, terminating tyramine release and allowing forward locomotion and head bending to resume.

APPENDIX II: Additional publications

I made contributions to the following publications during the course of my thesis research.

Wang, Y., Zhang, X., Xin, Q., Hung, W., **Florman, J**., Huo, J., Xu, T., Xie, Y., Alkema, M. J., Zhen, M., & Wen, Q. (2020). Flexible motor sequence generation during stereotyped escape responses. *eLife*, *9*, e56942. https://doi.org/10.7554/eLife.56942

-I generated transgenic strains used in the study.

Philbrook, A., Ramachandran, S., Lambert, C. M., Oliver, D., **Florman, J.**, Alkema, M. J., Lemons, M., & Francis, M. M. (2018). Neurexin directs partner-specific synaptic connectivity in *C. elegans*. *eLife*, *7*, e35692. https://doi.org/10.7554/eLife.35692

- I performed behavioral experiments and analyzed data.

Awal, M. R., Austin, D., **Florman, J.**, Alkema, M., Gabel, C. V., & Connor, C. W. (2018). Breakdown of Neural Function under Isoflurane Anesthesia: In Vivo, Multineuronal Imaging in Caenorhabditis elegans. *Anesthesiology*, *129*(4), 733–743. https://doi.org/10.1097/ALN.0000000000002342.

-I generated transgenic stains used in this study.

Venkatachalam, V., Ji, N., Wang, X., Clark, C., Mitchell, J. K., Klein, M., Tabone, C. J., **Florman, J**., Ji, H., Greenwood, J., Chisholm, A. D., Srinivasan, J., Alkema, M., Zhen, M., & Samuel, A. D. (2016). Pan-neuronal imaging in roaming Caenorhabditis elegans. *Proceedings of the National Academy of Sciences of the United States of America*, *113*(8), E1082–E1088. https://doi.org/10.1073/pnas.1507109113

-I generated transgenic stains used in this study.

Bibliography

Alkema, M. J. *et al.* (2005) 'Tyramine functions independently of octopamine in the Caenorhabditis elegans nervous system', *Neuron*, 46(2), pp. 247–260. doi: 10.1016/j.neuron.2005.02.024.

Allen, A. R. *et al.* (2006) 'Modulation of contractile function through neuropeptide Y receptors during development of cardiomyocyte hypertrophy', *Journal of Pharmacology and Experimental Therapeutics*, 319(3), pp. 1286–1296. doi: 10.1124/jpet.106.110445.

An, J. H. *et al.* (2005) 'Regulation of the Caenorhabditis elegans oxidative stress defense protein SKN-1 by glycogen synthase kinase-3', *Proceedings of the National Academy of Sciences of the United States of America*, 102(45), pp. 16275–16280. doi: 10.1073/pnas.0508105102.

Arantes-Oliveira, N., Berman, J. R. and Kenyon, C. (2003) 'Healthy Animals with Extreme Longevity', *Science*, 302(5645), p. 611. doi: 10.1126/science.1089169.

Asikainen, S. *et al.* (2005) 'Selective sensitivity of Caenorhabditis elegans neurons to RNA interference', *NeuroReport*, 16(18), pp. 1995–1999. doi: 10.1097/00001756-200512190-00005.

Ayyadevara, S. *et al.* (2005) 'Lifespan and stress resistance of Caenorhabditis elegans are increased by expression of glutathione transferases capable of metabolizing the lipid peroxidation product 4-hydroxynonenal', *Aging Cell*, 4(5), pp. 257–271. doi: 10.1111/j.1474-9726.2005.00168.x.

Balasubramaniam, A. *et al.* (1988) 'Comparison of the effects of neuropeptide Y (NPY) and 4-norleucine-NPY on isolated perfused rat hearts; effects of NPY on atrial and ventricular strips of rat heart and on rabbit heart mitochondria', *Regulatory Peptides*, 21(3–4), pp. 289–299. doi: 10.1016/0167-0115(88)90012-2.

Barbieri, M. *et al.* (2003) 'Insulin/IGF-I-signaling pathway: An evolutionarily conserved mechanism of longevity from yeast to humans', *American Journal of Physiology - Endocrinology and Metabolism*, 285(5 48-5), pp. 1064–1071. doi: 10.1152/ajpendo.00296.2003.

Bargmann, C. I. and Avery, L. (1995) 'Chapter 10 Laser Killing of Cells in Caenorhabditis elegans', in *Methods in cell biology*. Academic Press, pp. 225–250. doi: 10.1016/S0091-679X(08)61390-4.

Bastiani, C. A. *et al.* (2003) 'Caenorhabditis elegans Gαq Regulates Egg-Laying Behavior via a PLCβ-Independent and Serotonin-Dependent Signaling Pathway and Likely Functions Both in the Nervous System and in Muscle', *Genetics*, 165(4), pp. 1805–1822. Available at: http://www.genetics.org/content/165/4/1805.short (Accessed: 29 May 2014).

Bauknecht, P. and Jékely, G. (2017) ‘Ancient coexistence of norepinephrine, tyramine, and octopamine signaling in bilaterians’, *BMC Biology*. BMC Biology, 15(1), pp. 1–12. doi: 10.1186/s12915-016-0341-7.

Bean, B. P., Nowycky, M. C. and Tsien, R. W. (1984) ‘β-Adrenergic modulation of calcium channels in frog ventricular heart cells’, *Nature*, 307(5949), pp. 371–375. doi: 10.1038/307371a0.

Bentley, B. *et al.* (2016) ‘The Multilayer Connectome of Caenorhabditis elegans’, *PLoS Computational Biology*, 12(12). doi: 10.1371/journal.pcbi.1005283.

Berger, A. J., Hart, A. C. and Kaplan, J. M. (1998) ‘Gα s -Induced Neurodegeneration in Caenorhabditis elegans’, *The Journal of Neuroscience*, 18(8), pp. 2871–2880. doi: 10.1523/JNEUROSCI.18-08-02871.1998.

Bhardwaj, A. *et al.* (2018) ‘FLP-18 functions through the G-protein coupled receptors NPR-1 and NPR-4 to modulate reversal length in Caenorhabditis elegans.’, *The Journal of neuroscience : the official journal of the Society for Neuroscience*, 38(20), pp. 1955–17. doi: 10.1523/JNEUROSCI.1955-17.2018.

Bhardwaj, A., Pandey, P. and Babu, K. (2020) ‘Control of locomotory behavior of caenorhabditis elegans by the immunoglobulin superfamily protein RIG-3’, *Genetics*, 214(1), pp. 135–145. doi: 10.1534/genetics.119.302872.

Bhatla, N. and Horvitz, H. R. (2015) ‘Light and Hydrogen Peroxide Inhibit C. elegans Feeding through Gustatory Receptor Orthologs and Pharyngeal Neurons’, *Neuron*. Elsevier Inc., 85(4), pp. 804–818. doi: 10.1016/j.neuron.2014.12.061.

Blitz, D. M. *et al.* (1999) ‘Different proctolin neurons elicit distinct motor patterns from a multifunctional neuronal network’, *Journal of Neuroscience*, 19(13), pp. 5449–5463. doi: 10.1523/jneurosci.19-13-05449.1999.

De Boer, P. A. C. M. *et al.* (1997) ‘Functional role of peptidergic anterior lobe neurons in male sexual behavior of the snail Lymnaea stagnalis’, *Journal of Neurophysiology*, 78(6), pp. 2823–2833. doi: 10.1152/jn.1997.78.6.2823.

Boland, B. *et al.* (1992) ‘ATP activates P2x-contracting and P2y-relaxing purinoceptors in the smooth muscle of mouse vas deferens’, *British Journal of Pharmacology*, 107(4), pp. 1152–1158. doi: 10.1111/j.1476-5381.1992.tb13422.x.

Borovac Štefanović, L. *et al.* (2015) ‘Oxidative status and the severity of clinical symptoms in patients with post-traumatic stress disorder’, *Annals of Clinical Biochemistry*, 52(1), pp. 95–104. doi: 10.1177/0004563214528882.

Brenner, S. (1974) ‘The genetics of Caenorhabditis elegans.’, *Genetics*, 77(1),

pp. 71–94.

Brundage, L. *et al.* (1996) ‘Mutations in a C. elegans Gqα gene disrupt movement, egg laying, and viability’, *Neuron*, 16(5), pp. 999–1009. doi: 10.1016/S0896-6273(00)80123-3.

Burnstock, G. (1976) ‘Do some nerve cells release more than one transmitter?’, *Neuroscience*, 1(4), pp. 239–248. doi: 10.1016/0306-4522(76)90054-3.

Burnstock, G. and Verkhratsky, A. (2010) ‘Vas deferens - A model used to establish sympathetic cotransmission’, *Trends in Pharmacological Sciences*. Elsevier Ltd, 31(3), pp. 131–139. doi: 10.1016/j.tips.2009.12.002.

Busch, K. E. *et al.* (2012) ‘Tonic signaling from O 2 sensors sets neural circuit activity and behavioral state’, *Nature Neuroscience*. Nature Publishing Group, 15(4), pp. 581–591. doi: 10.1038/nn.3061.

Calabrese, E. J. (2008) ‘Stress biology and hormesis: The Yerkes-Dodson Law in psychology - A special case of the hormesis dose response’, *Critical Reviews in Toxicology*, 38(5), pp. 453–462. doi: 10.1080/10408440802004007.

Camhi, J. M. (1984) *Neuroethology: Nerve Cells and the Natural Behavior of Animals*. Sunderland: Sinauer Associates Inc.

Cannon, W. B. (1915) *Bodily Changes in Pain, Hunger, Fear and Rage; An Account of Recent Researches into the Function of Emotional Excitement*. NEW YORK AND LONDON D. APPLETON AND COMPANY.

Chalasani, S. H. *et al.* (2007) ‘Dissecting a circuit for olfactory behaviour in Caenorhabditis elegans’, *Nature*, 450(7166), pp. 63–70. doi: 10.1038/nature06292.

Chalfie, M. *et al.* (1985) ‘The neural circuit for touch sensitivity in Caenorhabditis elegans.’, *The Journal of neuroscience : the official journal of the Society for Neuroscience*, 5(4), pp. 956–64. Available at: http://www.ncbi.nlm.nih.gov/pubmed/3981252.

Chalfie, M. and Sulston, J. (1981) ‘Developmental genetics of the mechanosensory neurons of Caenorhabditis elegans’, *Developmental Biology*, 82(2), pp. 358–370. doi: 10.1016/0012-1606(81)90459-0.

Chang, Y. J. *et al.* (2015) ‘Modulation of locomotion and reproduction by FLP neuropeptides in the nematode Caenorhabditis elegans’, *PLoS ONE*, 10(9), pp. 1–16. doi: 10.1371/journal.pone.0135164.

Chen, D. *et al.* (2016) ‘The Neuropeptides FLP-2 and PDF-1 act in Concert to Arouse Caenorhabditis elegans Locomotion.’, *Genetics*, 204(November), p. genetics.116.192898. doi: 10.1534/genetics.116.192898.

Chen, T. W. E. A. (2013) ‘Ultrasensitive fluorescent proteins for imaging neuronal activity’, *Nature*, 499(7458), pp. 295–300. doi: 10.1038/nature12354.

Chew, Y. L. *et al.* (2018) ‘An Afferent Neuropeptide System Transmits Mechanosensory Signals Triggering Sensitization and Arousal in C. elegans’, *Neuron*. Elsevier Inc., 99(6), pp. 1233-1246.e6. doi: 10.1016/j.neuron.2018.08.003.

Chiang, W. C. *et al.* (2012) ‘HSF-1 regulators DDL-1/2 link insulin-like signaling to heat-shock responses and modulation of longevity’, *Cell*. Elsevier Inc., 148(1–2), pp. 322–334. doi: 10.1016/j.cell.2011.12.019.

Choi, S. *et al.* (2013) ‘Analysis of NPR-1 reveals a circuit mechanism for behavioral quiescence in C.elegans’, *Neuron*. Elsevier Inc., 78(5), pp. 869–880. doi: 10.1016/j.neuron.2013.04.002.

Choi, S. *et al.* (2015) ‘Sensory Neurons Arouse C. elegans Locomotion via Both Glutamate and Neuropeptide Release’, *PLoS Genetics*, 11(7), pp. 1–20. doi: 10.1371/journal.pgen.1005359.

Chronis, N., Zimmer, M. and Bargmann, C. I. (2007) ‘Microfluidics for in vivo imaging of neuronal and behavioral activity in Caenorhabditis elegans’, *Nature Methods*, 4(9), pp. 727–731. doi: 10.1038/nmeth1075.

Chun, L. *et al.* (2015) ‘Metabotropic GABA signalling modulates longevity in C. elegans’, *Nature Communications*. Nature Publishing Group, 6. doi: 10.1038/ncomms9828.

Coates, J. C. and Bono, M. De (2002) ‘Antagonistic pathways in neurons exposed to body fluid regulate social feeding in Caenorhabditis elegans’, *Nature*, 419(6910), pp. 925–929. doi: 10.1038/nature01065.1.

Cohen, M. *et al.* (2009) ‘Coordinated regulation of foraging and metabolism in C. elegans by RFamide neuropeptide signaling.’, *Cell metabolism*. Elsevier Ltd, 9(4), pp. 375–85. doi: 10.1016/j.cmet.2009.02.003.

Croll, N. A. (1975) ‘Components and patterns in the behaviour of the nematode Caenorhabditis elegans’, *Journal of Zoology*, 176(2), pp. 159–176.

Curtis, A. L. *et al.* (2012) ‘Predator stress engages corticotropin-releasing factor and opioid systems to alter the operating mode of locus coeruleus norepinephrine neurons’, *Neuropharmacology*. Elsevier Ltd, 62(4), pp. 1737–1745. doi: 10.1016/j.neuropharm.2011.11.020.

Cypser, J. R. and Johnson, T. E. (2002) ‘Multiple stressors in Caenorhabditis elegans induce stress hormesis and extended longevity’, *Journals of Gerontology - Series A Biological Sciences and Medical Sciences*, 57(3), pp. 109–114. doi: 10.1093/gerona/57.3.B109.

Dal Santo, P. *et al.* (1999) ‘The inositol trisphosphate receptor regulates a 50-second behavioral rhythm in C. elegans.’, *Cell*, 98(6), pp. 757–67. doi: 10.1016/s0092-8674(00)81510-x.

Danese, A. *et al.* (2009) ‘Adverse childhood experiences and adult risk factors for age-related disease: Depression, inflammation, and clustering of metabolic risk markers’, *Archives of Pediatrics and Adolescent Medicine*, 163(12), pp. 1135–1143. doi: 10.1001/archpediatrics.2009.214.

Daskalakis, N. P., Lehrner, A. and Yehuda, R. (2013) ‘Endocrine Aspects of Post-traumatic Stress Disorder and Implications for Diagnosis and Treatment’, *Endocrinology and Metabolism Clinics of North America*. Elsevier Inc, 42(3), pp. 503–513. doi: 10.1016/j.ecl.2013.05.004.

Dielenberg, R. A., Hunt, G. E. and McGregor, I. S. (2001) ‘“When a rat smells a cat”: The distribution of Fos immunoreactivity in rat brain following exposure to a predatory odor’, *Neuroscience*, 104(4), pp. 1085–1097. doi: 10.1016/S0306-4522(01)00150-6.

Domeier, T. L. *et al.* (2008) ‘IP3 receptor-dependent Ca2+ release modulates excitation-contraction coupling in rabbit ventricular myocytes’, *American Journal of Physiology - Heart and Circulatory Physiology*, 294(2), pp. 596–604. doi: 10.1152/ajpheart.01155.2007.

Donnelly, J. L. *et al.* (2013) ‘Monoaminergic orchestration of motor programs in a complex C. elegans behavior.’, *PLoS biology*, 11(4), p. e1001529. doi: 10.1371/journal.pbio.1001529.

Dorman, J. B. *et al.* (1995) ‘The age-1 and daf-2 genes function in a common pathway to control the lifespan of Caenorhabditis elegans’, *Genetics*, 141(4), pp. 1399–1406.

Drechsler, C. (1937) ‘Some Hyphomycetes That Prey on Free-Living Terricolous Nematodes’, *Mycologia*, 29(4), pp. 447–552.

Du, W. *et al.* (2016) ‘HID-1 is required for homotypic fusion of immature secretory granules during maturation’, *eLife*, 5(OCTOBER2016), pp. 1–22. doi: 10.7554/eLife.18134.

Edelstein, A. D. *et al.* (2014) ‘Advanced methods of microscope control using μManager software’, *Journal of Biological Methods*, 1(2), p. 10. doi: 10.14440/jbm.2014.36.

Edwards, D. H., Heitler, W. J. and Krasne, F. B. (1999) ‘Fifty years of a command neuron: the neurobiology of escape behavior in the crayfish.’, *Trends in neurosciences*, 22(4), pp. 153–61. Available at: http://www.ncbi.nlm.nih.gov/pubmed/10203852.

Edwards, S. L. *et al.* (2008) ‘A novel molecular solution for ultraviolet light detection in Caenorhabditis elegans’, *PLoS Biology*, 6(8), pp. 1715–1729. doi: 10.1371/journal.pbio.0060198.

Ellis, J. L. and Burnstock, G. (1990) ‘Neuropeptide Y neuromodulation of sympathetic co-transmission in the guinea-pig vas deferens’, *British Journal of Pharmacology*, 100(3), pp. 457–462. doi: 10.1111/j.1476-5381.1990.tb15828.x.

Elphick, M. R. and Mirabeau, O. (2014) ‘The evolution and variety of RFamide-type neuropeptides: Insights from deuterostomian invertebrates’, *Frontiers in Endocrinology*, 5(JUN), pp. 1–11. doi: 10.3389/fendo.2014.00093.

Essers, M. A. G. *et al.* (2004) ‘FOXO transcription factor activation by oxidative stress mediated by the small GTPase Ral and JNK’, *EMBO Journal*, 23(24), pp. 4802–4812. doi: 10.1038/sj.emboj.7600476.

Eve Marder and Dirk Bucher (2001) ‘Central pattern generators and the control of rhythmic movements’, *Current Biology*, 11(23), pp. R986–R996.

Everitt, B. J. *et al.* (1984) ‘Differential co-existence of neuropeptide Y (NPY)-like immunoreactivity with catecholamines in the central nervous system of the rat’, *Neuroscience*, 11(2). doi: 10.1016/0306-4522(84)90036-8.

Fares, H. and Greenwald, I. (2001) ‘Genetic analysis of endocytosis in caenorhabditis elegans: Coelomocyte uptake defective mutants’, *Genetics*, 159(1), pp. 133–145.

Feder, J. H. *et al.* (1992) ‘The consequences of expressing hsp70 in Drosophila cells at normal temperatures’, *Genes and Development*, 6(8), pp. 1402–1413. doi: 10.1101/gad.6.8.1402.

Fire, A. *et al.* (1998) ‘Potent andspecific genetic interference by double-stranded RNA in Caenorhabditis elegans’, *Nature*, 391(February), pp. 806–811. Available at: https://www.nature.com/articles/35888.pdf.

Fontana, L., Partridge, L. and Longo, V. D. (2010) ‘Extending healthy life span - From yeast to humans’, *Science*, 328, pp. 321–326. doi: 10.1126/science.1172539.

Fried, G. *et al.* (1985) ‘Evidence for differential localization of noradrenaline and neuropeptide Y in neuronal storage vesicles isolated from rat vas deferens’, *Journal of Neuroscience*, 5(2), pp. 450–458. doi: 10.1523/jneurosci.05-02-00450.1985.

Fried, G., Lundberg, J. M. and Theodorsson-Norheim, E. (1985) ‘Subcellular storage and axonal transport of neuropeptide Y (NPY) in relation to catecholamines in the cat’, *Acta Physiologica Scandinavica*, 125(1), pp. 145–154. doi: 10.1111/j.1748-1716.1985.tb07701.x.

Frooninckx, L. *et al.* (2012) ‘Neuropeptide GPCRs in C. elegans.’, *Frontiers in endocrinology*, 3(December), p. 167. doi: 10.3389/fendo.2012.00167.

Fuller, M. D. *et al.* (2010) ‘Molecular mechanism of calcium channel regulation in the fight-or-flight response’, *Science Signaling*, 3(141), pp. 1–11. doi: 10.1126/scisignal.2001152.

Garcia, L. R., Mehta, P. and Sternberg, P. W. (2001) ‘Regulation of distinct muscle behaviors controls the C. elegans male’s copulatory spicules during mating’, *Cell*, 107(6), pp. 777–788. doi: 10.1016/S0092-8674(01)00600-6.

Garrison, J. L. *et al.* (2012) ‘Oxytocin/Vasopressin-Related Peptides Have an Ancient Role in Reproductive Behavior’, *Science*, 338(6106), pp. 540–543. doi: 10.1126/science.1226201.

Gershkovich, M. M. *et al.* (2019) ‘Pharmacological and functional similarities of the human neuropeptide y system in C. elegans challenges phylogenetic views on the FLP/NPR system’, *Cell Communication and Signaling*. Cell Communication and Signaling, 17(1), pp. 1–15. doi: 10.1186/s12964-019-0436-1.

Gilliam, L. K., Palmer, J. P. and Taborsky, G. J. (2007) ‘Tyramine-mediated activation of sympathetic nerves inhibits insulin secretion in humans’, *Journal of Clinical Endocrinology and Metabolism*, 92(10), pp. 4035–4038. doi: 10.1210/jc.2007-0536.

Gollasch, M. *et al.* (1991) ‘Thyrotropin-releasing hormone induces opposite effects on Ca2+ channel currents in pituitary cells by two pathways’, *Proceedings of the National Academy of Sciences of the United States of America*, 88(22), pp. 10262–10266. doi: 10.1073/pnas.88.22.10262.

Gray, J. M., Hill, J. J. and Bargmann, C. I. (2005) ‘A circuit for navigation in Caenorhabditis elegans.’, *Proceedings of the National Academy of Sciences of the United States of America*, 102(9), pp. 3184–91. doi: 10.1073/pnas.0409009101.

Hashmi, S. *et al.* (2013) ‘A C. elegans model to study human metabolic regulation’, *Nutrition and Metabolism*, 10(1), pp. 1–11. doi: 10.1186/1743-7075-10-31.

Hawk, J. D. *et al.* (2018) ‘Integration of Plasticity Mechanisms within a Single Sensory Neuron of C. elegans Actuates a Memory’, *Neuron*, 97(2), pp. 356-367.e4. doi: 10.1016/j.neuron.2017.12.027.

Hawlena, D. and Schmitz, O. J. (2010) ‘Herbivore physiological response to predation risk and implications for ecosystem nutrient dynamics’, *Proceedings of the National Academy of Sciences of the United States of America*, 107(35), pp. 15503–15507. doi: 10.1073/pnas.1009300107.

Hayon, G., Abeles, M. and Lehmann, D. (2005) ‘A model for representing the dynamics of a system of synfire chains’, *Journal of Computational Neuroscience*, 18(1), pp. 41–53. doi: 10.1007/s10827-005-5479-1.

Henderson, S. T. and Johnson, T. E. (2001) ‘daf-16 integrates developmental and environmental inputs to mediate aging in the nematode Caenorhabditis elegans’, *Current Biology*, 11(24), pp. 1975–1980. doi: 10.1016/S0960-9822(01)00594-2.

Hills, T., Brockie, P. J. and Maricq, A. V. (2004) ‘Dopamine and Glutamate Control Area-Restricted Search Behavior in Caenorhabditis elegans’, *Journal of Neuroscience*, 24(5), pp. 1217–1225. doi: 10.1523/JNEUROSCI.1569-03.2004.

Hokfelt, T., Elfvin, L. G. and Elde, R. (1977) ‘Occurrence of somatostatin-like immunoreactivity in some peripheral sympathetic noradrenergic neurons’, *Proceedings of the National Academy of Sciences of the United States of America*, 74(8), pp. 3587–3591. doi: 10.1073/pnas.74.8.3587.

Honda, Y. and Honda, S. (1999) ‘ The daf-2 gene network for longevity regulates oxidative stress resistance and Mn-superoxide dismutase gene expression in Caenorhabditis elegans ’, *The FASEB Journal*, 13(11), pp. 1385–1393. doi: 10.1096/fasebj.13.11.1385.

Honner, V. and Docherty, J. R. (1999) ‘Investigation of the subtypes of α1-adrenoceptor mediating contractions of rat vas deferens’, *British Journal of Pharmacology*, 128(6), pp. 1323–1331. doi: 10.1038/sj.bjp.0702913.

Hoover, C. M. *et al.* (2014) ‘A novel CaM kinase II pathway controls the location of neuropeptide release from Caenorhabditis elegans motor neurons.’, *Genetics*, 196(3), pp. 745–65. doi: 10.1534/genetics.113.158568.

Horn, J. P. and Swanson, L. W. (2013) *Principles of Neural Science*. 5th edn. Edited by E. R. Kandel et al. New York: McGraw Hill.

Hsu, A. L., Murphy, C. T. and Kenyon, C. (2003) ‘Regulation of aging and age-related disease by DAF-16 and heat-shock factor’, *Science*, 300(5622), pp. 1142–1145. doi: 10.1126/science.1083701.

Huang, K. M., Cosman, P. and Schafer, W. R. (2006) ‘Machine vision based detection of omega bends and reversals in C. elegans’, *Journal of Neuroscience Methods*, 158(2), pp. 323–336. doi: 10.1016/j.jneumeth.2006.06.007.

Huffhines, L., Noser, A. and Patton, S. R. (2016) ‘The Link Between Adverse Childhood Experiences and Diabetes’, *Current Diabetes Reports*. Current Diabetes Reports, 16(6), pp. 1–9. doi: 10.1007/s11892-016-0740-8.

Husson, S. J. *et al.* (2005) ‘Discovering neuropeptides in Caenorhabditis elegans

by two dimensional liquid chromatography and mass spectrometry', *Biochemical and Biophysical Research Communications*, 335(1), pp. 76–86. doi: 10.1016/j.bbrc.2005.07.044.

Husson, S. J. *et al.* (2007) 'Neuropeptidergic signaling in the nematode Caenorhabditis elegans.', *Progress in neurobiology*, 82(1), pp. 33–55. doi: 10.1016/j.pneurobio.2007.01.006.

Huster, M. *et al.* (2010) ' A complex of Ca V 1.2/PKC is involved in muscarinic signaling in smooth muscle ', *The FASEB Journal*, 24(8), pp. 2651–2659. doi: 10.1096/fj.09-149856.

Insel, T. R. (1992) 'Oxytocin - A neuropeptide for affiliation: Evidence from behavioral, receptor autoradiographic, and comparative studies', *Psychoneuroendocrinology*, 17(1), pp. 3–35. doi: 10.1016/0306-4530(92)90073-G.

Islas-Trejo, A. *et al.* (1997) ' Structure and Expression of the Caenorhabditis elegans Protein Kinase C2 Gene ', *Journal of Biological Chemistry*, 272(10), pp. 6629–6640. doi: 10.1074/jbc.272.10.6629.

Jan, L. Y. and Jan, Y. N. (1982) 'Peptidergic transmission in sympathetic ganglia of the frog.', *The Journal of Physiology*, 327(1), pp. 219–246. doi: 10.1113/jphysiol.1982.sp014228.

Jasper, H. (2008) 'SKNy Worms and Long Life', *Cell*, pp. 915–916. doi: 10.1016/j.cell.2008.03.002.

Jékely, G. (2013) 'Global view of the evolution and diversity of metazoan neuropeptide signaling', *Proceedings of the National Academy of Sciences of the United States of America*, 110(21), pp. 8702–8707. doi: 10.1073/pnas.1221833110.

Jin, D. Z., Ramazanoğlu, F. M. and Seung, H. S. (2007) 'Intrinsic bursting enhances the robustness of a neural network model of sequence generation by avian brain area HVC', *Journal of Computational Neuroscience*, 23(3), pp. 283–299. doi: 10.1007/s10827-007-0032-z.

Jin, X., Pokala, N. and Bargmann, C. I. (2016) 'Distinct Circuits for the Formation and Retrieval of an Imprinted Olfactory Memory', *Cell*. Elsevier Inc., 164(4), pp. 632–643. doi: 10.1016/j.cell.2016.01.007.

Jospin, M. *et al.* (2002) 'The L-type voltage-dependent Ca2+ channel EGL-19 controls body wall muscle function in Caenorhabditis elegans.', *The Journal of cell biology*, 159(2), pp. 337–48. doi: 10.1083/jcb.200203055.

Kagawa-Nagamura, Y. *et al.* (2018) 'Role of tyramine in calcium dynamics of GABAergic neurons and escape behavior in Caenorhabditis elegans', *Zoological*

Letters. Zoological Letters, 4(1), pp. 1–14. doi: 10.1186/s40851-018-0103-1.

Kamp, T. J. and Hell, J. W. (2000) 'Regulation of cardiac L-type calcium channels by protein kinase A and protein kinase C', *Circulation research*, 87(12), pp. 1095–1102. Available at: http://graphics.tx.ovid.com/ovftpdfs/FPDDNCLBFGAJAP00/fs004/ovft/live/gv006/00003012/00003012-200012080-00008.pdf.

Kang, C. and Avery, L. (2009) 'Systemic regulation of starvation response in Caenorhabditis elegans', *Genes & Development*, 23(1), pp. 12–17. doi: 10.1101/gad.1723409.

Kasakov, L. *et al.* (1988) 'Direct evidence for concomitant release of noradrenaline, adenosine 5′-triphosphate and neuropeptide Y from sympathetic nerve supplying the guinea-pig vas deferens', *Journal of the Autonomic Nervous System*, 22(1), pp. 75–82. doi: 10.1016/0165-1838(88)90156-7.

Katz, P. (1998) 'Neuromodulation Intrinsic to the Central Pattern Generator for Escape Swimming in Tritoniaa', *Annals of the New York Academy of Sciences*. Available at: http://onlinelibrary.wiley.com/doi/10.1111/j.1749-6632.1998.tb09048.x/full (Accessed: 7 May 2014).

Kawano, T. *et al.* (2011) 'An imbalancing act: gap junctions reduce the backward motor circuit activity to bias C. elegans for forward locomotion.', *Neuron*. Elsevier Inc., 72(4), pp. 572–86. doi: 10.1016/j.neuron.2011.09.005.

Kenyon, C. *et al.* (1993) 'A C. elegans mutant that lives twice as long as wild type', *Nature*, 366(6454), pp. 461–464. doi: 10.1038/366461a0.

Kenyon, C. (2010) 'A pathway that links reproductive status to lifespan in Caenorhabditis elegans', *Annals of the New York Academy of Sciences*, 1204, pp. 156–162. doi: 10.1111/j.1749-6632.2010.05640.x.

Van Kesteren, R. E. *et al.* (1995) 'Structural and functional evolution of the vasopressin/oxytocin superfamily: Vasopressin-related conopressin is the only member present in Lymnaea, and is involved in the control of sexual behavior', *Journal of Neuroscience*, 15(9), pp. 5989–5998. doi: 10.1523/jneurosci.15-09-05989.1995.

Khraiwesh, B. and Salehi-Ashtiani, K. (2017) 'Alternative poly(A) tails meet miRNA targeting in Caenorhabditis elegans', *Genetics*, 206(2), pp. 755–756. doi: 10.1534/genetics.117.202101.

Kim, K. and Li, C. (2004) 'Expression and regulation of an FMRFamide-related neuropeptide gene family in Caenorhabditis elegans', *Journal of Comparative Neurology*, 475(4), pp. 540–550. doi: 10.1002/cne.20189.

Kimura, K. D. *et al.* (1997) 'Daf-2, an insulin receptor-like gene that regulates

longevity and diapause in Caenorhabditis elegans', *Science*, 277(5328), pp. 942–946. doi: 10.1126/science.277.5328.942.

Komuniecki, R. W. *et al.* (2004) 'Biogenic amine receptors in parasitic nematodes: What can be learned from Caenorhabditis elegans?', *Molecular and Biochemical Parasitology*, 137(1), pp. 1–11. doi: 10.1016/j.molbiopara.2004.05.010.

Korn, H. and Faber, D. S. (2005) 'The Mauthner cell half a century later: A neurobiological model for decision-making?', *Neuron*, 47(1), pp. 13–28. doi: 10.1016/j.neuron.2005.05.019.

Korswagen, H. C. *et al.* (1997) 'An activating mutation in a Caenorhabditis elegans Gs protein induces neural degeneration.', *Genes & Development*, 11(12), pp. 1493–1503. doi: 10.1101/gad.11.12.1493.

Krebs, R. A. and Feder, M. E. (1997) 'Deleterious consequences of Hsp70 overexpression in Drosphilla melanogaster larvae', *Cell Stress & Chaperones*, 2(1), p. 60. doi: 10.1379/1466-1268(1997)002<0060:DCOHOI>2.3.CO;2.

Kubiak, T. M. *et al.* (2003) 'Differential Activation of "Social" and "Solitary" Variants of the Caenorhabditis elegans G Protein-coupled Receptor NPR-1 by Its Cognate Ligand AF9', *Journal of Biological Chemistry*, 278(36), pp. 33724–33729. doi: 10.1074/jbc.M304861200.

Kubiak, T. M. *et al.* (2008) 'FMRFamide-like peptides encoded on the flp-18 precursor gene activate two isoforms of the orphan Caenorhabditis elegans G-protein-coupled receptor Y58G8A.4 heterologously expressed in mammalian cells.', *Biopolymers*, 90(3), pp. 339–48. doi: 10.1002/bip.20850.

Kumsta, C. *et al.* (2017) 'Hormetic heat stress and HSF-1 induce autophagy to improve survival and proteostasis in C. Elegans', *Nature Communications*. Nature Publishing Group, 8. doi: 10.1038/ncomms14337.

Lackner, M. R., Nurrish, S. J. and Kaplan, J. M. (1999) 'Facilitation of Synaptic Transmission by EGL-30 Gq and EGL-8 PLC: DAG Binding to UNC-13 Is Required to Stimulate Acetylcholine Release', *Cell*, 24, pp. 335–346.

Landis, J. N. and Murphy, C. T. (2010) 'Integration of diverse inputs in the regulation of Caenorhabditis elegans DAF-16/FOXO', *Developmental Dynamics*, 239(5), pp. 1405–1412. doi: 10.1002/dvdy.22244.

Lashley, K. (1951) 'The problem of serial order in behavior', *Cerebral mechanisms in behavior*, (7), pp. 112–147. Available at: http://books.google.com/books?hl=en&lr=&id=AqnzXFRU_BoC&oi=fnd&pg=PA118&dq=The+Problem+of+Serial+Order+in+Behavior&ots=hPyCJTnlTq&sig=nuMFcEmlbxnE5a9fH72casFdhyk.

Lee, I. *et al.* (2012) ‘Metabolic Rate Regulates L1 Longevity in C. elegans’, *PLoS ONE*, 7(9), pp. 1–10. doi: 10.1371/journal.pone.0044720.

Lee, J. H. *et al.* (2016) ‘Protein kinase a subunit balance regulates lipid metabolism in Caenorhabditis elegans and mammalian adipocytes’, *Journal of Biological Chemistry*, 291(39), pp. 20315–20328. doi: 10.1074/jbc.M116.740464.

Leifer, A. M. *et al.* (2011) ‘Optogenetic manipulation of neural activity in freely moving Caenorhabditis elegans.’, *Nature methods*, 8(2), pp. 147–52. doi: 10.1038/nmeth.1554.

Li, C. *et al.* (1999) ‘Neuropeptide Gene Families in the Nematode Caenorhabditis elegans’, *Annals of the New York Academy of Sciences*, 897(1), pp. 239–252. doi: 10.1111/j.1749-6632.1999.tb07895.x.

Li, C. and Kim, K. (2008) ‘Neuropeptides’, in *WormBook*. The C. elegans Research Community, WormBook, pp. 1–36. doi: 10.1895/wormbook.1.142.1.

Li, C. and Kim, K. (2014) ‘Family of FLP Peptides in Caenorhabditis elegans and Related Nematodes.’, *Frontiers in endocrinology*, 5(October), p. 150. doi: 10.3389/fendo.2014.00150.

Li, C., Kim, K. and Nelson, L. S. (1999) ‘FMRFamide-related neuropeptide gene family in Caenorhabditis elegans.’, *Brain research*, 848(1–2), pp. 26–34. Available at: http://www.ncbi.nlm.nih.gov/pubmed/15236235.

Li, H. Y. and Sawchenko, P. E. (1998) ‘Hypothalamic effector neurons and extended circuitries activated in “neurogenic” stress: A comparison of footshock effects exerted acutely, chronically, and in animals with controlled glucocorticoid levels’, *Journal of Comparative Neurology*, 393(2), pp. 244–266. doi: 10.1002/(SICI)1096-9861(19980406)393:2<244::AID-CNE8>3.0.CO;2-2.

Li, M.-R. and Greenside, H. (2006) ‘Stable propagation of a burst through a one-dimensional homogeneous excitatory chain model of songbird nucleus HVC’, *Physical Review E*, 74(1), p. 011918. doi: 10.1103/PhysRevE.74.011918.

Lim, M. M. and Young, L. J. (2006) ‘Neuropeptidergic regulation of affiliative behavior and social bonding in animals’, *Hormones and Behavior*, 50(4), pp. 506–517. doi: 10.1016/j.yhbeh.2006.06.028.

Lin, K. *et al.* (2001) ‘Regulation of the Caenorhabditis elegans longevity protein DAF-16 by insulin/IGF-1 and germline signaling.’, *Nature genetics*, 28(2), pp. 139–45. doi: 10.1038/88850.

Lionaki, E. and Tavernarakis, N. (2013) ‘Assessing Aging and Senescent Decline in Caenorhabditis elegans: Cohort Survival Analysis’, in *Cell Senescence*, pp. 473–484. doi: 10.1007/978-1-62703-239-1_31.

Lithgow, G. J. and Walker, G. A. (2002) ‘Stress resistance as a determinate of C. elegans lifespan’, *Mechanisms of Ageing and Development*, 123(7), pp. 765–771. doi: 10.1016/S0047-6374(01)00422-5.

Liu, S., Schulze, E. and Baumeister, R. (2012) ‘Temperature- and touch-sensitive neurons couple cng and trpv channel activities to control heat avoidance in caenorhabditis elegans’, *PLoS ONE*, 7(3). doi: 10.1371/journal.pone.0032360.

Liu, Y. *et al.* (1994) ‘Preferential localization of a vesicular monoamine transporter to dense core vesicles in PC12 cells’, *Journal of Cell Biology*, 127(5), pp. 1419–1433. doi: 10.1083/jcb.127.5.1419.

Lockard, M. A., Ebert, M. S. and Bargmann, C. I. (2017) ‘Oxytocin mediated behavior in invertebrates: An evolutionary perspective’, *Developmental Neurobiology*, 77(2), pp. 128–142. doi: 10.1002/dneu.22466.

Long, M. a, Jin, D. Z. and Fee, M. S. (2010) ‘Support for a synaptic chain model of neuronal sequence generation.’, *Nature*. Nature Publishing Group, 468(7322), pp. 394–399. doi: 10.1038/nature09514.

Lundberg, J. M. *et al.* (1982) ‘Neuropeptide Y (NPY)-like immunoreactivity in peripheral noradrenergic neurons and effects of NPY on sympathetic function’, *Acta Physiologica Scandinavica*, 116(4), pp. 477–480. doi: 10.1111/j.1748-1716.1982.tb07171.x.

Lundberg, J. M. *et al.* (1983) ‘High levels of neuropeptide Y in peripheral noradrenergic neurons in various mammals including man’, *Neuroscience Letters*, 42(2), pp. 167–172. doi: 10.1016/0304-3940(83)90401-9.

Lundberg, J. M. *et al.* (1985) ‘Co-release of neuropeptide Y and catecholamines during physical exercise in man’, *Biochemical and Biophysical Research Communications*, 133(1), pp. 30–36. doi: 10.1016/0006-291X(85)91837-6.

Lundberg, J. M. *et al.* (1986) ‘Frequency- and reserpine-dependent chemical coding of sympathetic transmission: Differential release of noradrenaline and neuropeptide Y from pig spleen’, *Neuroscience Letters*, 63(1), pp. 96–100. doi: 10.1016/0304-3940(86)90020-0.

Lundberg, J. M. *et al.* (1989) ‘Co-release of neuropeptide Y and noradrenaline from pig spleen in vivo: Importance of subcellular storage, nerve impulse frequency and pattern, feedback regulation and resupply by axonal transport’, *Neuroscience*, 28(2), pp. 475–486. doi: 10.1016/0306-4522(89)90193-0.

Lundberg, J. M. and Stjarne, L. (1984) ‘Neuropeptide Y (NPY) depresses the secretion of 3H-noradrenaline and the contractile response evoked by field stimulation, in rat vas deferens’, *Acta Physiologica Scandinavica*, 120(3), pp. 477–479. doi: 10.1111/j.1748-1716.1984.tb07410.x.

Luo, J. *et al.* (2014) ‘Neuropeptide receptors npr-1 and npr-2 regulate caenorhabditis elegans avoidance response to the plant stress hormone methyl salicylate’, *Genetics*, 199(2), pp. 523–531. doi: 10.1534/genetics.114.172239.

Maguire, S. M. *et al.* (2011) ‘The C. elegans touch response facilitates escape from predacious fungi.’, *Current biology : CB*. Elsevier Ltd, 21(15), pp. 1326–30. doi: 10.1016/j.cub.2011.06.063.

Maryon, E. B., Saari, B. and Anderson, P. (1998) ‘Muscle-specific functions of ryanodine receptor channels in Caenorhabditis elegans.’, *Journal of cell science*, 111 (Pt 1, pp. 2885–95. Available at: http://www.ncbi.nlm.nih.gov/pubmed/9730981.

Matsuzaki, H. *et al.* (2003) ‘Insulin-induced phosphorylation of FKHR (Foxo1) targets to proteasomal degradation’, *Proceedings of the National Academy of Sciences*, 100(20), pp. 11285–11290. doi: 10.1073/pnas.1934283100.

McDermott, B. J. *et al.* (1997) ‘Evidence for Y1 and Y2 subtypes of neuropeptide Y receptors linked to opposing postjunctional effects observed in rat cardiac myocytes’, *European Journal of Pharmacology*, 336(2–3), pp. 257–265. doi: 10.1016/S0014-2999(97)01258-2.

Merriam, E. B., Netoff, T. I. and Banks, M. I. (2005) ‘Bistable network behavior of layer I interneurons in auditory cortex’, *Journal of Neuroscience*, 25(26), pp. 6175–6186. doi: 10.1523/JNEUROSCI.0512-05.2005.

Mesa, R. *et al.* (2011) ‘HID-1, a new component of the peptidergic signaling pathway’, *Genetics*, 187(2), pp. 467–483. doi: 10.1534/genetics.110.121996.

Michael Piper, H., Cherie Millar, B. and McDermott, B. J. (1989) ‘The negative inotropic effect of neuropeptide Y on the ventricular cardiomyocyte’, *Naunyn-Schmiedeberg’s Archives of Pharmacology*, 340(3), pp. 333–337. doi: 10.1007/BF00168519.

Miller, G. E., Chen, E. and Parker, K. J. (2011) ‘Psychological stress in childhood and susceptibility to the chronic diseases of aging: Moving toward a model of behavioral and biological mechanisms.’, *Psychological Bulletin*, 137(6), pp. 959–997. doi: 10.1037/a0024768.

Miller, K., Emerson, M. and Rand, J. (1999) ‘G o α and Diacylglycerol Kinase Negatively Regulate the G q α Pathway in C. elegans’, *Neuron*, 24, pp. 323–333. Available at: http://www.sciencedirect.com/science/article/pii/S0896627300808478 (Accessed: 1 June 2014).

Miller, M. W. and Sadeh, N. (2014) ‘Traumatic stress, oxidative stress and post-Traumatic stress disorder: Neurodegeneration and the accelerated-aging

hypothesis', *Molecular Psychiatry*, 19(11), pp. 1156–1162. doi: 10.1038/mp.2014.111.

Mirabeau, O. and Joly, J. S. (2013) 'Molecular evolution of peptidergic signaling systems in bilaterians', *Proceedings of the National Academy of Sciences of the United States of America*, 110(22). doi: 10.1073/pnas.1219956110.

Moore, F. L. (1992) 'Evolutionary Precedents for Behavioral Actions of Oxytocin and Vasopressin', *Annals of the New York Academy of Sciences*, 652(1), pp. 156–165. doi: 10.1111/j.1749-6632.1992.tb34352.x.

Murphy, C. T., Lee, S. J. and Kenyon, C. (2007) 'Tissue entrainment by feedback regulation of insulin gene expression in the endoderm of Caenorhabditis elegans', *Proceedings of the National Academy of Sciences of the United States of America*, 104(48), pp. 19046–19050. doi: 10.1073/pnas.0709613104.

Nagai, T. *et al.* (2002) 'A variant of yellow fluorescent protein with fast and efficient maturation for cell-biological applications.', *Nature biotechnology*, 20(1), pp. 87–90. doi: 10.1038/nbt0102-87.

Nagel, G. *et al.* (2003) 'Channelrhodopsin-2, a directly light-gated cation-selective membrane channel', *Proceedings of the National Academy of Sciences*, 100(24), pp. 13940–13945. doi: 10.1073/pnas.1936192100.

Nusbaum, M. P. and Beenhakker, M. P. (2002) 'A small-systems approach to motor pattern generation', *Nature*, 417(6886), pp. 343–350. doi: 10.1038/417343a.

O'Hagan, R., Chalfie, M. and Goodman, M. B. (2005) 'The MEC-4 DEG/ENaC channel of Caenorhabditis elegans touch receptor neurons transduces mechanical signals.', *Nature neuroscience*, 8(1), pp. 43–50. doi: 10.1038/nn1362.

Ogg, S. *et al.* (1997) 'The Fork head transcription factor DAF-16 transduces insulin-like metabolic and longevity signals in C. elegans', *Nature*, 389(6654), pp. 994–999. doi: 10.1038/40194.

Oh, J. Y. *et al.* (2015) 'Plasma catecholamine levels before and after paroxetine treatment in patients with panic disorder', *Psychiatry Research*. Elsevier, 225(3), pp. 471–475. doi: 10.1016/j.psychres.2014.11.065.

Oki, Y., Teraoka, H. and Kitazawa, T. (2017) 'Neuropeptide Y (NPY) inhibits spontaneous contraction of the mouse atrium by possible activation of the NPY1 receptor', *Autonomic and Autacoid Pharmacology*, 37(2), pp. 23–28. doi: 10.1111/aap.12055.

Osterrieder, W. *et al.* (1982) 'Injection of subunits of cyclic AMP-dependent protein kinase into cardiac myocytes modulates Ca2+ current', *Nature*,

298(5874), pp. 576–578. doi: 10.1038/298576a0.

Park, J. H. *et al.* (1997) ‘Structure and expression of the gsa-1 gene encoding a G protein alpha(s) subunit in C. elegans.’, *Gene*, 194(2), pp. 183–90. Available at: http://www.ncbi.nlm.nih.gov/pubmed/9272860.

Pierce, S. B. (2001) ‘Regulation of DAF-2 receptor signaling by human insulin and ins-1, a member of the unusually large and diverse C. elegans insulin gene family’, *Genes & Development*, 15(6), pp. 672–686. doi: 10.1101/gad.867301.

Piggott, B. J. *et al.* (2011) ‘The neural circuits and synaptic mechanisms underlying motor initiation in C. elegans.’, *Cell*. Elsevier Inc., 147(4), pp. 922–33. doi: 10.1016/j.cell.2011.08.053.

Pirri, J. K. *et al.* (2009) ‘A Tyramine-Gated Chloride Channel Coordinates Distinct Motor Programs of a Caenorhabditis elegans Escape Response’, *Neuron*. Elsevier Ltd, 62(4), pp. 526–538. doi: 10.1016/j.neuron.2009.04.013.

Pirri, J. K., Rayes, D. and Alkema, M. J. (2015) ‘A Change in the Ion Selectivity of Ligand-Gated Ion Channels Provides a Mechanism to Switch Behavior’, *PLoS Biology*, 13(9), pp. 1–20. doi: 10.1371/journal.pbio.1002238.

Pokala, N. *et al.* (2014) ‘Inducible and titratable silencing of Caenorhabditis elegans neurons in vivo with histamine-gated chloride channels.’, *Proceedings of the National Academy of Sciences of the United States of America*, 111(7), pp. 2770–5. doi: 10.1073/pnas.1400615111.

Prahlad, V., Cornelius, T. and Morimoto, R. I. (2008) ‘Regulation of the cellular heat shock response in Caenorhabditis elegans by thermosensory neurons’, *Science*, 320(5877), pp. 811–814. doi: 10.1126/science.1156093.

Prahlad, V. and Morimoto, R. I. (2009) ‘Integrating the stress response: lessons for neurodegenerative diseases from C. elegans’, *Trends in Cell Biology*, 19(2), pp. 52–61. doi: 10.1016/j.tcb.2008.11.002.

Queiroz, G., Talaia, C. and Gonçalves, J. (2003) ‘ATP Modulates Noradrenaline Release by Activation of Inhibitory P2Y Receptors and Facilitatory P2X Receptors in the Rat Vas Deferens’, *Journal of Pharmacology and Experimental Therapeutics*, 307(2), pp. 809–815. doi: 10.1124/jpet.103.054809.

Rabasa, C. and Dickson, S. L. (2016) ‘Impact of stress on metabolism and energy balance’, *Current Opinion in Behavioral Sciences*. Elsevier Ltd, 9, pp. 71–77. doi: 10.1016/j.cobeha.2016.01.011.

Rattan, S. I. S. and Ali, R. E. (2007) ‘Hormetic prevention of molecular damage during cellular aging of human skin fibroblasts and keratinocytes’, *Annals of the New York Academy of Sciences*, 1100, pp. 424–430. doi: 10.1196/annals.1395.047.

Rodriguez, M. *et al.* (2013) ‘Worms under stress: C. elegans stress response and its relevance to complex human disease and aging’, *Trends in Genetics*. Elsevier Ltd, 29(6), pp. 367–374. doi: 10.1016/j.tig.2013.01.010.

Rogers, C. *et al.* (2003) ‘Inhibition of Caenorhabditis elegans social feeding by FMRFamide-related peptide activation of NPR-1.’, *Nature neuroscience*, 6(11), pp. 1178–85. doi: 10.1038/nn1140.

De Rosa, M. J. *et al.* (2019) ‘The flight response impairs cytoprotective mechanisms by activating the insulin pathway’, *Nature*. Springer US, pp. 135–138. doi: 10.1038/s41586-019-1524-5.

Rosoff, M. L. *et al.* (1993) ‘The flp-1 propeptide is processed into multiple, highly similar FMRFamide-like peptides in Caenorhabditis elegans’, *Peptides*, 14(2), pp. 331–338. doi: 10.1016/0196-9781(93)90049-M.

Rosoff, M. L., Burglin, T. R. and Li, C. (1992) ‘Alternatively spliced transcripts of the flp-1 gene encode distinct FMRFamide-like peptides in Caenorhabditis elegans’, *Journal of Neuroscience*, 12(6), pp. 2356–2361. doi: 10.1523/jneurosci.12-06-02356.1992.

Sanders, J. *et al.* (2014) ‘Homeostasis in C. elegans sleep is characterized by two behaviorally and genetically distinct mechanisms’, *eLife*, 3, pp. 1–21. doi: 10.7554/elife.04380.

Sassone-Corsi, P. (2012) ‘The Cyclic AMP pathway’, *Cold Spring Harbor Perspectives in Biology*, 4(12), pp. 3–5. doi: 10.1101/cshperspect.a011148.

Schindelin, J. *et al.* (2012) ‘Fiji: An open-source platform for biological-image analysis’, *Nature Methods*, 9(7), pp. 676–682. doi: 10.1038/nmeth.2019.

Selye, H. (1936) ‘A syndrome produced by diverse nocuous agents’, *Nature*, p. 32. doi: 10.1038/138032a0.

Selye, H. (1946) ‘The General Adaptation Syndrome and the Diseases of Adaptation’, *The Journal of Clinical Endocrinology*, 6(2), pp. 117–230. doi: 10.1210/jcem-6-2-117.

Sharp, G. W. G. and Straub, S. G. (2012) ‘Evolving insights regarding mechanisms for the inhibition of insulin release by norepinephrine and heterotrimeric G proteins’, *American Journal of Physiology - Cell Physiology*, 302(12). doi: 10.1152/ajpcell.00282.2011.

Shipley, F. B. *et al.* (2014) ‘Simultaneous optogenetic manipulation and calcium imaging in freely moving C. elegans’, *Frontiers in Neural Circuits*, 8(March), pp. 1–8. doi: 10.3389/fncir.2014.00028.

Sieburth, D., Madison, J. M. and Kaplan, J. M. (2007) ‘PKC-1 regulates secretion

of neuropeptides.', *Nature neuroscience*, 10(1), pp. 49–57. doi: 10.1038/nn1810.

Smith, N. C. E. and Burnstock, G. (2004) 'Mechanisms underlying postjunctional synergism between responses of the vas deferens to noradrenaline and ATP', *European Journal of Pharmacology*, 498(1–3), pp. 241–248. doi: 10.1016/j.ejphar.2004.07.055.

Spanier, B. *et al.* (2005) 'Caenorhabditis elegans neprilysin NEP-1: An effector of locomotion and pharyngeal pumping', *Journal of Molecular Biology*, 352(2), pp. 429–437. doi: 10.1016/j.jmb.2005.06.063.

Speese, S. *et al.* (2007) 'UNC-31 (CAPS) is required for dense-core vesicle but not synaptic vesicle exocytosis in Caenorhabditis elegans', *Journal of Neuroscience*, 27(23), pp. 6150–6162. doi: 10.1523/JNEUROSCI.1466-07.2007.

Starich, T. A. *et al.* (2009) 'Interactions between innexins UNC-7 and UNC-9 mediate electrical synapse specificity in the Caenorhabditis elegans locomotory nervous system', *Neural Development*, 4(1), pp. 1–28. doi: 10.1186/1749-8104-4-16.

Stawicki, T. M. *et al.* (2013) 'Neuropeptides function in a homeostatic manner to modulate excitation-inhibition imbalance in C. elegans.', *PLoS genetics*, 9(5), p. e1003472. doi: 10.1371/journal.pgen.1003472.

Stiernagle, T. (2006) 'Maintenance of C. elegans.', *WormBook : the online review of C. elegans biology*, (1999), pp. 1–11. doi: 10.1895/wormbook.1.101.1.

Strawn, J. R. and Geracioti, T. D. (2008) 'Noradrenergic dysfunction and the psychopharmacology of posttraumatic stress disorder', *Depression and Anxiety*, 25(3), pp. 260–271. doi: 10.1002/da.20292.

Streb, H. *et al.* (1983) 'Release of Ca2+ from a nonmitochondrial intracellular store in pancreatic acinar cells by inositol-1,4,5-trisphosphate', *Nature*, 306(5938), pp. 67–69. doi: 10.1038/306067a0.

Suzuki, H. *et al.* (2003) 'In vivo imaging of C. elegans mechanosensory neurons demonstrates a specific role for the MEC-4 channel in the process of gentle touch sensation', *Neuron*, 39(6), pp. 1005–1017. doi: 10.1016/j.neuron.2003.08.015.

Swierczek, N. a *et al.* (2011) 'High-throughput behavioral analysis in C. elegans.', *Nature methods*, 8(7), pp. 592–8. doi: 10.1038/nmeth.1625.

Thorn, R. G. and Barron, G. L. (1984) 'Carnivorous mushrooms', *Science*, 224(4644), pp. 76–78. doi: 10.1126/science.224.4644.76.

Toth, P. T. *et al.* (1993) 'Mechanism of presynaptic inhibition by neuropeptide Y at sympathetic nerve terminals', *Nature*, 364(6438), pp. 635–639. doi:

10.1038/364635a0.

Travers, M. *et al.* (2010) ‘Indirect predator effects on clutch size and the cost of egg production’, *Ecology Letters*, 13(8), pp. 980–988. doi: 10.1111/j.1461-0248.2010.01488.x.

Tsalik, E. L. *et al.* (2003) ‘LIM homeobox gene-dependent expression of biogenic amine receptors in restricted regions of the C. elegans nervous system’, *Developmental Biology*, 263(1), pp. 81–102. doi: 10.1016/S0012-1606(03)00447-0.

Tullet, J. M. A. *et al.* (2017) ‘The SKN-1/Nrf2 transcription factor can protect against oxidative stress and increase lifespan in C. elegans by distinct mechanisms’, *Aging Cell*, 16(5), pp. 1191–1194. doi: 10.1111/acel.12627.

Varshney, L. R. *et al.* (2011) ‘Structural properties of the Caenorhabditis elegans neuronal network’, *PLoS Computational Biology*, 7(2). doi: 10.1371/journal.pcbi.1001066.

Venkatachalam, V. *et al.* (2015) ‘Pan-neuronal imaging in roaming Caenorhabditis elegans.’, *Proceedings of the National Academy of Sciences of the United States of America*, p. 201507109. doi: 10.1073/pnas.1507109113.

Vergara, J., Tsien, R. Y. and Delay, M. (1985) ‘Inositol 1,4,5-trisphosphate: A possible chemical link in excitation-contraction coupling in muscle’, *Proceedings of the National Academy of Sciences of the United States of America*, 82(18), pp. 6352–6356. doi: 10.1073/pnas.82.18.6352.

Vervaeke, K. *et al.* (2010) ‘Rapid Desynchronization of an Electrically Coupled Interneuron Network with Sparse Excitatory Synaptic Input’, *Neuron*, 67(3), pp. 435–451. doi: 10.1016/j.neuron.2010.06.028.

Volpe, P. *et al.* (1985) ‘Inositol 1,4,5-trisphosphate induces calcium release from sarcoplasmic reticulum of skeletal muscle’, *Nature*, 316(6026), pp. 347–349. doi: 10.1038/316347a0.

Van Voorhies, W. A. and Ward, S. (1999) ‘Genetic and environmental conditions that increase longevity in Caenorhabditis elegans decrease metabolic rate’, *Proceedings of the National Academy of Sciences of the United States of America*, 96(20), pp. 11399–11403. doi: 10.1073/pnas.96.20.11399.

Wagenaar, D. A. *et al.* (2010) ‘A Hormone-Activated Central Pattern Generator for Courtship’, *Current Biology*. Elsevier Ltd, 20(6), pp. 487–495. doi: 10.1016/j.cub.2010.02.027.

Wahlestedt, C. *et al.* (1985) ‘Neuropeptide Y potentiates noradrenaline-evoked vasoconstriction: Mode of action’, *Journal of Pharmacology and Experimental Therapeutics*, 234(3), pp. 735–741.

Wahlestedt, C. *et al.* (1990) 'Norepinephrine and neuropeptide Y: Vasoconstrictor cooperation in vivo and in vitro', *American Journal of Physiology - Regulatory Integrative and Comparative Physiology*, 258(3 27-3), pp. 736–742. doi: 10.1152/ajpregu.1990.258.3.r736.

Wakabayashi, T., Kitagawa, I. and Shingai, R. (2004) 'Neurons regulating the duration of forward locomotion in Caenorhabditis elegans', *Neuroscience Research*, 50(1), pp. 103–111. doi: 10.1016/j.neures.2004.06.005.

Wang, Y. *et al.* (2020) 'Flexible motor sequence generation during stereotyped escape responses', *eLife*, 9, pp. 1–27. doi: 10.7554/eLife.56942.

Weiss, K. R. *et al.* (1992) 'Peptidergic co-transmission in Aplysia: Functional implications for rhythmic behaviors', *Experientia*, 48(5), pp. 456–463. doi: 10.1007/BF01928164.

Weiss, S. *et al.* (2012) 'Modulation of distinct isoforms of L-type calcium channels by G q-coupled receptors in Xenopus oocytes: Antagonistic effects of Gβγ and protein kinase C', *Channels*, 6(6), pp. 426–437. doi: 10.4161/chan.22016.

Westfall, T. C. *et al.* (1988) 'Cardiovascular effects and modulation of noradrenergic neurotransmission following central and peripheral administration of neuropeptide Y', *Synapse*, 2(3), pp. 299–307. doi: 10.1002/syn.890020320.

Westfall, T. C., Yang, C. L. and Curfman-Falvey, M. (1995) 'Neuropeptide-Y-ATP interactions at the vascular sympathetic neuroeffector junction', *Journal of Cardiovascular Pharmacology*, 26(5), pp. 682–687. doi: 10.1097/00005344-199511000-00002.

White, J. G. *et al.* (1986) 'The Structure of the Nervous System of the Nematode Caenorhabditis elegans', *Philosophical Transactions of the Royal Society B: Biological Sciences*, 314(1165), pp. 1–340. doi: 10.1098/rstb.1986.0056.

Wicks, S. R. and Rankin, C. H. (1995) 'Integration of mechanosensory stimuli in Caenorhabditis elegans.', *The Journal of neuroscience : the official journal of the Society for Neuroscience*, 15(3 Pt 2), pp. 2434–2444.

Witvliet, D. *et al.* (2020) 'Connectomes across development reveal principles of brain maturation in C. elegans', *bioRxiv*, pp. 1–26. doi: 10.1101/2020.04.30.066209.

Wolf, E. J. *et al.* (2016) 'Accelerated DNA methylation age: Associations with PTSD and neural integrity', *Psychoneuroendocrinology*. Elsevier Ltd, 63, pp. 155–162. doi: 10.1016/j.psyneuen.2015.09.020.

Wood, D. E. and Nusbaum, M. P. (2002) 'Extracellular Peptidase Activity Tunes Motor Pattern Modulation', *Journal of Neuroscience*, 22(10), pp. 4185–4195. doi: 10.1523/jneurosci.22-10-04185.2002.

Wragg, R. T. *et al.* (2007) ‘Tyramine and octopamine independently inhibit serotonin-stimulated aversive behaviors in Caenorhabditis elegans through two novel amine receptors’, *Journal of Neuroscience*, 27(49), pp. 13402–13412. doi: 10.1523/JNEUROSCI.3495-07.2007.

Wu, D. *et al.* (1992) ‘Activation of phospholipase C by α1-adrenergic receptors is mediated by the α subunits of Gq family’, *Journal of Biological Chemistry*, 267(36), pp. 25798–25802.

Xu, S. and Chisholm, A. D. (2011) ‘A Gαq-Ca2+ signaling pathway promotes actin-mediated epidermal wound closure in C. elegans’, *Current Biology*. Elsevier Ltd, 21(23), pp. 1960–1967. doi: 10.1016/j.cub.2011.10.050.

Yaffe, K. *et al.* (2010) ‘Posttraumatic Stress Disorder and Risk of Dementia Among US Veterans’, *Archives of General Psychiatry*, 67(6), p. 608. doi: 10.1001/archgenpsychiatry.2010.61.

Yamada, K. *et al.* (2010) ‘Olfactory Plasticity Is Regulated by Pheromonal Signaling in Caenorhabditis elegans’, *Science*, 329(5999), pp. 1647–1650. doi: 10.1126/science.1192020.

Yehuda, R. *et al.* (1998) ‘Plasma norepinephrine and 3-methoxy-4-hydroxyphenylglycol concentrations and severity of depression in combat posttraumatic stress disorder and major depressive disorder’, *Biological Psychiatry*, 44(1), pp. 56–63. doi: 10.1016/S0006-3223(98)80007-3.

Yemini, E., Kerr, R. A. and Schafer, W. R. (2011) ‘Tracking movement behavior of multiple worms on food’, *Cold Spring Harbor Protocols*, 6(12), pp. 1483–1487. doi: 10.1101/pdb.prot067025.

Zheng, M. *et al.* (2012) ‘Calcium imaging of multiple neurons in freely behaving C. elegans’, *Journal of Neuroscience Methods*. Elsevier B.V., 206(1), pp. 78–82. doi: 10.1016/j.jneumeth.2012.01.002.

Zukowska-Grojec, Z., Konarska, M. and McCarty, R. (1988) ‘Differential plasma catecholamine and neuropeptide Y responses to acute stress in rats’, *Life Sciences*, 42(17), pp. 1615–1624. doi: 10.1016/0024-3205(88)90440-7.

Zukowska-Grojec, Z., Marks, E. S. and Haass, M. (1987) ‘Neuropeptide Y is a potent vasoconstrictor and a cardiodepressant in rat’, *American Journal of Physiology - Heart and Circulatory Physiology*, 253(5). doi: 10.1152/ajpheart.1987.253.5.h1234.

Zukowska-Grojec, Z. and Vaz, A. C. (1988) ‘Role of neuropeptide Y (NPY) in cardiovascular responses to stress’, *Synapse*, 2(3), pp. 293–298. doi: 10.1002/syn.890020319.